

ADA 050677

2

RADC-TR-77-410
Final Technical Report
December 1977



RELIABILITY STUDY OF DOPED ALUMINUM CONDUCTOR FILMS

James Black

Motorola Semiconductor Products Group

HU INU.
DDC FILE COPY

DDC
RECEIVED
MAR 3 1978
F

Approved for public release; distribution unlimited.

ROME AIR DEVELOPMENT CENTER
Air Force Systems Command
Griffis Air Force Base, New York 13441

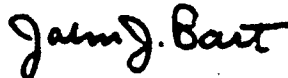
use 237670

jet

This report has been reviewed by the RADC Information Office (OI) and is releasable to the National Technical Information Service (NTIS). At NTIS it will be releasable to the general public, including foreign nations.


RADC-TR-77-410 has been reviewed and is approved for publication.

APPROVED:



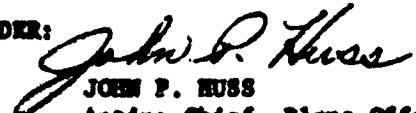
JOHN J. BART
Project Engineer

APPROVED:



JOSEPH J. NARESKY
Chief, Reliability & Compatibility Division

FOR THE COMMANDER:



JOHN P. HUSS
Acting Chief, Plans Office

If your address has changed or if you wish to be removed from the RADC mailing list, or if the addressee is no longer employed by your organization, please notify RADC (RRFP) Griffiss AFB NY 13441. This will assist us in maintaining a current mailing list.

Do not return this copy. Retain or destroy.

UNCLASSIFIED

SECURITY CLASSIFICATION OF THIS PAGE (When Data Entered)

REPORT DOCUMENTATION PAGE		READ INSTRUCTIONS BEFORE COMPLETING FORM
1. REPORT NUMBER 18 RADC-TR-77-410	2. GOVT ACCESSION NO.	3. RECIPIENT'S CATALOG NUMBER
4. TITLE (and Subtitle) 4 RELIABILITY STUDY OF DOPED ALUMINUM CONDUCTOR FILMS.	5. TYPE OF REPORT & PERIOD COVERED 9 Final Technical Report. May 1976 - August 1977.	6. CONTRACT OR GRANT NUMBER(s) N/A
7. AUTHOR(s) 10 James/Black	8. CONTRACT OR GRANT NUMBER(s) 15 F30602-76-C-8308 ^{REV}	
9. PERFORMING ORGANIZATION NAME AND ADDRESS Motorola Semiconductor Products Group ✓ 5005 E. McDowell Road Phoenix AZ 85008 Div. 237670	10. PROGRAM ELEMENT, PROJECT, TASK AREA & WORK UNIT NUMBERS 62702F 16 2338 23380115 17 01	
11. CONTROLLING OFFICE NAME AND ADDRESS Rome Air Development Center (RBRP) ✓ Griffiss AFB NY 13441	12. REPORT DATE 11 December 1977	
14. MONITORING AGENCY NAME & ADDRESS (if different from Controlling Office) Same	13. NUMBER OF PAGES 100 12 112p.	15. SECURITY CLASS. (of this report) UNCLASSIFIED
16. DISTRIBUTION STATEMENT (of this Report) Approved for public release; distribution unlimited.		15a. DECLASSIFICATION/DOWNGRADING SCHEDULE N/A
17. DISTRIBUTION STATEMENT (of the abstract entered in Block 20, if different from Report) Same		
18. SUPPLEMENTARY NOTES RADC Project Engineer: John J. Bart		
19. KEY WORDS (Continue on reverse side if necessary and identify by block number) Silicon Doped Aluminum Conductor Films Microelectronic Devices Electromigration Corrosion Resistance Activation Energy Analysis		
20. ABSTRACT (Continue on reverse side if necessary and identify by block number) A reliability study of silicon doped aluminum conductor films for semiconductor device use is presented. The solid state dissolution process of silicon in aluminum is discussed and the morphology of etch pits that can form in silicon due to these processes are described. Processes for depositing Al/Si alloy films are briefly mentioned and the structure of the films as deposited and after various heat treatments is studied. The electromigration failure mode of metal induced by high current densities and temperatures is presented along with the results of previous studies of pure aluminum, other aluminum		

DDC
 REPRODUCED
 MAR 3 1978
 F

237 670

JOB



UNCLASSIFIED

SECURITY CLASSIFICATION OF THIS PAGE (When Data Entered)

alloys and aluminum silicon alloys. Current results on low temperature (<210°C) studies of small grained and glassed Al/Si alloys indicate that they fail by an electrical open circuit due to the growth of voids resulting from the electromigration of Al in Al. The activation energy for this process for small grained (~1.4µm) glassed alloys is 0.544 eV, a value consistent with grain boundary diffusion of Al. Equations describing the low temperature lifetimes of these small grain, glassed alloys as a function of conductor geometry, current density and temperature are given with design charts. At elevated temperatures (>185°C - 240°C depending upon the device sensitivity) which often are employed for device life testing, two other failure modes were observed which are due to the electromigration of Si through Al. These are the shunting or shorting of shallow junctions at (-) ohmic contacts to the alloy and increase in contact resistance at (+) ohmic contacts to the alloy. These failures exhibit an activation energy of 0.89 eV consistent with that attributed for the diffusion of Si in Al dislocations. An equation describing the lifetime of the test device used which failed at the (-) contact is given as a function of conductor geometry, current density and temperature.

Si alloy additions to Al accelerate the anodic corrosion rate while the cathodic corrosion rate of the alloys are similar to that of pure Al. Also alloy films that have been etched to remove exposed silicon particulates corrode in a manner similar to pure aluminum.

The surface reconstruction of small grained Al/Si alloys produces more hillocks, but smaller hillocks than does small grained pure aluminum. The silicon does not prevent hillock growth. The ultrasonic wire bondability of the alloy films is excellent as is the adhesion of the alloys to thermally grown SiO₂ when deposited onto hot substrates. The electrical resistivity of the silicon alloys is similar to pure aluminum. Residual silicon particulates at the interface between thermally grown SiO₂ and passivation glass do not electrically interfere with devices if the particles are small compared to device spacing/

A study of data obtained by others at high temperatures where failure was attributed to the electromigration of Si in Al indicates the same activation energy for the process as was obtained in this work.

The small grain, glassed Al/Si alloy metallization is considered to be reliable and it is recommended that the MIL-M-38510C specification for small grain, glassed Al/Si alloys be reduced from the present maximum current density limit of 5×10^5 A/cm².

UNCLASSIFIED

SECURITY CLASSIFICATION OF THIS PAGE (When Data Entered)

TABLE OF CONTENTS

<u>Section</u>	<u>Title</u>	<u>Page No.</u>
1.0	Introduction	1
2.0	Technical Discussion	1
2.1	Solid State Dissolution of Si in Al	2
2.2	Al-Si alloy Film Deposition and Structure	11
2.2.1	Film Structure-Experimental	12
2.3	Electromigration	17
2.3.1	Theory	24
2.3.2	Previous Experimental Work-General	25
2.3.3	Previous Experimental Work-Al/Si Alloys	29
2.3.4	Low Temperature Al/Si Alloy Electromigration	33
2.3.5	High Temperature Al/Si Alloy Electro- migration	53
2.4	Al/Si Alloy Film Corrosion	69
2.5	Al/Si Alloy Film Surface Reconstruction	79
2.6	Al/Si Alloy Wire Bondability	82
2.7	Adhesion of Al/Si Alloy Films to SiO ₂	85
2.8	Resistivity of Al/Si Alloys	86
2.9	Sheet Resistivity at the Thermal Oxide- Passivation Glass Interface	90
3.0	Further Observations of High Temperature Al/Si Alloy Electromigration	92
4.0	Conclusions and Recommendations	95
Appendix I	References	98
Appendix II	Acknowledgments	100

<input type="checkbox"/> Wire Section	<input checked="" type="checkbox"/>
<input type="checkbox"/> R ff Section	<input type="checkbox"/>
BY	
DISTRIBUTION/AVAILABILITY CODES	
SPECIAL	
A	

LIST OF FIGURES

<u>Figure No.</u>	<u>Title</u>	<u>Page No.</u>
1	Aluminum silicon phase diagram	3
2	The diffusivity of silicon in solid aluminum	5
3	The morphology of silicon dissolution pits	6
4	SEM picture of the silicon substrate after Al (large grained) has been removed	7
5	Dark field optical micrographs showing the number and size of dissolution pits in 111 silicon after three aging times (405°C)	9
6	SEM micrograph of dissolution pits which occurred using Al-1% Si metallization	10
7	As deposited Al/Si alloy films	13
8	Al/Si alloy films after 15 min. at 500°C	16
9	Si particles in as deposited Al/Si alloy films	19
10	Al/Si alloy films after 15 min. at 500°C followed by a fast cool and Al etch	20
11	Al/Si alloy films after 15 min. at 500°C followed by slow cooling and Al etch	21
12	Al/Si alloy films after 15 min. at 500°C, fast cool, 161 hours at 300°C followed by fast cooling and Al etch	22
13	Three possible locations where electro-migration can occur in polycrystalline aluminum	23
14	Median time to failure of some aluminum alloys as a function of current density j , temperature T , and cross section area A	26
15	Growth of voids and hillocks in small grained aluminum	27

<u>Figure No.</u>	<u>Title</u>	<u>Page No.</u>
16	An electron beam induced current (EBIC) mode photograph of a one mil wide Al-2% Cu stripe during an electromigration experiment in the SEM	28
17	Etch pits formed by electromigration of Si through Al (negative terminal)	31
18	Si build-up by electromigration of Si through Al (positive terminal)	31
19	Chemical diffusion in bulk Al-Si alloys	32
20	Low temperature electromigration test die	39
21	Log normal plot of A 19 device cell stressed at 167°C at $J = 8 \times 10^5$ A/cm ²	40
22	Voids formed in Al/Si alloys during electromigration test at low temperatures	41
23	Cracked passivation glass due to hillock growth before and after glass removal	42
24	Al-0.79% Si alloy data relating median time to failure to film geometry, current density and temperature	43
25	Al-1.9% Si alloy data relating median time to failure to film geometry, current density and temperature	44
26	Al-3% Si alloy data relating median time to failure to film geometry, current density and temperature	45
27	Combined Al/Si alloy data relating % device failure to film geometry, current density and temperature	47
28	50% failure time of Al/Si alloy films with 10 ⁻⁷ cm ² cross sectional area	49
29	1% failure time of Al/Si alloy films with 10 ⁻⁷ cm ² cross sectional area	50
30	0.1% failure time of Al/Si alloy films with 10 ⁻⁷ cm ² cross sectional area	51

<u>Figure No</u>	<u>Title</u>	<u>Page No.</u>
31	0.01. failure time of Al/Si alloy films with 10^{-7} cm ² cross sectional area	52
32	Schematic of high temperature test structure cross section prior to passivation	54
33	(a) 80 x 80 mil high temperature test structure. (b) Enlarged view of diffused region, ohmic contact and wire bond pad	55
34	Bimodal failure distribution	58
35	Device stressed at 310 ⁰ C and J = 4.95 x 10 ⁵ A/cm ² prior to passivation glass removal	59
36	Device shown in Figure 35 after removal of passivation glass	60
37	Device shown in Figures 35 and 36 after aluminum etch	61
38	+ and - terminals after passivation glass, aluminum and thermal oxide etch	62
39	+ and - terminals before and after passivation glass removal	64
40	Contacts shown in Figure 39 after aluminum etch	65
41	Typical voids and hillocks observed in high temperature Al/Si alloy films due to aluminum electromigration in Al	66
42	Al/Si alloy median time to failure due to the electromigration of Si in Al related to film geometry, current density and temperature	68
43	Al/Si alloy high temperature median time to failure due to void formation related to film geometry current density and temperature	70
44	Al/Si alloy failures due to the electromigration of Al in Al and Si in Al	71
45	The corrosion test pattern with 0.5 mil line widths and 0.5 mil spacings	73

<u>Figure No.</u>	<u>Title</u>	<u>Page No.</u>
46	The anodic corrosion for Al-Si alloy films and a pure Al film	74
47	The cathodic corrosion for Al-Si alloy films and a pure Al film	75
48	(a) A typical Al-3% Si sample showing characteristic spotty corrosion at the anode stripes after 180 hours at 85/85/20. (b) The center stripes at higher magnification showing local corrosion spots	76
49	Local corrosion spots on Al-0.79% Si metallization after 180 hours at 85/85/20	77
50	(a) A pure Al test sample showing the corrosion characteristics after 180 hours at 85/85/20. (b) A high magnification view of the top part of Figure 50a showing cathodic corrosion	78
51	Al/Si alloy films thermally cycled 10 times from 25°C to 450°C	81
52	Passivation glass cracks due to thermal cycling	83
53	Power-time bonding windows for Al/Si alloy films to 0.001" Al-1% Si wire at a load of 30 grams	84
54	Measured resistivity of three Al/Si alloy films	88
55	Resistivity ratio room temperature to liquid nitrogen temperature as a function of alloy silicon content	89
56	ECL data compared to data generated by the high temperature test device and low temperature data	94

LIST OF TABLES

<u>Table No.</u>	<u>Title</u>	<u>Page No.</u>
I	Grain Size of Alloy Films After Various Thermal Treatments	15
II	Maximum Si Particle Size	18
III	Si Particle Density	18
IV	Al/Si Alloy Conductor Dimensions	35
V	Low Temperature Al/Si Alloy Test Conditions and Results	37-38
VI	High Temperature Test Device Dimensions	57
VII	High Temperature Al/Si Alloy Test Conditions and Results	67
VIII	Metal-SiO ₂ Adhesion Test Results	88
IX	Stripe Leakage Current at 10 Volts	91
X	High Temperature ECL Test Data Obtained from Reference 24	93

EVALUATION

This technical report describes the evaluation of silicon doped aluminum conductors under a variety of stress conditions that would be encountered in their use as interconnection paths on microelectronic devices. This work supports the objectives of TPO-5, "C³ Systems Availability," and the associated project 2338, "Assurance Technology for Electronics."

The data generated on the mechanisms of electromigration, film corrosion resistance and other sources of device degradation associated with the silicon doping material will be used to upgrade MIL-M-38510D, "General Specification for Microcircuits," and the associated test procedures defined in MIL-STD-883B, "Test Methods and Procedures for Microelectronics."

This work not only advanced the understanding of the influence of silicon doped aluminum metallization on microelectronic device reliability, but also points out the need for continued evaluation of other metallization systems used in microcircuit fabrication. These additional studies are being planned as part of RADC's solid state reliability program.


JOHN J. BART
Reliability Physics Section
Reliability Branch

RELIABILITY STUDY OF DOPED ALUMINUM CONDUCTOR FILMS

1.0 Introduction

The objective of this study is to provide information concerning the effect silicon doped aluminum conductor films have on the reliability of integrated circuits when these films are used to interconnect active device areas. The study of alloys containing 3.5% or less silicon includes electromigration failure by aluminum transport as well as electromigration failure by silicon transport. In addition the films were characterized as to their wire bondability, their sensitivity to corrosion, their adherence to glass, electrical leakage at the passivation glass-thermal oxide interface, their resistance to surface reconstruction during thermal cycling and their electrical resistance as a function of temperature. The films were also characterized as to effects caused by thermal treatment.

Pure aluminum has been used extensively as a metallization for semiconductor devices and was characterized in a RADC sponsored program in 1968^{1*}. The results of this work led to the design rules now used by industry for the manufacture of reliable integrated circuits using aluminum metal. Since about 1966 a class of semiconductor devices utilizing shallow junctions and requiring elevated heat treatments after metallization appeared which could not be manufactured with pure aluminum metallization but could be produced utilizing aluminum doped with 1-3% silicon. The reason for this is described in the next section of this report. The effects these slight additions of silicon to aluminum might have on the reliability of semiconductor devices was not known even though millions of these parts have been in use with an exceptionally good long-term reliability record. It is the purpose of this study to provide a better understanding of these alloys and to establish guide lines for their manufacture and use.

Section 2 of this report represents the technical portion while the conclusions and recommendations are presented in Section 4.

2.0 Technical Discussion

There are many modes by which a metallization system can effect the reliability of a semiconductor integrated circuit. All must be understood and controlled if devices are to be designed and constructed for reliable operation. Some metallization properties which are of interest are:

1. electrical volume resistance
2. ohmic contact to both n and p type silicon
3. adherence to silicon
4. adherence to silicon dioxide

*References are listed in the Appendix.

5. metallurgical interactions with silicon
6. chemical reactions with silicon dioxide
7. resistance to surface reconstruction
8. adherence of passivation films to the metallization
9. corrosion susceptibility
10. ease of deposition in a controlled manner
11. ease of patterning and removing all components of the metallization
12. electromigration characteristics
13. electromigration of solute ions and its effect on ohmic contacts
14. wire bondability and bond integrity.

Guided by the resources available for this present program and by their anticipated importance level to reliability, over one half of the above items were selected for study. These are reported on in the following sections.

2.1 Solid State Dissolution of Si in Al*

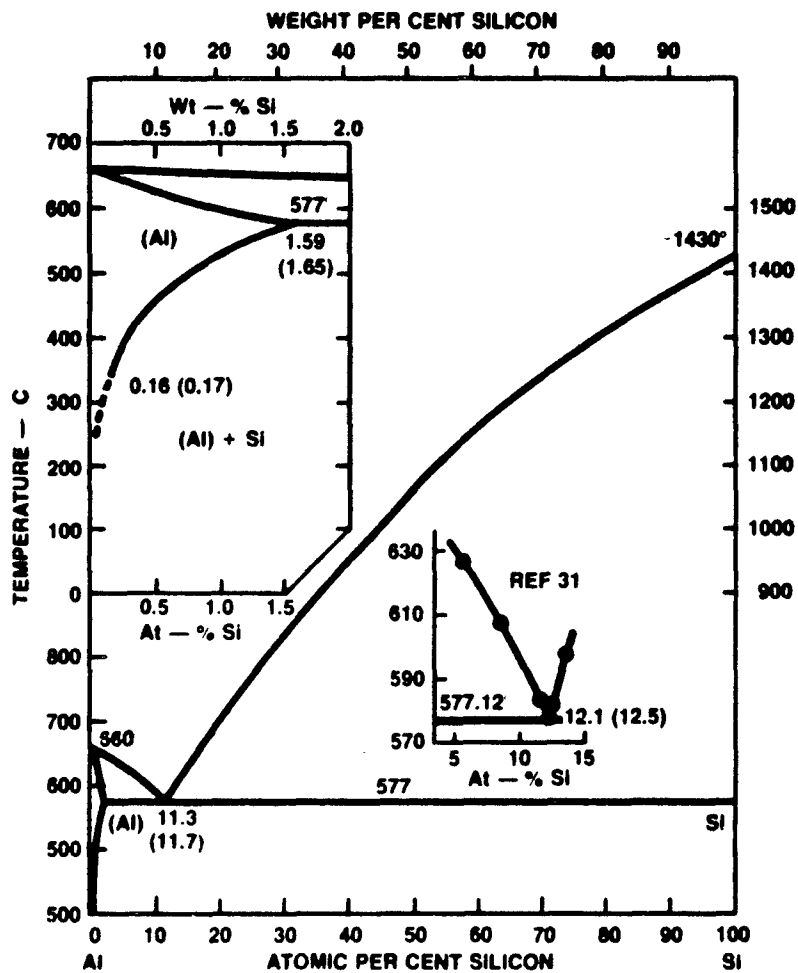
The reactions which occur at the aluminum-silicon contact areas affect both the initial processing yield of devices and the long term stability. Aluminum and silicon form a simple eutectic system (Figure 1). For this discussion the enlarged portion of the diagram shown in the upper left insert is of importance. The pie shaped region labeled (A1) is a solid region whose crystalline structure is identical to pure aluminum except that some of the aluminum ions have been substituted by silicon ions. This is the region of "solid solution." The lower curved boundary of that region is called the "solvus" curve and defines the maximum amount of silicon that can dissolve into aluminum as a function of temperature.

Below and to the right of the solvus curve is a solid region containing a mixture of essentially pure silicon crystals and crystals whose composition is determined by the solvus curve. As shown, below about 200°C well annealed aluminum silicon alloys consist of a mixture of nearly pure aluminum and pure silicon crystals. When aluminum in contact with silicon is heated silicon rapidly dissolves by a solid state diffusion process (below 577°C) into the aluminum to saturate the solution at a composition determined by the solvus curve. Upon slow cooling the dissolved silicon precipitates out of solution forming a mixture of silicon and aluminum crystals at lower temperatures.

At the eutectic temperature of 577°C, the solubility of silicon in aluminum is 1.59 atomic percent and this solubility drops rapidly with temperature. A plot of log atomic percent silicon vs. $1/T$ of the solvus curve using the data given by Hansen³ is linear from 300°C to just before the eutectic temperature, indicating that aluminum and small amounts of silicon form a near ideal solution. The activation energy for the dissolution of silicon in aluminum as determined from the slope of this curve is 0.52 eV. The solid solubility of aluminum in silicon has been carefully measured only at high temperatures ($T > 600^\circ\text{C}$). From extrapolation of the data to lower temperatures,

*The etch pit study reported here was done by E. Hall of Motorola and published as reference 2.

FIGURE 1. ALUMINUM-SILICON PHASE DIAGRAM



E3602

this solubility is more than 100 times less than that of silicon in aluminum.

The diffusivity of silicon in thin film aluminum is much higher than in bulk samples^{4,5,6}, (Figure 2). Also the activation energy is appreciably lower, presumably indicating a much stronger grain boundary contribution. For example, at 500°C a silicon atom moves nearly 1½ microns a second in a thin aluminum film. The diffusion coefficient of aluminum in silicon again has been determined only at high temperatures (1000-1400°C). At 1000°C it is 10^{-13} cm²/sec.

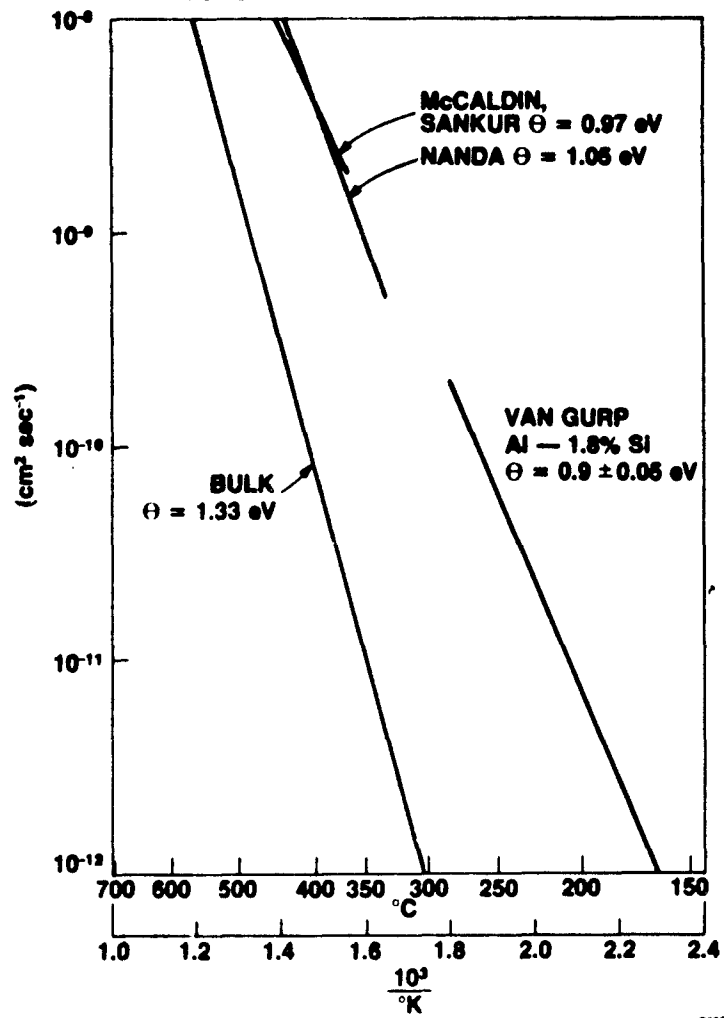
When an aluminum-silicon contact is annealed at elevated temperatures several interface reactions can occur. Because of the high solubility and diffusion of silicon in aluminum, silicon will move into and through the aluminum thin film during processing and sometimes at device operating temperatures. However, aluminum will not enter the silicon. Experimentally this solid state dissolution process is not uniform at the contact but occurs locally, creating pits^{1,2}. On single crystal silicon the dissolution pits are crystallographic in shape*. (Figure 3). On (100) silicon, the pits are rectangular with the side walls being (111) planes and the flat bottom being a (100) plane. On (111) silicon, the pits are triangular with the side walls and base being (111) planes. The above pit shapes are probably the minimum energy configurations since pits are normally not found with other crystallographic planes. Experimentally it is also found that pits in (100) silicon are deeper than pits in a comparable contact area of (111) oriented silicon. Pits in (111) silicon generally have large lateral dimensions and are shallow. The dissolution process at an aluminum-polysilicon contact occurs uniformly over the interface and no isolated pits are formed. Aluminum fills these pits and if they grow large enough, the underlying or an adjacent semiconductor junction will be shorted.

The location of etch pits depends on many factors. The most important factor appears to be the general availability of aluminum, as pointed out by Black¹. Since the maximum size and not the total number of pits is important in considering shorted junctions in semiconductor devices, the pits closest to large regions of unalloyed aluminum are then the most critical. At very small Al-Si contacts one large etch pit may form which can extend under the oxide.

Away from the leading edge other factors may be important in determining pit location. Dislocations are not the determining factor for etch pit location; however, at each dislocation there probably is an etch pit. Scratches in the silicon have been observed to act as nucleation sites and when the dissolution rate is low (temperature low) these type of surface imperfections will play a role of increasing importance. The location of the aluminum grain boundaries also influences the location of etch pits. This grain boundary effect is most important when the aluminum thin film has a large grain size (>5 μ). Figure 4 shows an SEM picture of the silicon substrate after the aluminum has been removed. The etch pits are fairly shallow and have flat

* Dissolution pits in highly doped silicon are not crystallographic in shape.

FIGURE 2. THE DIFFUSIVITY OF SILICON IN SOLID ALUMINUM



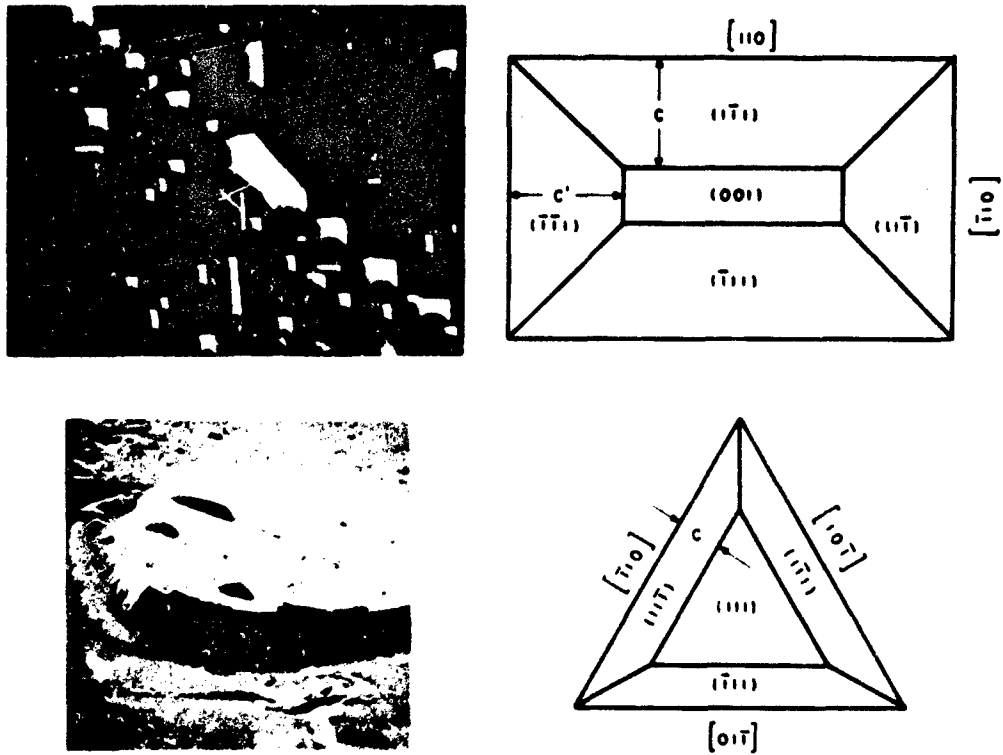
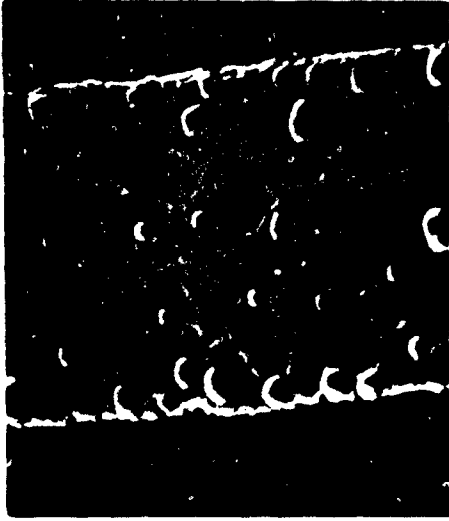


FIGURE 3. THE MORPHOLOGY OF SILICON DISSOLUTION PITS. THE SEM PHOTOGRAPHS ON THE LEFT ARE REPLICAS OF Al-Si CONTACTS AFTER REMOVAL OF THE Al. THE DRAWING INDICATES THE CRYSTALLOGRAPHIC SHAPE OF THESE PITS IN (100) AND (111) ORIENTED SILICON.



1 MIL



FIGURE 4. SEM PICTURE OF THE SILICON SUBSTRATE AFTER Al (LARGE GRAINED) HAS BEEN REMOVED ILLUSTRATING THAT THE PITTS IN THIS CASE ARE PRIMARILY FORMED NEAR GRAIN BOUNDARIES AND TRIPLE POINTS.

bottoms. The Al grain boundaries have been delineated by the precipitated silicon and most pits are near the grain boundaries and triple points. Also, some pits seem to straddle a grain boundary. The location of etch pits may be influenced by several other factors. Stresses between SiO_2 and Si at the edge of an ohmic contact cut may increase the rate of dissolution in this area. Also any oxide left at the Al-Si interface will greatly influence the rate of reaction.

The overall dissolution process can be separated into three stages: 1) an incubation period to penetrate any native SiO_2 present, 2) the time required to satisfy solubility of silicon in the aluminum, and 3) a coarsening process whereby the overall silicon solubility remains constant but a few pits grow at the expense of others. The driving force for this third state of dissolution is a reduction of surface free energy per unit volume.

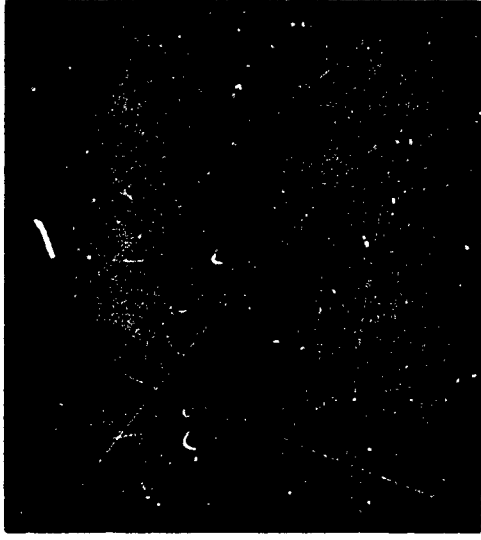
Figure 5 shows dark field photographs of etch pit formation on silicon which has been stored at 405°C for increasing times. It can be seen that the number of pits drastically decreases between 12900 minutes and 22800 minutes, but the size of the pits and hence their depth increases. This coarsening reaction may create long term reliability problems depending on the device operating temperature.

In order to minimize this Al-Si reaction, device manufacturers intentionally alloy the aluminum film with greater than 1% silicon during deposition to internally satisfy solubility requirements during subsequent elevated temperature treatments. This greatly reduces the number and size of etch pits but does not totally eliminate the problem as shown in Figure 6. These small etch pits form because non-uniform distribution of the silicon in aluminum creates small regions which can most easily satisfy solubility requirements from the substrate.

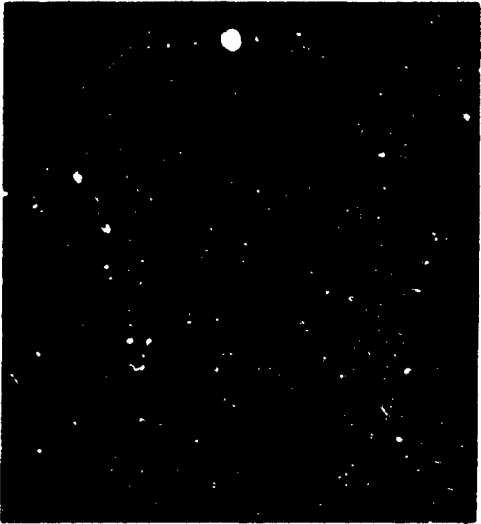
Although the maximum amount of silicon that can dissolve into aluminum below the eutectic temperature is only 1.59 atomic percent, in practice it has been determined that for very shallow junction devices, the yield improves if a 2 atomic percent alloy is used. The lower yield at 1.6% Si is believed due to the coarsening of the etch pits where the larger ones continue to grow at the expense of the smaller ones. Even though the aluminum alloy is saturated with silicon the etch pits can continue to grow by this process and may electrically short junctions. The addition of extra silicon to the alloy is believed to result in further epitaxial growth from the saturated solid solution at the silicon substrate contact reducing the effects of etch pit coarsening.

The distribution of silicon in aluminum depends both on the annealing temperature and the rate of cool. Fast cooling results in a dispersion of fine silicon precipitates located at aluminum grain boundaries. If the Al-Si contact is slow cooled, silicon will grow epitaxially on the substrate, creating mesas, and will precipitate at the top surface of the aluminum metallization. The epitaxially regrowth regions are p-doped since Al has an acceptor level of 0.057 eV above the valence band. These regrowth regions can influence the electrical characteristics of the contact. The barrier height of Al-nSi Schottky barrier diodes is particularly sensitive to the amount of this regrowth region^{7,8}. Fast cooled diodes produce a barrier height of 0.68 eV.

1 μM



t = 12900 MIN.



t = 1210 MIN.



t = 22800 MIN.

FIGURE 5. DARK FIELD OPTICAL MICROGRAPHS SHOWING THE NUMBER AND SIZE OF DISSOLUTION PITS IN (III) SILICON AFTER THREE AGING TIMES (405°C). THE ALUMINUM HAS BEEN REMOVED.

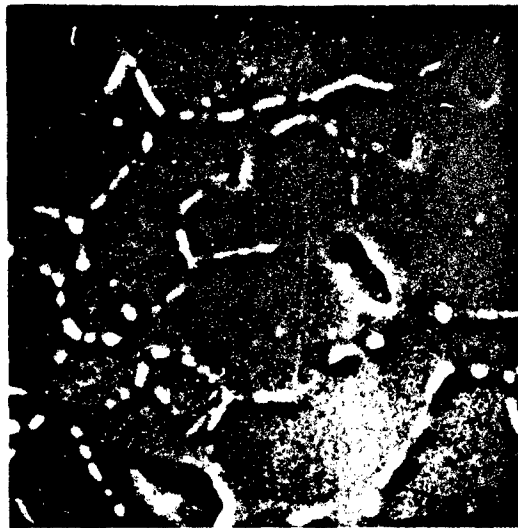


**FIGURE 6. SEM MICROGRAPH OF
DISSOLUTION PITS
WHICH OCCURRED
USING Al-1% Si
METALLIZATION.**

E3807

However, slow cooling or annealing at low temperatures causes the barrier height to slowly increase to values up to 0.74 eV. Even at low temperatures, this process should occur, only at a slower rate.

2.2 Al-Si Alloy Film Deposition and Structure

The structure and properties of aluminum-silicon alloy films are strongly dependent on the techniques used to deposit the films and on subsequent heat treatments and cooling rates. Because of the disparity in vapor pressure between aluminum and silicon (10:1) it is difficult to deposit the alloy in a reproducible manner from a single source by evaporation and condensation processes. Generally two separate electron beam sources with separate evaporation rate meters are used to deposit the alloy. Flash evaporation techniques may also be employed where small bits of the alloy are sequentially evaporated to completion or an alloy wire is fed into a crucible at a rate where complete evaporation takes place.

Motorola utilizes two different techniques to deposit the alloy. Both employ dual sources and rate meters. The first system deposits the film on substrates heated to about 450°C to obtain films with aluminum crystals having a lateral dimension of 4-5 microns. The second deposits the alloy film on substrates held at near 420°C resulting in aluminum grains with lateral dimensions of about 1.4 microns. It was this latter production line process which was utilized to deposit the films employed in this present study. The small grained films were chosen because it was believed that these were more representative of films in general use and probably are the worst case situation as far as electromigration resistance is concerned because of the high density of grain boundaries.

When Al/Si alloy films are heated during device processing silicon rapidly diffuses from the silicon particles (and crystalline substrate at ohmic contacts) by a solid state process and substitutionally enters the aluminum crystalline lattice to satisfy solid solubility limits at the elevated temperature. While held at the elevated temperature residual silicon in the form of particulates can coarsen by these solid state dissolution and diffusion processes. Certain large silicon crystals can grow at the sacrifice of small particulates where the driving force is the reduction of interfacial energy between the aluminum and silicon. By this process the net silicon surface to volume ratio decreases. Silicon can also be transported from the particulates to the single crystal silicon substrate of a device and build up silicon at ohmic contacts. This process is favorable since it greatly reduces the net aluminum-silicon interfacial energy.

Upon cooling the aluminum becomes super-saturated and the excess silicon is expected to participate out of solution preferentially on existing particulates of silicon or on the single crystal silicon substrate at ohmic contacts. If all of the silicon is in solution rapid cooling from elevated temperatures would expect to form a large number of small crystallites while slow cooling would tend to grow fewer but larger crystals.

An extensive study of the precipitation behavior of evaporated Al/Si films with up to 1.8% Si was published by G. J. van Gurp⁵. Since our observations

on the film structure was essentially in agreement with his conclusions they are given below in a somewhat condensed form:

After deposition of an Al/Si film alloy by flash evaporation onto a 200°C substrate, the Si, which is mainly present as a finely divided precipitate is not distributed homogeneously in the film, but is predominantly present in a Si-rich layer at the substrate-film interface. Subsequent aging at temperatures above about 200°C makes these precipitates grow to bigger shapes so that the number decreases. Above 300°C, Si is dissolved and the resistance of the Al/Si film increases. After annealing at a temperature where Si is in solid solution and subsequent quenching in ice water, all of the Si is retained in solution. Upon cooling at a moderate rate some Si is precipitated, partly as a thin layer on the substrate. During very slow cooling, usually all of the Si is precipitated and the thin layer on the substrate is not formed. The precipitation causes a resistance decrease.

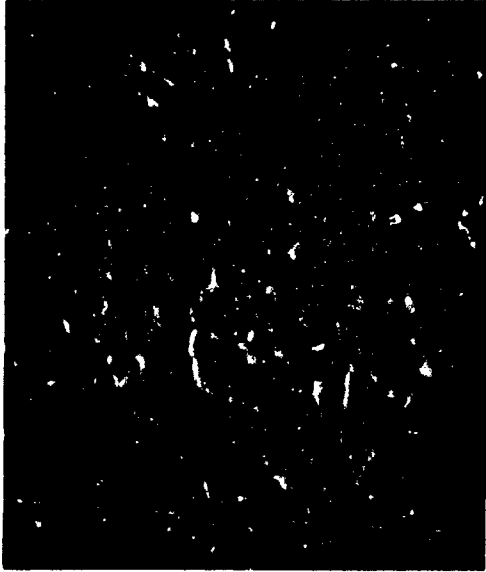
Aging of a supersaturated solution of Si in Al leads to precipitation of Si on Al grain boundaries. Microscopy shows that the shape of the precipitates is cylindrical with height equal to the film thickness. The cross section is almost circular for very small Si contents or very small aging time. Thereafter the precipitates become elongated along Al grain boundaries. At high Si content, however, more or less circular cross sections are found after very slow cooling from 550°C.

The kinetics of the precipitation is described as a two dimensional diffusion-limited process with diffusion coefficient much greater than in bulk Al-Si. This enhancement is mainly caused by diffusion along dislocation lines, the density of which is found to be of the order of 10^{10} cm⁻². The activation energy for this diffusion is 0.85 - 0.9 eV.

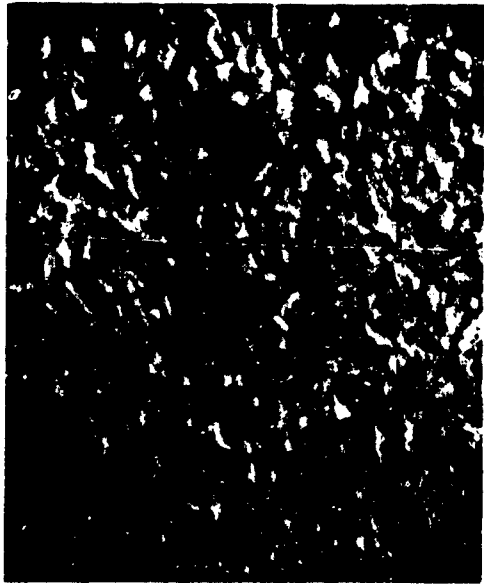
2.2.1 Film Structure - Experimental

Three alloys of silicon were deposited on oxidized silicon wafers by our small grained Al/Si alloy production line using separate sources as previously discussed. The substrate temperature during deposition was maintained at 420°C. The substrates were oxidized silicon wafers with an oxide thickness of about 900 Å units thick. The thin thermal oxide was used to permit better heat sinking of the films and to reduce unwanted thermal gradient effects. During each alloy metallization run a substrate for EBIC studies was also metallized. In addition a sapphire substrate was included from which the composition of the alloy was determined by dissolution of the film and atomic absorption spectrometry. The silicon composition of the three alloys was 0.79%, 1.9% and 3%. The thickness of the films were determined by means of a Dektak profilometer to be near 7000 Å.

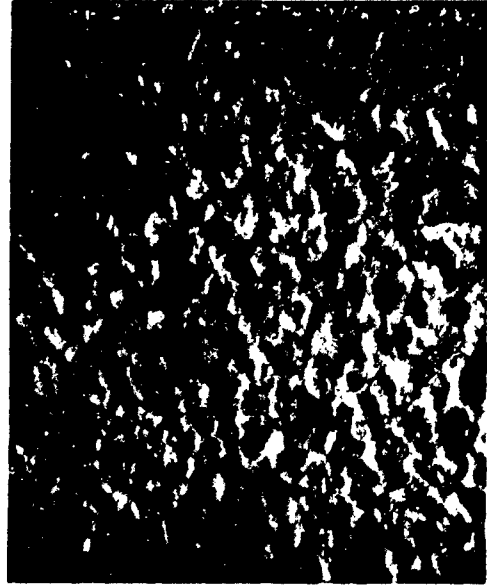
Figure 7 presents scanning electron microscope views at a magnification of 5000 X of the topography of these alloy films as deposited. Although the



0.79% Si



1.9% Si



3% Si

FIGURE 7. As DEPOSITED Al/Si ALLOY FILMS. 5000X $\angle = 25^\circ$.

films are quite flat the individual grains of the alloys are observable. These grains are individual single crystals of the metal and differ from their near neighbors in that their crystal lattices are oriented in different directions. Their average grain sizes are given in Table I along with grain sizes of the alloys after receiving various heat treatments as discussed below. It should be noted that the grain size of the alloy deposited on a 420°C substrate is 1.2 - 1.4 μm in lateral dimension while films of pure Al deposited in the same manner yield films with crystal sizes in the order of 4-5 μm in dimension. It is apparent that the silicon inhibits grain growth during film deposition.

When the films are subjected to a 500°C ambient for 15 minutes--a possible device manufacturing step after metallization--the grains grow to 5 μm for the 0.79% Si alloy, 4.1 μm for the 1.9% Si alloy and 3.6 μm for the 3% Si alloy as shown in the SEM views of Figure 8. Note that these large grains are somewhat difficult to discern mainly because the aluminum oxide which formed on the surface of the as deposited small grain film remains intact. Note, also, that the surface roughens and hillocks appear on the surface. This surface reconstruction is discussed in more detail in Section 2.5 of this report. Grain coarsening proceeds by the gradual elimination of small grains with energetically unfavorable shapes or orientations relative to their immediate neighbors.

If a deposited alloy film is heat treated at 500°C for 15 minutes, brought to room temperature and then annealed for 161 hours at 300°C further grain growth occurs depending upon the amount of silicon content of the alloy. Al 0.79% Si alloy produced average grains of 5.3 μm , Al 1.9% Si alloy produced an average grain size of 4.9 μm while Al 3.0% Si alloy produced grains of 3.7 μm . The silicon in the grain boundaries tends to pin down the grain boundaries reducing the grain growth with increasing Si content.

When the deposited alloys are temperature cycled by fast heating and cooling from room temperature (25°C) to 450°C for ten cycles being held 10 minutes at each temperature enhanced grain growth occurs as shown in Table I. See Figure 51 in Section 2.5 of this report for SEM micrographs of these films. Again there is less growth with increasing silicon content. It is believed that the enhanced grain coarsening obtained by temperature cycling is brought about by stress introduced into the film by thermal cycling. It is known that one of the most important variables controlling grain size in an aluminum alloy is the amount of cold work. With small amounts of cold work the grain size obtained is relatively large. As the cold work increases the grain size obtained decreases asymptotically.

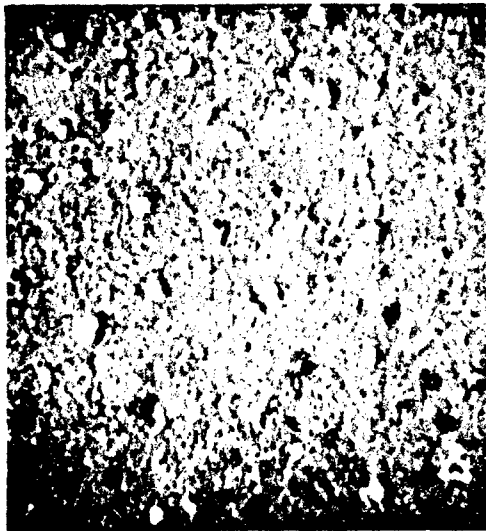
The size and distribution of the silicon in the three Al/Si alloys after various heat treatments and cooling schedules was determined by selectively etching away the aluminum to expose the silicon and inspecting the samples with an SEM. The formula of the aluminum etch used is:

water	-	2 parts by volume
nitric acid	-	1 part
acetic acid	-	1 part
phosphoric acid	-	16 parts

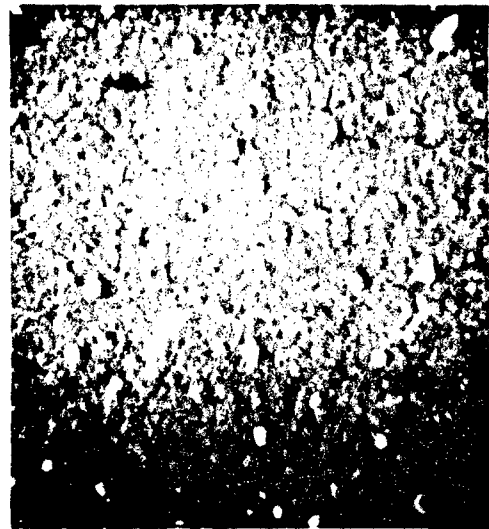
The as deposited Al/Si alloy films after aluminum removal are shown in

TABLE I
Grain Size of Alloy Films After Various Thermal Treatments

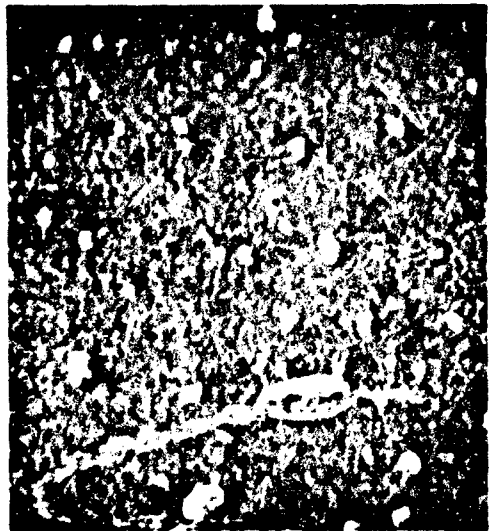
Thermal Treatment	% Si		
	.79	1.9	3.0
As Deposited	1.2 μm	1.4 μm	1.4 μm
After 15 min. at 500°C	5 μm	4.1 μm	3.6 μm
After 15 min at 500°C Plus 161 hours at 300°C	5.3 μm	4.9 μm	3.7 μm
After 10 cycles 25°C to 450°C with 10 min at each Temperature per cycle	7.2 μm	6.0 μm	5.8 μm



0.79% Si



1.9% Si



3% Si

FIGURE 8. Al/Si ALLOY FILMS AFTER 15 MINUTES AT 500°C. 2000X

E3609

the SEM micrographs of Figure 9 which were taken at a magnification of 5000 X and an angle of 25° . The 0.79% Si alloy showed a particle density of about 3.75×10^6 per cm^2 and particles up to $0.39 \mu\text{m}$ in lateral dimension. The 1.9% Si alloy has a Si particle density of 5.7×10^6 and a maximum particle size of $0.39 \mu\text{m}$ (similar to the 0.79% Si alloy). The 3.0% Si alloy exhibited a particle density similar to that of the 1.9% alloy, however the size of the particles were in general greater with the maximum being $0.56 \mu\text{m}$.

When the films were heated to 500°C for a period of 15 minutes and subjected to a fast cool by quickly removing them from the furnace into air coarsening of the silicon was observed as shown in Figure 10 which are SEM micrographs taken at a magnification of 5000 X. The 0.79% Si alloy had elongated particles ($2.8 \mu\text{m}$ long) growing along grain boundaries and at tripple points with a particle density of 1.2×10^6 per cm^2 . The 1.9% Si alloy formed more spherical particles with a density of 8.4×10^6 per cm^2 and a maximum size of $2 \mu\text{m}$. The 3.0% Si alloy grew similar shaped and sized particles as did the 1.9% Si alloy however the particle density increased to 1.9×10^7 per cm^2 .

Further coarsening of the Si particles occurred when the films were heated for 15 minutes at 500°C and then cooled slowly by turning off the furnace and allowing it to cool at an initial rate of about 2°C per minute. (See Figure 11). The Si particles for the alloys grew to a maximum size of about $3 \mu\text{m}$ with the particle density being 2.3×10^5 per cm^2 for the 0.79% Si alloy, 3×10^6 per cm^2 for the 1.9% Si alloy and 5×10^6 per cm^2 for the 3% Si alloy.

When these alloy films were heated to 500°C for 15 minutes, cooled at a fast rate by quickly pulling them out of the furnace into room temperature air, and then heated at 300°C for 161 hours and cooled quickly it was found that the extended anneal at 300°C caused very little change in the Si distribution and structure. Figure 12 shows the Si formed in the quenched and annealed films. These appear similar to Figure 10 which shows the silicon structure of the quenched, but unannealed films.

The data on the maximum silicon particle size and particle density for the various heat treatments as described above are summarized in Tables II and III.

2.3 Electromigration

Electromigration is the transport of ions through a conductor resulting from the passage of direct current. It is caused by a modification of the self diffusion of the metal from a random process to a directional one by the presence of charge carrier flow. Electrons or holes flowing in a material will exert a force on the stationary atoms of the conductor by momentum exchange. If this force is large enough and if the atom is in a suitable position, the atom will move. For aluminum, a suitable site is one with a vacant lattice positioned "downstream" from the electron flow, since such a site can be found in the lattice (vacancy), or on the surface of a grain (grain boundary or grain surface) there are three modes of electromigration. (Figure 13). Normally the large current densities (greater than 10^4 amps/ cm^2) needed to cause electromigration will melt the conductor. However thin film metallization on semiconductor devices are extremely well heat sunk. Thus very high

Table II

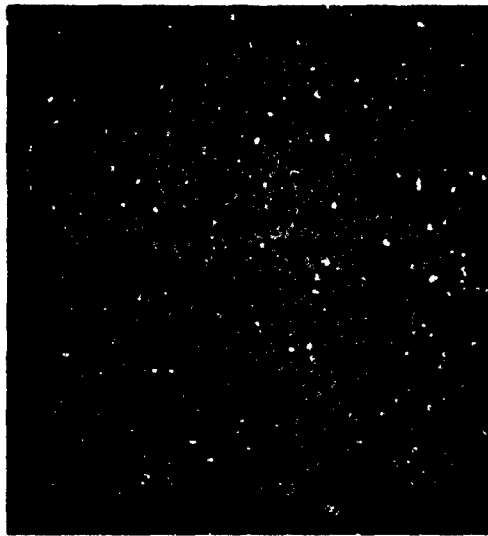
Maximum Si Particle Size

Heat Treatment	0.79% Si	1.9% Si	3.0% Si
As Deposited	0.39 μm	0.39 μm	0.56 μm
500°C for 15 minutes and fast cooled	2.8 μm (long)	2.0 μm	2.0 μm
500°C for 15 minutes and cooled slowly	3 μm	3 μm	3 μm
500°C for 15 minutes, fast cooled, plus 161 hours at 300°C.	2.8 μm	2 μm	2 μm

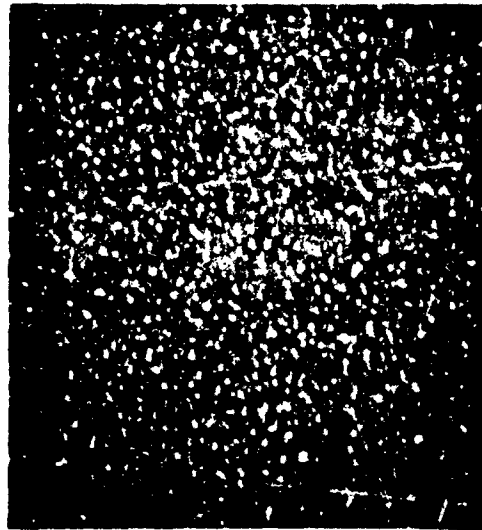
Table III

Si Particle Density
(Particles per cm^2)

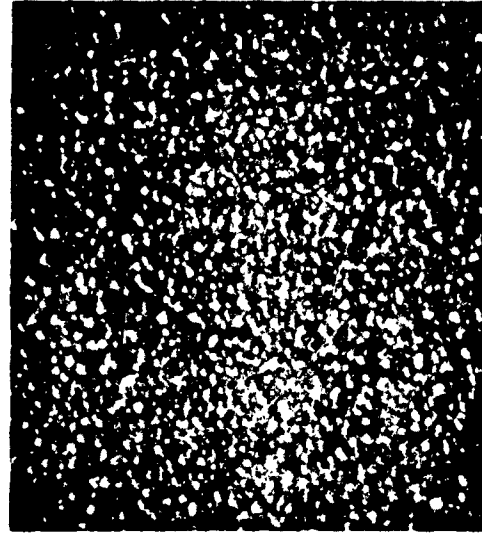
Heat Treatment	0.79% Si	1.9% Si	3.0% Si
As deposited	3.7×10^8	5.7×10^8	5.7×10^8
500°C for 15 minutes and fast cooled.	1.2×10^6	8.4×10^6	1.9×10^7
500°C for 15 minutes and cooled slowly	2.3×10^5	3.0×10^6	5.0×10^6
500°C for 15 minutes, fast cooled plus 161 hours at 300°C	1.2×10^6	8.4×10^6	1.9×10^7



0.79% Si



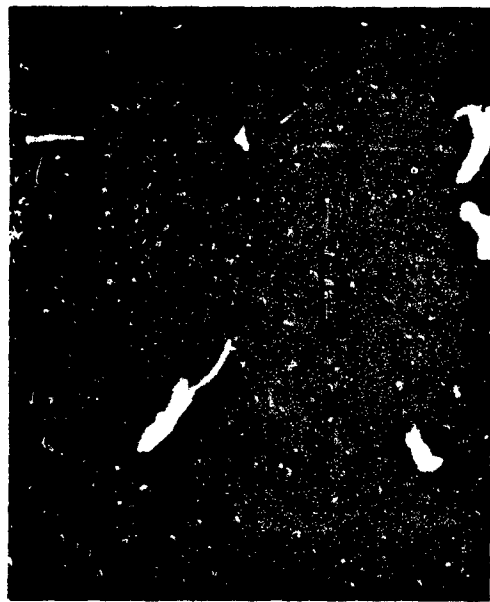
1.9% Si



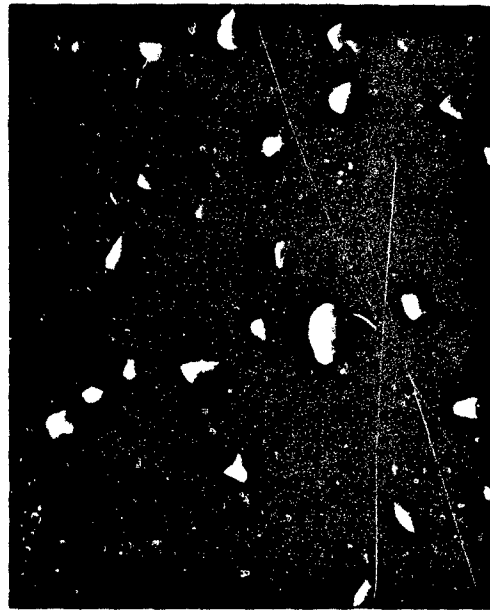
3% Si

FIGURE 9. SI PARTICLES IN AS DEPOSITED Al/Si ALLOY FILMS.
5000X, $\angle = 25^\circ$

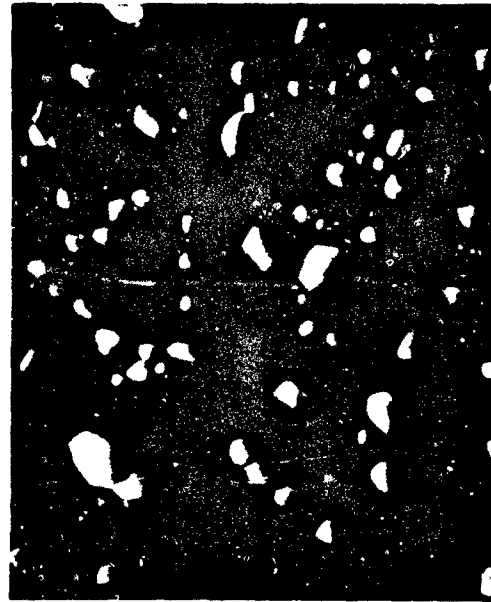
ESR10



0.79% Si



1.9% Si



3% Si

FIGURE 10. Al/Si ALLOY FILMS AFTER 15 MIN. AT 500°C FOLLOWED BY A FAST COOL AND Al ETCH. 5000X



0.79% Si



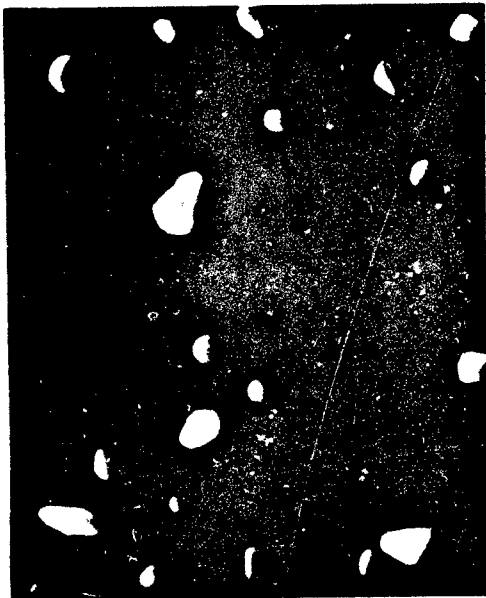
1.9% Si



3% Si

FIGURE 11. Al/Si ALLOY FILMS AFTER 15 MIN. AT 500°C FOLLOWED BY SLOW COOLING AND Al ETCH. 5000X

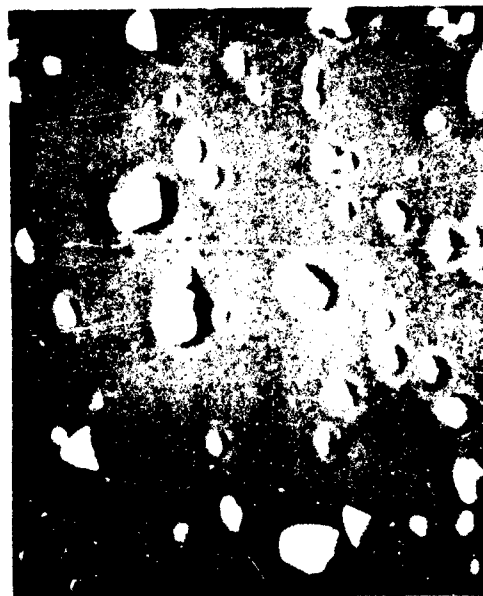
ES12



1.9% Si



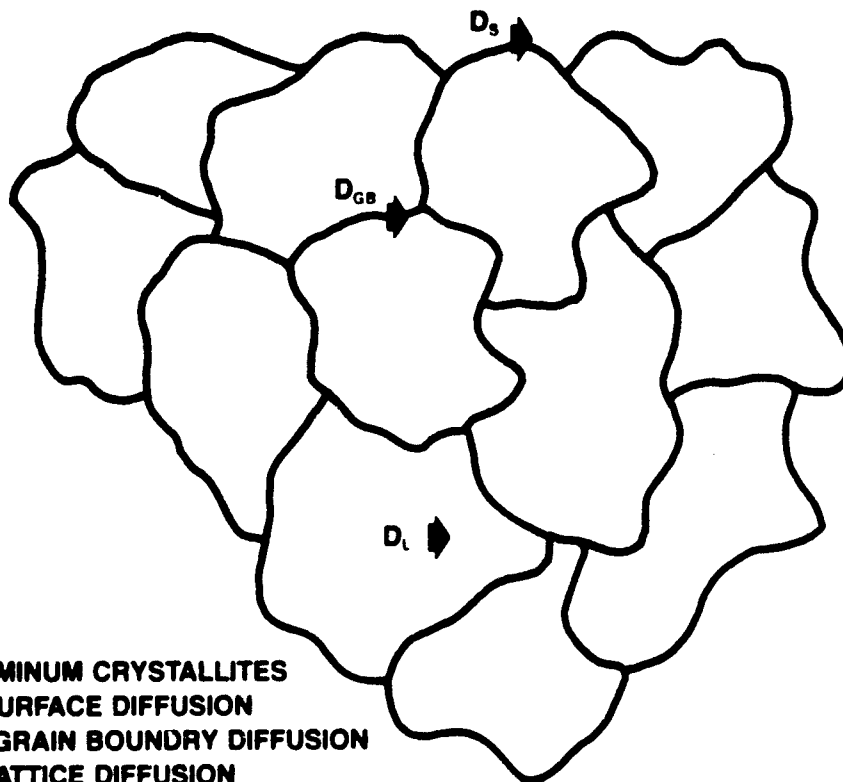
0.79% Si



3% Si

FIGURE 12. Al/Si ALLOY FILMS AFTER 15 MIN. AT 500°C, FAST COOL, 161 HOURS AT 300°C FOLLOWED BY FAST COOLING AND Al ETCH. 5000X

ESM13



ALUMINUM CRYSTALLITES
 D_s SURFACE DIFFUSION
 D_{GB} GRAIN BOUNDARY DIFFUSION
 D_l LATTICE DIFFUSION

FIGURE 13. THREE POSSIBLE LOCATIONS WHERE ELECTROMIGRATION CAN OCCUR IN POLYCRYSTALLINE ALUMINUM.

E3814

current densities can be applied and the Joule heating kept to a minimum. The electromigration force in this case is enough to cause an appreciable flow of atoms at normal operating conditions over the lifetime of the device. With the flow of atoms will be a simultaneous flow of vacancies in the opposite direction. These vacancies will coalesce at some flux divergences forming a void or causing thinning in the metallization. Typical divergences result from a temperature gradient, a change in grain size, or a current density gradient. Another common gradient found in integrated circuits creating divergences is due to a change in conductor self diffusion coefficient as the conductor changes from silicon to aluminum or from aluminum to silicon. Locally the resistance and thus the temperature of the metallization will increase, accelerating the rate of electromigration. The metallization fails when the conductor finally opens at one of the these sites.

A recent review of electromigration in thin films has been written by F. d'Heurle and R. Rosenberg⁹. It contains a fairly complete set of references of both experimental and theoretical work aimed at understanding this phenomena.

2.3.1 Theory

The theory of electromigration in an ideal material has been developed¹⁰ and predicts a flux of ions (atoms) J_a in a metallic film with a current density j of

$$J_a = \frac{ND}{kT} z^* q j \rho \quad (1)$$

where N is the atom density, D the diffusion coefficient, $D = D_0 e^{-Q/kT}$, D_0 the diffusion constant, k Boltzmann's constant, T the absolute temperature, z^* the effective charge of an ion, q , the electronic charge, ρ the electrical resistivity and Q the activation energy. This equation indicates that the flux is proportional to the current density and is strongly dependent of the diffusion mechanism (surface, grain boundary, lattice or a combination) of the atoms of the conductor. Failure of a thin metallization occurs when a flux divergence exists locally in the conductor. A first approximation of lifetime of a metallization, t_f is

$$t_f \sim 1/C \operatorname{div} J_a \quad (2)$$

where C is a constant. A major problem in this equation is how to handle the flux divergence $\operatorname{div} J_a$. It is impossible to predict $\operatorname{div} J_a$ a priori, nor is it constant in the local region during the film lifetime. Because of these difficulties, theoretical predictions are difficult and experimental results are presently the best method for studying the potential wearout of a metallization due to electromigration. The general approach is to use an equation of the form

$$t_f \propto MTF = A_n j^{-n} \exp(Q/kT) \quad (3)$$

where A_n is a constant related to the failure mechanism, geometry and material, and n is a constant related only to the mechanism. Chhabra¹¹ has shown that when the failure occurs from structural gradients $n = 1$ and when failure is controlled by temperature gradients $n = 3$.

2.3.2 Previous Experimental Work - General

Figure 14 is a plot of the experimental results obtained by J. Black¹² for pure aluminum. He showed the MTF of a set of conductors depends on the grain size and whether the metallization surface was coated. These observations illustrated that the diffusion coefficient found in equation 1 is a composite made up of surface, grain boundary, and lattice diffusion effects. The slope of his MTF vs. $1/T$ curves gave activation energies near those from grain boundary or lattice diffusion for the respective tests. Black also obtained a value of $n = 2.2$ for the exponent of current density. Several others have also obtained $n \sim 2$ instead of $n = 1$ as predicted by theory and some now believe that this fact is a result of the accelerated testing (see for example Figure 3 of reference 9). Although there has been much controversy over the j^2 term, Black's experimental curves are still the most complete for comparing the behavior of aluminum to other metallization schemes. The experiments performed by Black also indicated that the material lifetimes for similar grain size material depended on the conductor cross sectional area. This area dependence is included in the plots of Figure 14.

A time sequence of the effects of electromigration on a pure Al thin film is presented in the scanning electron microscope micrographs of Figure 15. In large grained samples voids nucleate at tripple points between the grains. For the small grained sample shown in the figure, it is not clear what flux divergence caused the nucleation of voids or the growth of hillocks. Void and hillock growth are shown in this sequence and show that the hillocks grow from the root. Normally hillocks of metal are seen interdispersed with the voids in a metal stripe which has been stressed for a long period of time. If test conditions are accelerated, failure usually occurs at the negative end of an aluminum sample where temperature gradients, current density gradients and other divergences are important.

The addition of certain alloying elements (e.g., Cu, Cr, Ni, Mg) to aluminum has been shown⁹ to greatly increase the lifetime of the thin film metallization. Since most of these alloy elements form precipitates which are located at grain boundaries, it is believed that the rate of aluminum grain boundary diffusion due to electromigration is reduced. For copper additions, lifetimes increase monotonically to 3-4% additions¹³ and local copper depletion is required before failure will occur¹⁴. (Figure 16). The MTF vs. $1/T$ for an Al-2% Cu metallization is given in Figure 14. The activation energy for the process is approximately equal to that of small grained aluminum but the curve is shifted downward. Thus at 200°C the alloy film lifetime is about 10 times better than large grained aluminum and 35 times better than small grained aluminum. However, at lower temperatures, the amount of improvement decreases and if the device operates below approximately 70°C, large grained aluminum metallization is more reliable.

Little work has been published on studies on sputtered materials. Sputtering normally produces very small grained films. Thus the atom flux in these films should be greater since there would be larger grain boundary contribution and a small bulk diffusion contribution. However, in fine grained materials the number of critical flux divergences may be greatly reduced and the lifetimes may be longer. In fact, in evaporated films it has recently been shown that the ratio of grain size to stripe width is important¹⁵.

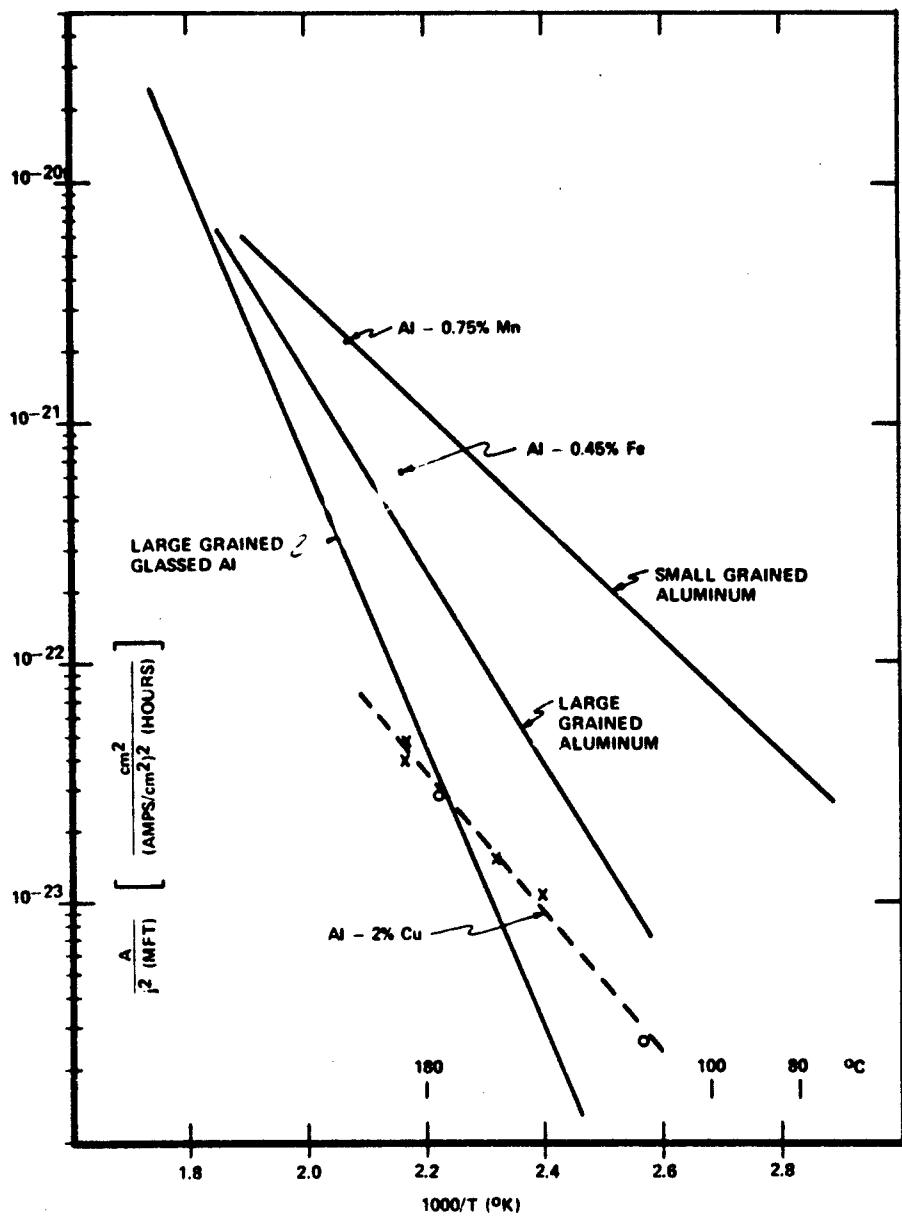


FIGURE 14. MEDIAN TIME TO FAILURE OF SOME ALUMINUM ALLOYS AS A FUNCTION OF CURRENT DENSITY j , TEMPERATURE T , AND CROSS-SECTION AREA A .

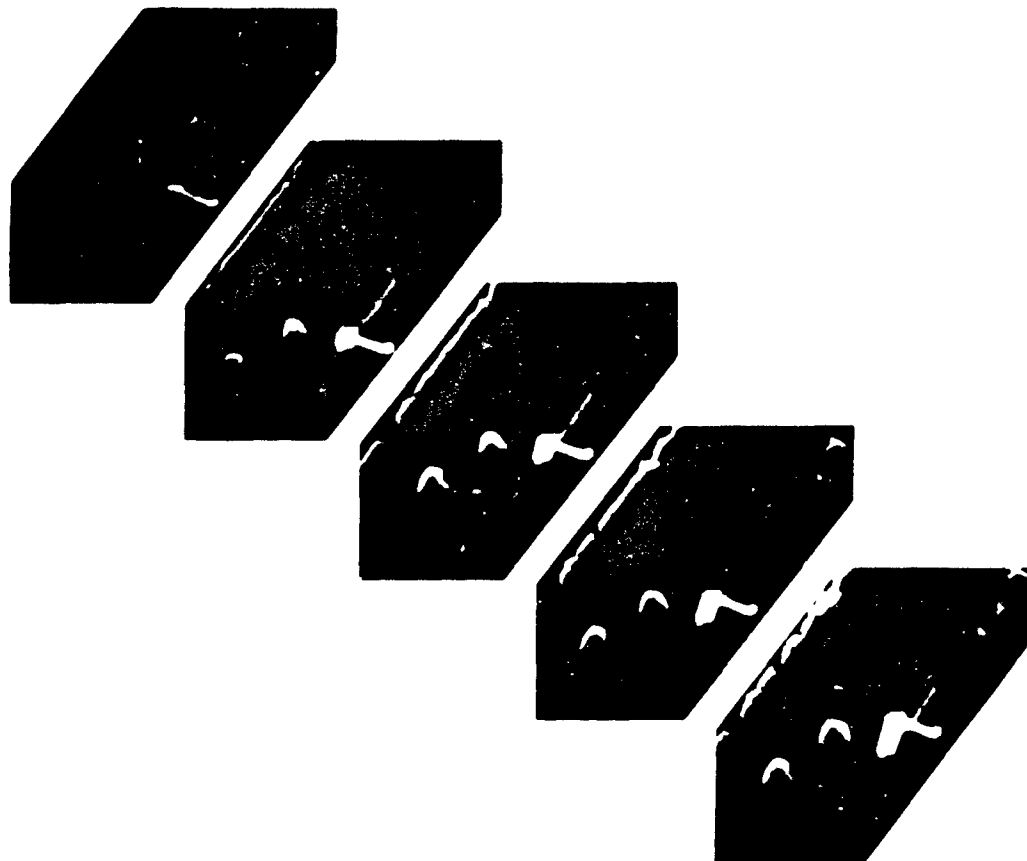


FIGURE 18. GROWTH OF VOIDS AND HILLOCKS IN SMALL GRAINED ALUMINUM.

12016

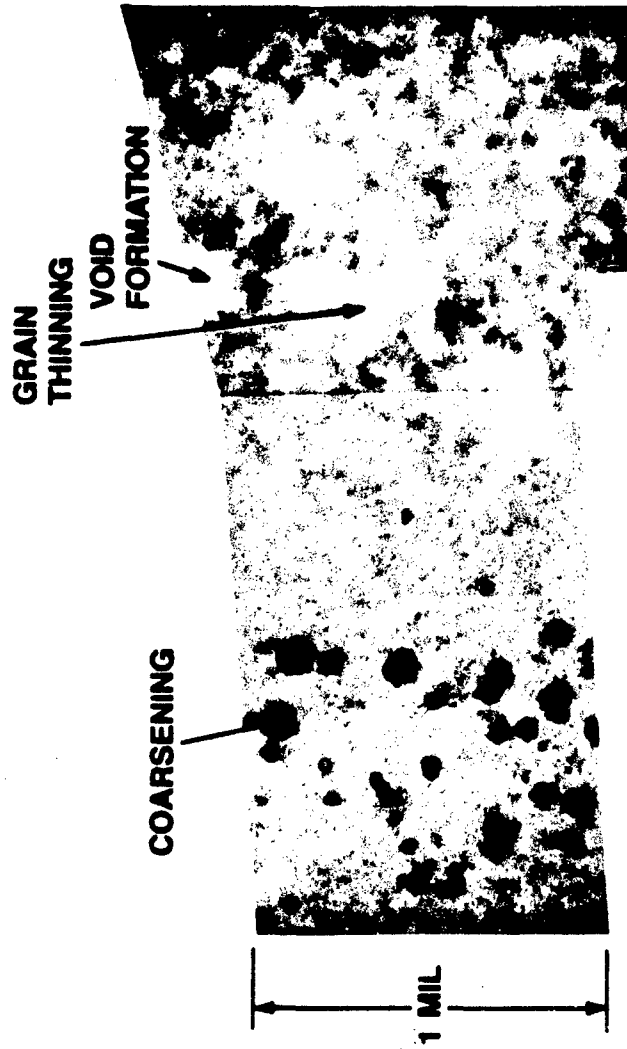


FIGURE 16. AN ELECTRON BEAM INCLUDED CURRENT (EBIC) MODE PHOTOGRAPH OF A ONE MIL WIDE Al-2% Cu STRIPE DURING AN ELECTROMIGRATION EXPERIMENT.

E3010

In the past it was believed that the dielectric layer over a thin film conductor increased lifetime under electromigration stress because it reduced surface diffusion or because it might eliminate the surface as a source of vacancies. It has been shown^{16,17,18} that a robust dielectric overcoat constrains the growth of hillocks and swelling of the stripe placing the metal under compression during electromigration. This compression of the metal then applies an opposing force on the metal ions than that due to the momentum exchange with electrons reducing electromigration and increasing lifetime.

The potential wearout of a thin film metallization on an actual device will depend on several factors besides those discussed above. The metallization cross section at a step is normally reduced from the nominal value thus increasing the local current density and lowering the lifetime. A metallization which goes from an oxide to a silicon contact area may experience a different amount of heat sinking thus creating a local temperature gradient and a slightly higher temperature in one region than another. Processing will affect the line width and the amount of undercutting if any. Lifetimes of metallization stripes on a given device will not scale as the current density to some power because of the relation between grain size and the line width. Finally, at ohmic contact regions and at bonding pads, current crowding exists which again alters the local current density.

2.3.3 Previous Experimental Work - Al/Si Alloys

In previous sections of this report electromigration and solid state dissolution of Si into Al have been discussed. In 1968 Black¹ described a then new wearout failure mode which resulted from a combination of these two effects. Silicon atoms can dissolve into the aluminum metal to satisfy solid solubility saturation conditions at the operating temperature and the dissolved silicon can electromigrate through the aluminum in the direction of electron flow.

Two distinct failure modes can result from these processes:

- (a) As the dissolved silicon near the contact to the substrate electromigrated away from that contact, the alloy is no longer saturated with silicon enabling additional silicon to dissolve from the substrate. The process is a continuous one allowing pits in the silicon contact to grow during device operation. These pits grow in those contacts where electrons leave the silicon and enter the aluminum. The ultimate failure is growth of a pit (filled with aluminum) until it shorts an adjacent or underlying junction.
- (b) Dissolved silicon in the conductor eventually electromigrates to a silicon contact where electrons are entering the silicon. Because of the continuous addition of silicon to the aluminum silicon alloy at this contact the alloy becomes supersaturated with silicon allowing the silicon to precipitate out of solution by epitaxially growing on the silicon crystal. The deposited silicon layer is resistive and failure is due to the increase in contact resistance.

Figure 17 is a SEM view of a ohmic contact to silicon after aluminum metal removal showing rectangular etch pits in the (100) oriented silicon. This contact had been stressed at 235°C for 250 hours at a current density in the metal greater than 10^5 A/cm². Electrons left the silicon at this contact and entered the aluminum. The largest pits occur at the edges of the contact where the conducting metal above the contact had the highest current density. The particulates of silicon near the center of this contact originated from the Al-3% Si alloy metallization.

Figure 18 is a view similar to that of Figure 17, except that this was the positive terminal contacting the aluminum where the electrons left the aluminum and entered the silicon. Silicon dissolved in the aluminum electromigrated to that contact where the solvent became supersaturated and then precipitated out on the silicon single crystal substrate.

Device failure caused by the electromigration of Si through Al to create etch pits at the (-) terminal or high resistive contacts at the (+) terminal were only observed at elevated temperatures. At lower temperatures (α230°C and below) failure of Al/Si alloy films was observed to be an open circuit caused by void formation. This lower temperature failure mode was predictable for glassed alloy films by considering them to be pure aluminum films and the failure was due to the electromigration of aluminum in aluminum.

van Gorp has reported on the electromigration of Si alloy films for Al-1.8 at.% Si for Al-0.3 at.% Si stressed at a current density of 2×10^6 amperes/cm²¹⁹. At 125°C the 1.8% Si alloy exhibited an order of magnitude longer lifetime than did a pure aluminum film even though the activation energy was 0.31 eV for the alloy while that of the pure aluminum was 0.55 eV. Since in the Al films voids and hillock growth was noted all along the conductor stripe and in the alloy a void formed only at the negative terminal and hillocks were formed at the positive terminal, van Gorp concluded that for the alloy grain boundary diffusion was suppressed by Si precipitated in the grain boundaries. The low activation energy of the alloy was attributed to the surface diffusion of aluminum ions. The transport of silicon by electromigration through the films was not observed. Learn²⁰ essentially repeated van Gorp's work and agreed with his results.

The study of the diffusion of Si in Al for wrought alloys has all been made above 450°C and the work was done about 30 years ago. The work of Buckle²¹ and Mehl et al²² on the diffusivity at elevated temperatures is presented in Figure 19. This indicates that D decreases somewhat as the percent silicon increases. Extrapolation to zero percent solute gives²³

$$D \sim 0.9e^{-1.33 \text{ eV}/kT} \quad (4)$$

This is the diffusion of silicon through the aluminum lattice with an activation energy of 1.33 eV.

Nanda observed the diffusion of silicon through aluminum films by heating (330-510°C) thin stripes of aluminum contacted by an evaporation deposited silicon spot and then observing the concentration profile down the stripe utilizing an electron microprobe. He observed an activation energy for the diffusion of Si through Al film to be 1.05 eV⁰. He concluded that grain



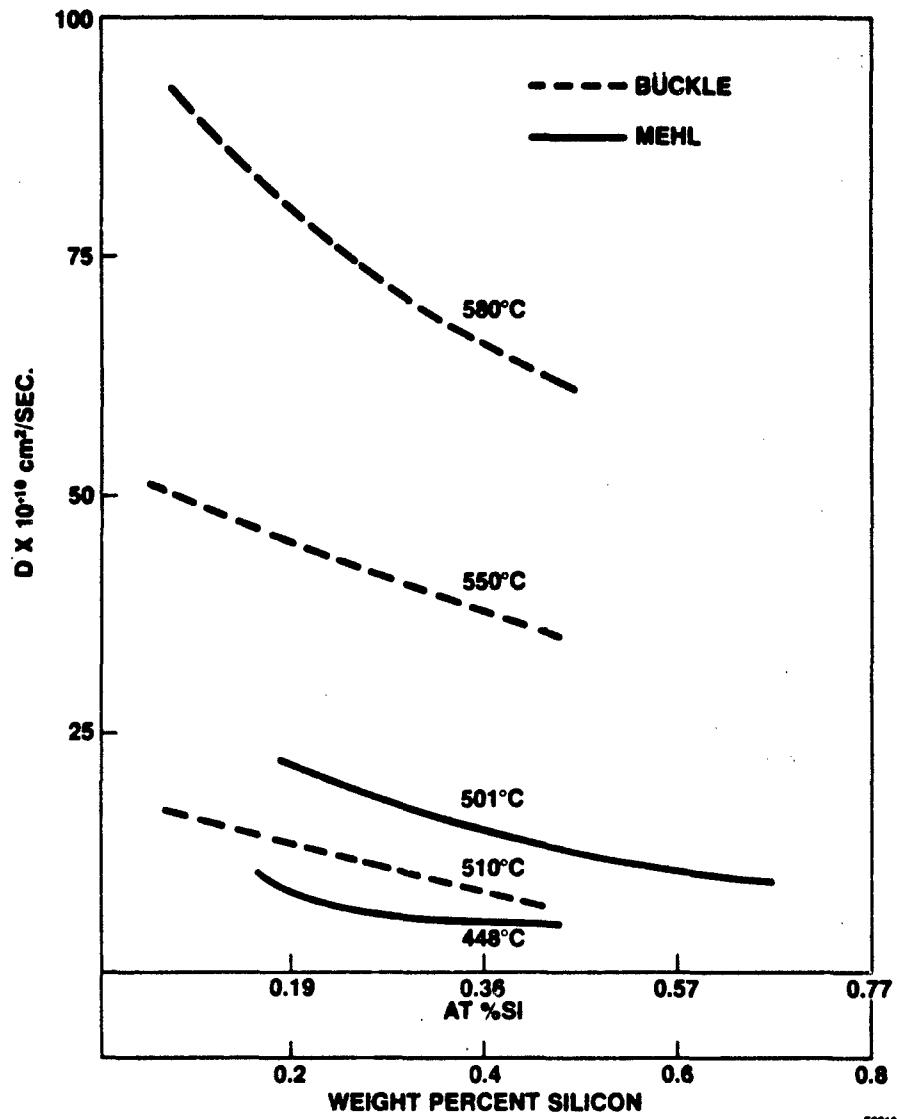
FIGURE 17. ETCH PITS FORMED BY ELECTROMIGRATION OF SI THROUGH AL (NEGATIVE TERMINAL).



FIGURE 18. SI BUILD-UP BY ELECTROMIGRATION OF SI THROUGH AL (POSITIVE TERMINAL).

63917

FIGURE 19. CHEMICAL DIFFUSION IN BULK Al-Si ALLOYS



boundary diffusion was the predominant mechanism for Si transport in the films.

McCaldin and Sankur⁴ also observed the diffusion of Si-Al film couples over the temperature range 360-560°C by measuring the resultant concentration gradient by an electron microprobe. The activation energy observed for the diffusion of Si in Al films was 0.79 eV. The low value compared to that for wrought alloys was attributed to diffusion down grain boundaries and dislocations.

In a more recent work van Gorp studied the precipitation of Si from a supersaturated Al-Si solid solution by resistance measurements and by microscopy⁵. He found that precipitation of silicon took place from the supersaturated solution at an appreciable rate only at temperatures above 150°C. The activation energy for the diffusion of Si in Al for Al-1.8 at.% Si was found to be 0.9 ± 0.05 eV. This low value compared to wrought alloy was attributed to diffusion down dislocations and grain boundaries.

It should be noted that in all of the above described experiments the films were not glassed and the grain size was relatively small enabling lattice, dislocation, grain boundary and surface diffusion paths. These data are plotted in Figure 2.

The Rome Air Development Center recently published a report on a reliability evaluation of emitter coupled logic microcircuits²⁴. When stressed at elevated temperatures ranging between 226°C and 292°C a major failure mode exhibited by one of the manufacturer's parts was due to the electromigration of silicon through the aluminum. Failure was due either to build up of silicon in the emitter contact region of the output transistor increasing the emitter resistance or by shunting the emitter base junction of the output transistor by the development of a pit in the silicon filled with aluminum. The shunt would occur at the point of maximum current density in the emitter metallization.

The following two sections of this report describe the results of experimental work on the electromigration properties of Al/Si alloys where the maximum Si content was 3.5% or less. The first section addresses the low temperature electromigration properties of these alloys ($T < 210^\circ\text{C}$) where failure is due to an open circuit resulting from the electromigration of the solvent. The second section addresses the high temperature failure mode resulting from the electromigration of the solute in the solvent.

2.3.4 Low Temperature Al/Si Alloy Electromigration

Because it was recognized that two basic processes could take place when Al/Si alloys are subjected to stress which results in electromigration, two experiments were designed to study these. One electromigration process is the electromigration of aluminum ions through the aluminum matrix which results in the growth of voids that eventually cause failure due to an open electrical circuit. The second electromigration process is the electromigration of silicon through the aluminum matrix which could cause device failure by the growth of pits in silicon at negative contacts to the aluminum or could cause

an increase in resistance at positive silicon contacts due to the build up of resistive silicon at those contacts. This section of this report describes experiments designed to study the electromigration of Al in Al while the following section addresses the electromigration of Si in Al.

At temperatures below about 230°C it had been observed that failure in Al/Si alloy films was due to the growth of voids which resulted from the electromigration of Al in Al. Failure occurs when a void grows across the conductor forming an open circuit. It was desirable to study this reaction to obtain data which would enable the prediction of the lifetime of these alloy film conductors and to specify maximum stress conditions for these films in order to obtain reliable long term operation. An experiment was designed to stress thin film alloy conductors at current densities ranging between about 8×10^5 amperes per square centimeter to about 2×10^6 A/cm². Three different alloys were selected with silicon contents being less than 1%, between 1 & 2% & greater than 2%. The grain size of the as deposited alloys was designed to be relatively small ($\approx 1.4 \mu\text{m}$) to represent worse case (high grain boundary density) films which probably would be typical in the semiconductor industry. These film conductors were to be tested over a temperature ranging from 110°C to 210°C.

The same films that were evaluated and whose deposition was described in Section 2.2 of this report were utilized to manufacture the devices to be placed on test. The silicon content of these alloys were 0.79%, 1.9% and 3% Si. The films deposited on 0.012 inch thick silicon substrates with a 900 Å thick thermal oxide layer were etched into narrow conductors utilizing a pattern which generated conductors 0.030 inches long and 0.0004 inches wide. One half of the films were then subjected to a silicon dissolving acid mixture to remove the residual silicon particles which remained on the thermal oxide substrate after the aluminum etch. This required a 3-5 second dip in a room temperature mixture of:

200 ml HNO₃
4 ml HF
20 ml Acetic acid

The thickness of the films were determined by means of a profilometer at two different sites per silicon wafer and the width of the stripe used was measured at five different positions on each wafer using a microscope and a filar eyepiece. Table IV presents the average widths, thicknesses and conductor cross sectional areas measured for the three alloys with and without residual silicon in the cleared areas. The thickness of the films with the silicon present was determined by the thickness measurements made on the same alloy where the residual silicon had been removed because the silicon particles did interfere with the profilometer measurement. Since the films of one alloy type were deposited at the same time the assumption that they are of the same thickness is reasonable.

After the films were measured they received a 8000 Å thick coat of passivation glass deposited by the chemical vapor deposition technique using silane and phosphene. The glass contained about 3% phosphorous. The glass

Table IV

Al/Si Alloy Conductor Dimensions

Conductor	Thickness (μm)	Width (μm)	Cross-sectional ($\text{cm}^2 \times 10^8$)
0.79% Si Si removed with Si	0.73 0.73	10.45 10.54	7.63 7.69
1.9% Si Si removed with Si	0.70 0.70	10.19 10.31	7.16 7.22
3% Si Si removed with Si	0.71 0.71	10.28 9.79	7.30 6.95

was removed at the bonding pads prior to lapping the back side of the wafers. The backs received a layer of titanium and then a layer of nickel for die bonding. The wafers were then scribed and broken into individual die and die bonded to TO-3 headers. Five mil diameter aluminum wires were used to connect the nominal 0.4 mil wide stripe to the electrical connections of the header. Finally caps were welded to the devices under a nitrogen ambient. A micrograph of a 80 x 80 mil square test die used for these experiments is presented in Figure 20. The nominally 0.4 mil wide test stripe is shown bonded and was used for all tests reported here.

Resistance measurements were then made of the devices and the very low and very high resistive devices were culled out of the sample. The parts were then put on test with each group consisting of between 15 and 20 devices. Generally the test continued until all or nearly all devices failed. An electronic recorder was utilized to record the time required for each device to fail. The data followed a log-normal distribution as shown in Figure 21 which shows the cumulative percent of the failed devices in one of the test runs plotted vs. time in hours on log-normal probability paper. The median time to failure and the standard deviation, σ , for each run was determined from such plots.

All film failures were due to voids growing in the film which eventually formed on electrically open circuits. The voids were randomly distributed along the stripes with many of them of sufficient size to nearly create an open circuit. Figure 22 presents SEM micrographs of voids which were typical of those distributed down the length of the stripes. Cracked passivation glass was also observed distributed along the length of the stripes which was caused by the accumulation of metal ions exerting sufficient pressure on the glass to cause it to fracture. One of these regions before and after the removal of the passivation glass is presented in Figure 23. No difference was observed in the electromigration behavior between those films which received an etch to remove the residual silicon in areas cleared of aluminum and those which contained the residual silicon.

The data obtained during this experiment are summarized in Table V. Here, the letter in the run number indicates the Al/Si alloy used where A = 0.79% Si, B = 1.9% Si and C = 3% Si. In these experiments the current density ranged from 7.6×10^5 to 2×10^6 A/cm² while the temperature varied from 110°C to 210°C. The film cross sectional areas and the metal grain sizes were relatively invariant. The median time to failure for these thirty experiments ranged from 68 hours to 630 hours and the standard deviations ranged from 0.23 to 0.65 with the majority grouped near the average of 0.40.

Figures 24, 25 and 26 present Arrhenius plots of the data for the three alloys. The unit plotted along the ordinate of those contains the product of the width and thickness of the films in centimeters in the numerator and the product of the current density squared and the median times to failure (MTF) in hours where the failure is due to an open conductor. The equations describing these plots drawn by the least squares method are:

$$\text{Al - 0.79 \% Si: } \frac{\text{wt}}{j^2 \text{ MTF}} = 5.723 \times 10^{-16} \exp - \frac{0.545}{kT}$$

Table V
Low Temperature Al/Si Alloy Test Conditions and Results

Run #	Current ma	Film Area cm ² x 10 ⁸	Temperature °C	10 ³ °K	Current Density A/cm ² x 10 ⁻⁶	MTF hours	Std. Dev. σ	wt JZ MTF x 10 ²²
1A	61.07	7.64	167	2.273	0.80	288	.34	4.14
1B	60.18	7.16	167	2.273	0.84	345	.44	2.94
1C	59.55	6.95	167	2.273	0.86	380	.43	2.44
2A	58.14	7.65	190	2.160	0.76	202	.44	6.51
2B	63.01	7.16	190	2.160	0.80	213	.65	5.36
2C	58.11	7.30	190	2.160	0.80	223	.37	5.17
3A	63.18	7.55	210	2.070	0.85	125	.54	8.90
3B	56.95	7.50	210	2.070	0.80	139	.63	8.14
3C	58.12	7.50	210	2.070	0.80	139	.40	8.28
4A	76.90	7.69	167	2.273	1.00	170	.48	4.52
4B	72.48	7.22	167	2.273	1.00	269	.35	2.68
4C	69.75	6.95	167	2.273	1.00	280	.35	2.46
5A	76.38	7.69	192	2.151	0.99	105	.23	7.42
5B	78.20	7.22	192	2.151	1.08	89	.49	6.93
5C	73.20	6.95	192	2.151	1.05	129	.45	4.85
6A	76.98	7.69	210	2.070	1.00	68	.52	11.3
6B	71.34	7.22	210	2.070	0.99	75	.45	9.86
6C	69.14	6.95	210	2.070	1.00	85	.41	8.26
7A	152.2	7.63	110	2.611	2.00	560	.46	0.342
7B	143.4	7.16	110	2.611	2.00	560	.36	0.321
7C	146.2	7.30	110	2.611	2.00	493	.38	0.369

Continued...

Table V (Continued)

Run #	Current ma	Film Area cm ² x 10 ⁸	Temperature °C	$\frac{10^3}{\mu K}$	Current Density A/cm ² x 10 ⁻⁶	MTF hours	Std. Dev. σ	$\frac{wt}{JZ MTF} \cdot 10^{22}$
8A	154.	7.69	137	2.44	2.00	178	0.23	1.07
8B	144.	7.22	137	2.44	1.98	245	0.31	0.75
8C	139.	6.95	137	2.44	1.98	292	0.47	0.61
9A	75.66	7.69	154	2.34	0.98	326	0.33	2.44
9B	72.38	7.22	154	2.34	1.00	346	0.46	2.01
9C	69.72	6.95	154	2.34	1.00	630	0.34	1.10
10A	154.	7.69	123	2.52	2.01	300	0.50	0.64
10E	144.	7.22	123	2.52	2.00	339	0.26	0.53
10C	139.	6.95	123	2.52	2.00	382	0.24	0.46

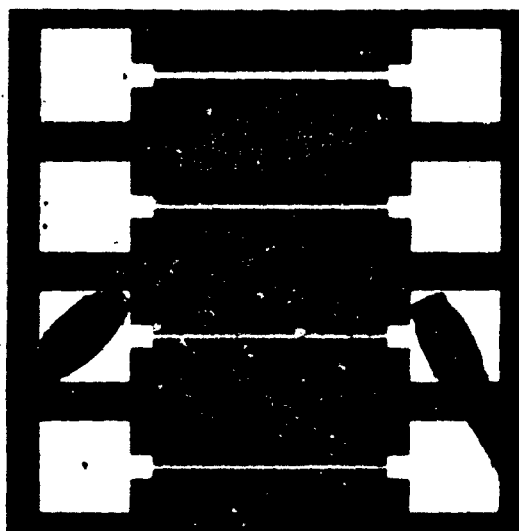


**FIGURE 20. LOW TEMPERATURE
ELECTROMIGRATION
TEST DIE.**

ES618

FIGURE 21. LOG NORMAL PLOT OF A 19 DEVICE CELL STRESSED AT 167°C AT $J = 8 \times 10^5$ A/cm²

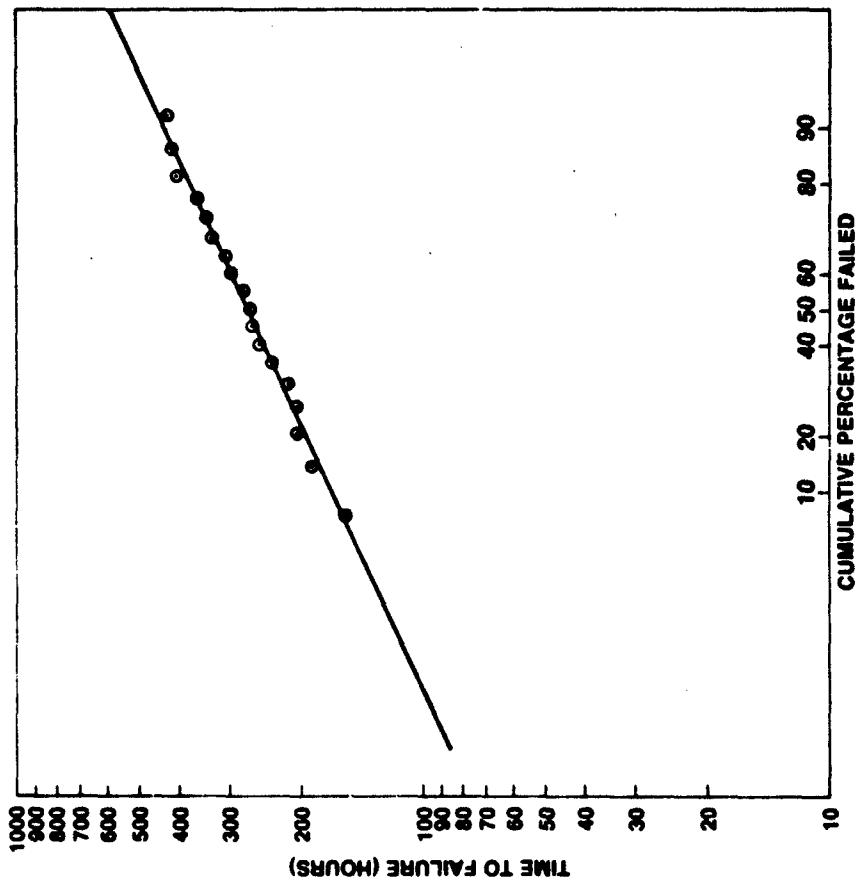




FIGURE 22. VOIDS FORMED IN Al/Si ALLOYS DURING ELECTROMIGRATION TEST AT LOW TEMPERATURES. 5000X

E-3021



**FIGURE 23. CRACKED PASSIVATION GLASS DUE TO HILLOCK GROWTH BEFORE
AND AFTER GLASS REMOVAL. 6000X**

E3022

FIGURE 24. Al — 0.79% Si ALLOY DATA RELATING MEDIAN TIME TO FAILURE TO FILM GEOMETRY, CURRENT DENSITY AND TEMPERATURE

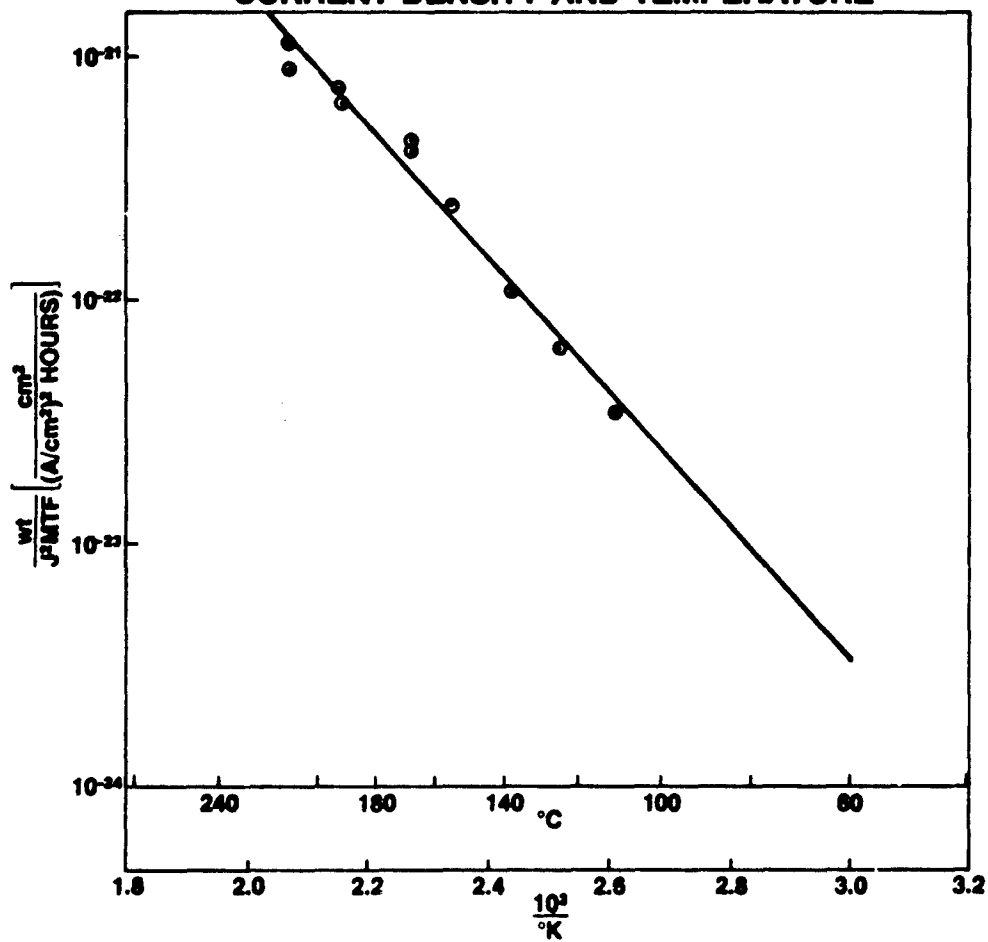
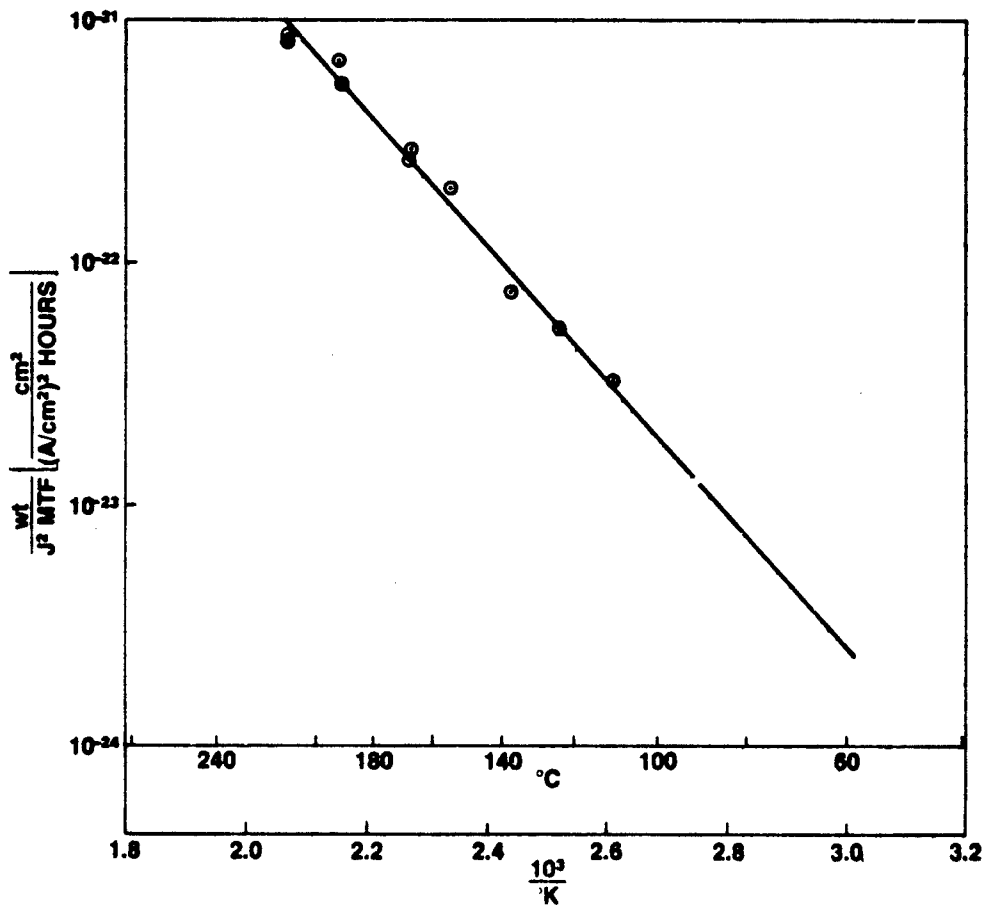
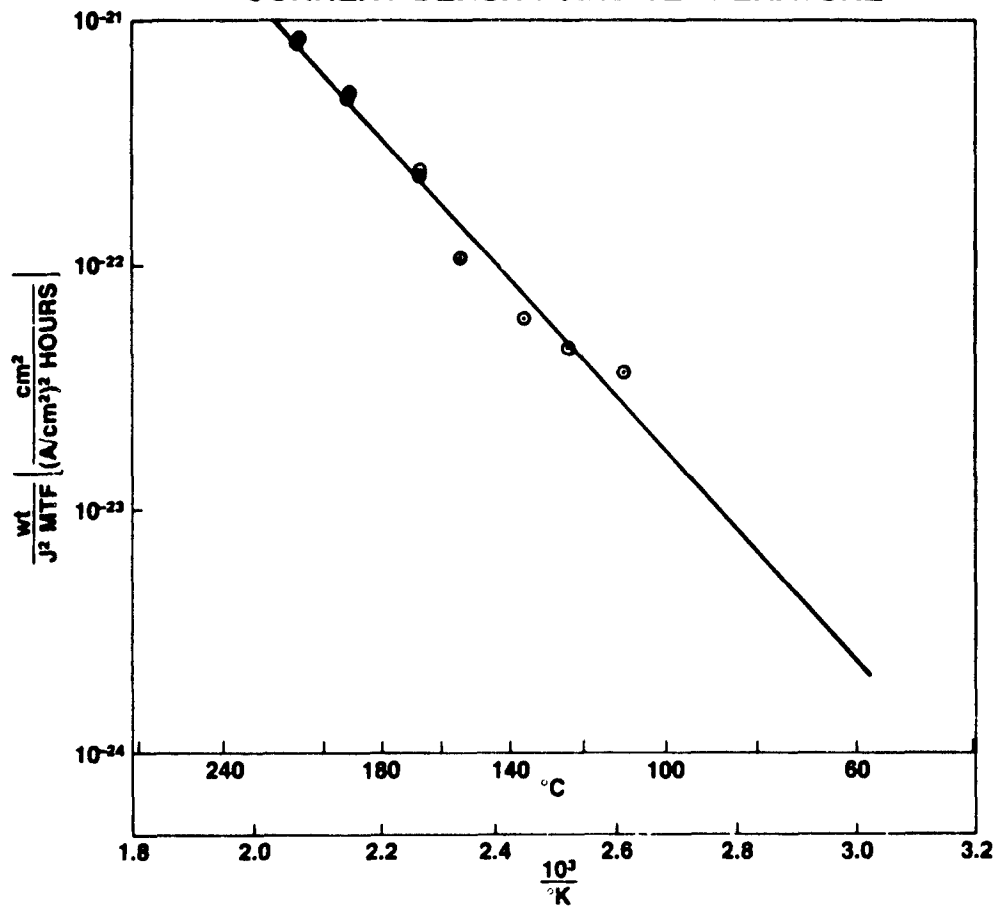


FIGURE 25. Al — 1.9% Si ALLOY DATA RELATING MEDIAN TIME TO FAILURE TO FILM GEOMETRY, CURRENT DENSITY AND TEMPERATURE



E324

FIGURE 26. AI — 3.0% SI ALLOY DATA RELATING MEDIAN TIME TO FAILURE TO FILM GEOMETRY, CURRENT DENSITY AND TEMPERATURE



where k is Boltzmann's constant $8.62 \times 10^{-5} \text{ eV/}^\circ\text{K}$
 T is the absolute temperature of the film
 w is the film width in cm
and t is the film thickness in cm.

from this one can express the median film lifetime to be:

$$\text{MTF} = \frac{wt}{J^2} 1.747 \times 10^{15} \exp \frac{0.545}{kT}$$

$$\text{Al - 1.9\% Si: } \frac{wt}{J^2 \text{ MTF}} = 5.623 \times 10^{-16} \exp - \frac{0.551}{kT}$$

$$\text{or MTF} = \frac{wt}{J^2} 1.778 \times 10^{15} \exp \frac{0.551}{kT}$$

$$\text{Al - 3\% Si: } \frac{wt}{J^2 \text{ MTF}} = 3.447 \times 10^{-16} \exp - \frac{0.540}{kT}$$

$$\text{or MTF} = \frac{wt}{J^2} 2.901 \times 10^{15} \exp \frac{0.540}{kT}$$

It is seen from the above that these plots are very nearly coincidental with activation energies of about 0.54 eV, a value attributed for the self diffusion of Al down grain boundaries. There is a slight ordering in the pre-exponential constants with silicon content providing slightly greater lifetimes as the silicon content of the alloys increase. This, however, is believed to be within experimental error which could arise during measurement of the cross sectional areas of the films. This is because the factor which is plotted along the ordinant of these figures varies as the cube of the cross sectional area.

A combined Arrhenius plot of these three alloy films including all thirty data points for the median time to failure is presented in Figure 27. The least squares method was used to determine the 50% failure line. Following Peck²⁵ the percentile lines were calculated using the average sigma of the thirty test cells using the log-normal distribution. The equations derived from this plot which describe the median lifetime are:

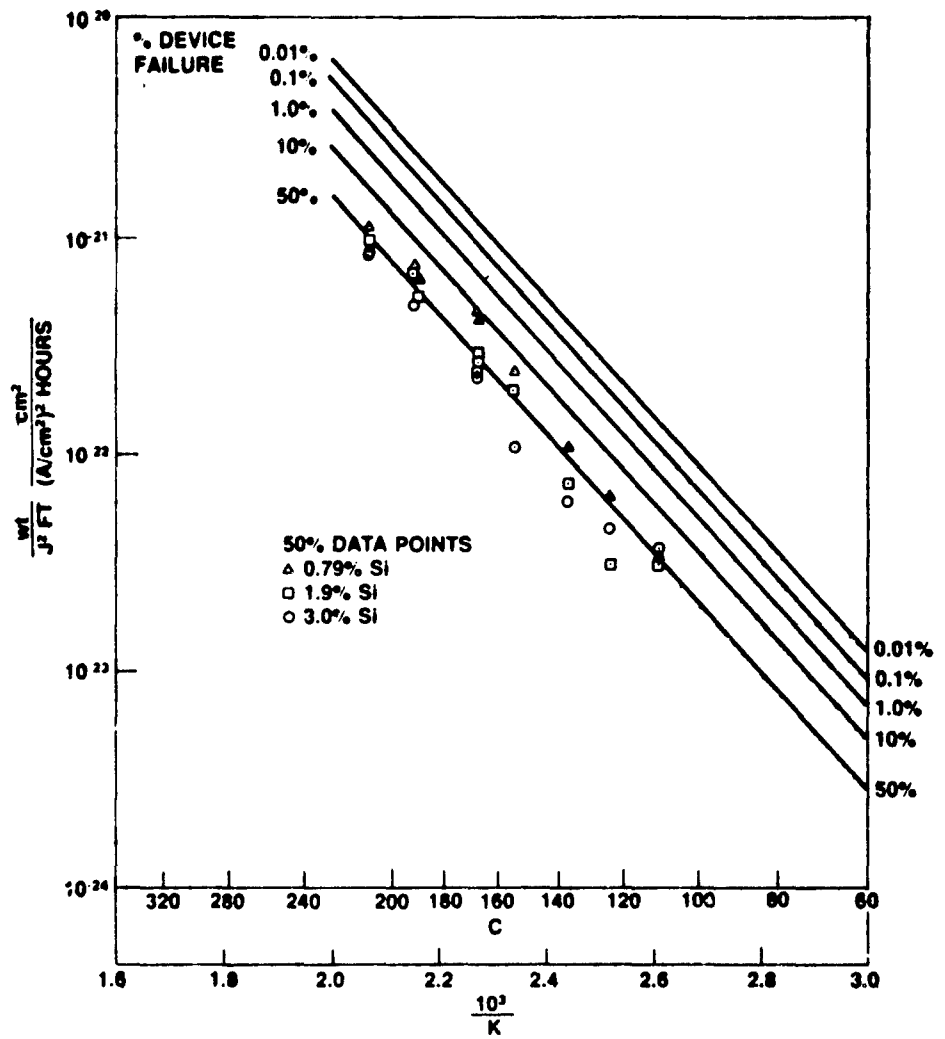
Combined Al/Si Alloys:

$$\frac{wt}{J^2 \text{ MTF}} = 4.727 \times 10^{-16} \exp - \frac{0.544}{kT}$$

$$\text{and MTF} = \frac{wt}{J^2} 2.116 \times 10^{15} \exp \frac{0.544}{kT}$$

It is of interest to note that the lifetime of the passivated alloy films are 2-3 times greater than pure small grained aluminum that was not passivated. (Compare Figure 27 with Figure 14). This can be attributed to the passivation glass which restricts hillock growth causing the metal to

FIGURE 27. COMBINED Al/Si ALLOY DATA RELATING % DEVICE FAILURE TIME TO FILM GEOMETRY, CURRENT DENSITY AND TEMPERATURE



E3826

go under compression. This compressive stress in turn applied a force to the electromigrating ion which is opposite to that due to the electron wind force resulting in increased lifetime¹⁸. Satake et al¹⁷ reported that a 5000 Å thick SiO₂ passivation glass increased electromigration lifetime of small grained films a factor of two over non-glassed films. In view of this it is concluded that the silicon addition to aluminum has very little effect on its rate of electromigration. At temperatures below about 210°C failure is due to the grain boundary electromigration of aluminum in aluminum forming voids and producing an electrical open circuit.

Figures 28, 29, 30, and 31 are engineering design charts for Al/Si films for 50%, 1%, 0.1% and 0.01% failure times. These present failure times as a function of temperature and current density for films possessing a cross sectional area of $1 \times 10^{-7} \text{ cm}^2$. Since lifetime to the percentage failure is a direct function of the cross sectional area of the conductor, one can directly scale the lifetime accordingly. If the conductor has $2 \times 10^{-7} \text{ cm}^2$ cross sectional area lifetime will be twice that shown on the chart. Likewise, if it is $5 \times 10^{-8} \text{ cm}^2$ it will fail at half the time indicated.

Figure 31 shows that for a conductor with a $1 \times 10^{-7} \text{ cm}^2$ cross sectional area and operating continuously on a device with a junction temperature of 125°C it will be expected to accumulate 0.01% device failures at the end of one year if the maximum current density is $2 \times 10^5 \text{ A/cm}^2$. This is a current of 20 ma.

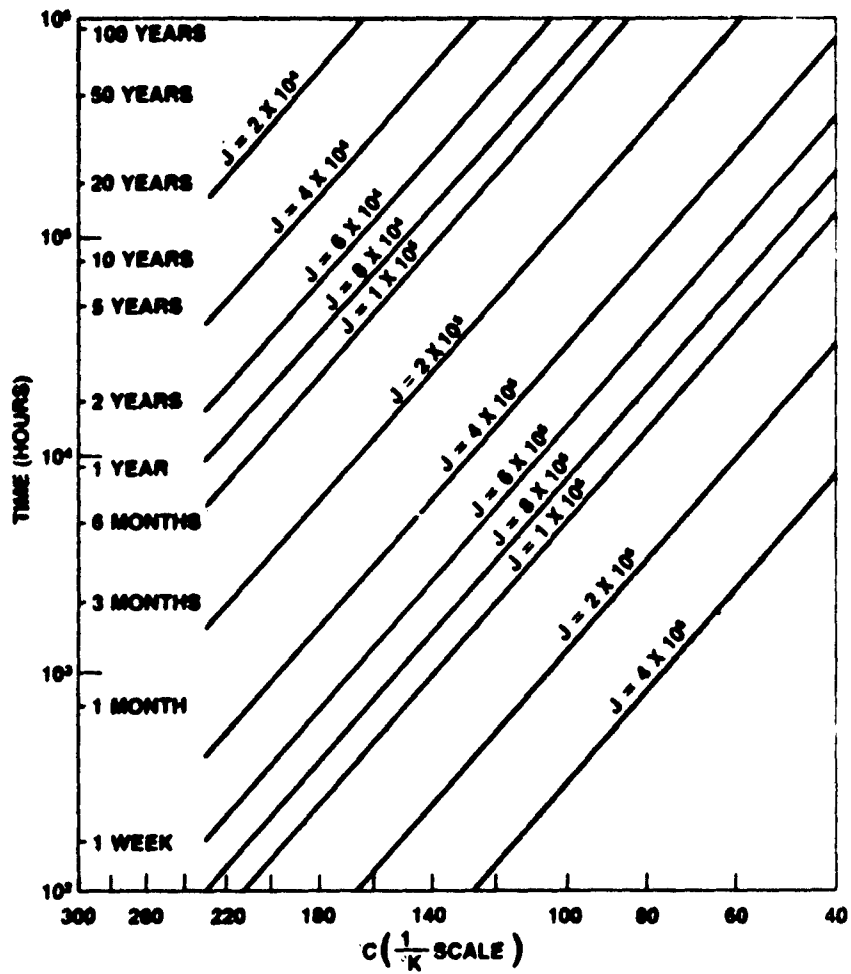
For a state-of-the-art conductor of $w = 5 \times 10^{-4} \text{ cm}$ and $t = 1 \times 10^{-4} \text{ cm}$ with an area of $5 \times 10^{-8} \text{ cm}^2$ to obtain 1 year data one must enter the charts at 2 years. At 175°C junction temperature, a common rating for many devices, these charts indicate that to achieve a 1% failure in 1 year a current density of $9 \times 10^4 \text{ A/cm}^2$ would be acceptable. A 0.1% failure in 1 year would require a maximum current density of $7 \times 10^4 \text{ A/cm}^2$ and a 0.01% failure in one year would limit the current density to $6 \times 10^4 \text{ A/cm}^2$. These are currents of 4.5 ma, 3.5 ma and 3 ma respectively.

In the future employing electron beam and x-ray lithography engineers are talking of 0.5 μm geometries in 0.5 μm thick aluminum films. These would be $2.5 \times 10^{-9} \text{ cm}^2$ in cross sectional area which is 1/40 of 10^{-7} cm^2 . To determine the 0.1% accumulative failure data for one year at 175°C one must enter the chart of Figure 30 at 40 years (3.5×10^5 hours) and find that the maximum current density cannot exceed about $1.7 \times 10^4 \text{ A/cm}^2$. This leads to a maximum current of 43 μa.

Alternately these data could easily be obtained from Figure 27 determining the value of $wt/J^2 \text{ FT}$ using the proper percentile line and temperature.

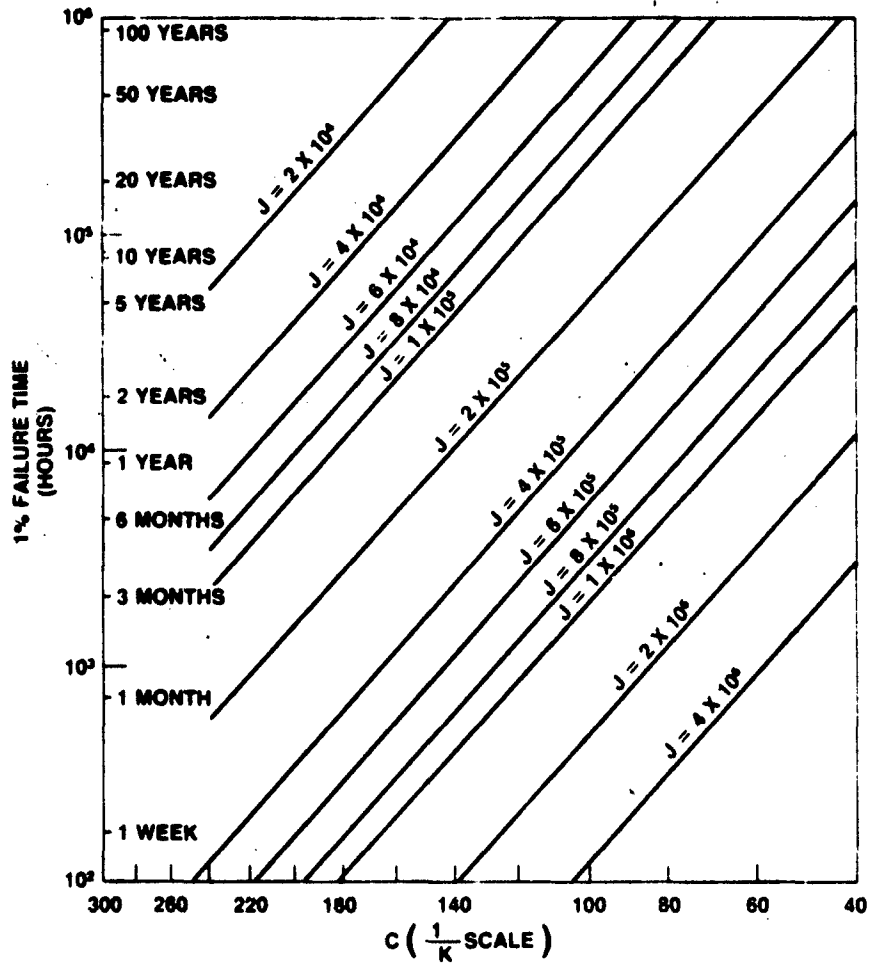
The results obtained in this work differ considerably from that reported by van Gurp¹⁹ and Learn²⁰. The former studied non-glassed very small grained Al/Si films of 0.3% and 1.8% Si as well as pure Al. When stressed at $J = 2 \times 10^6 \text{ A/cm}^2$ the pure Al exhibited an activation energy of 0.55 eV with voiding randomly distributed down the stripe. The 0.3% Si alloy had an activation energy of 0.32 eV while the 1.8% alloy had an activation energy of 0.31 eV. At 200°C the 0.3% Si alloy had a lifetime five times greater than pure Al while the 1.8% Si alloy exhibited an order of magnitude improvement

FIGURE 28. 50% FAILURE TIME OF Al/Si ALLOY FILMS WITH 10^{-7} cm² CROSS-SECTIONAL AREA



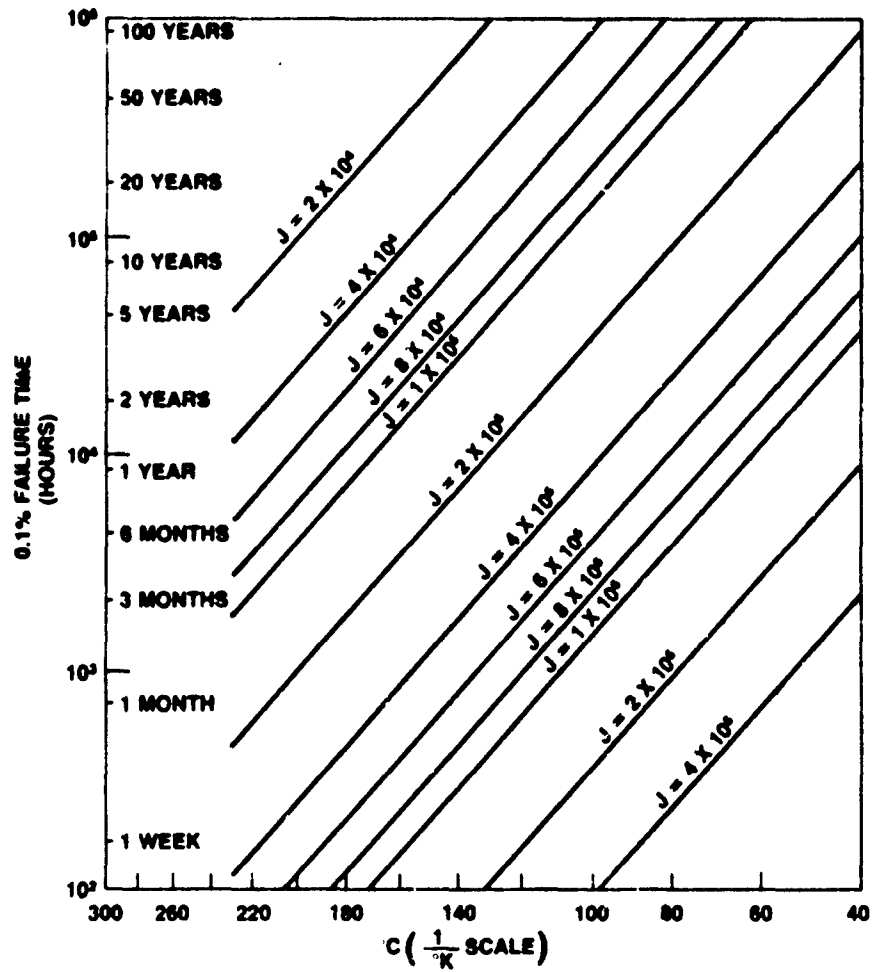
E3857

FIGURE 29. 1.0% FAILURE TIME OF Al/Si ALLOY FILMS WITH 10^{-7} cm² CROSS-SECTIONAL AREA



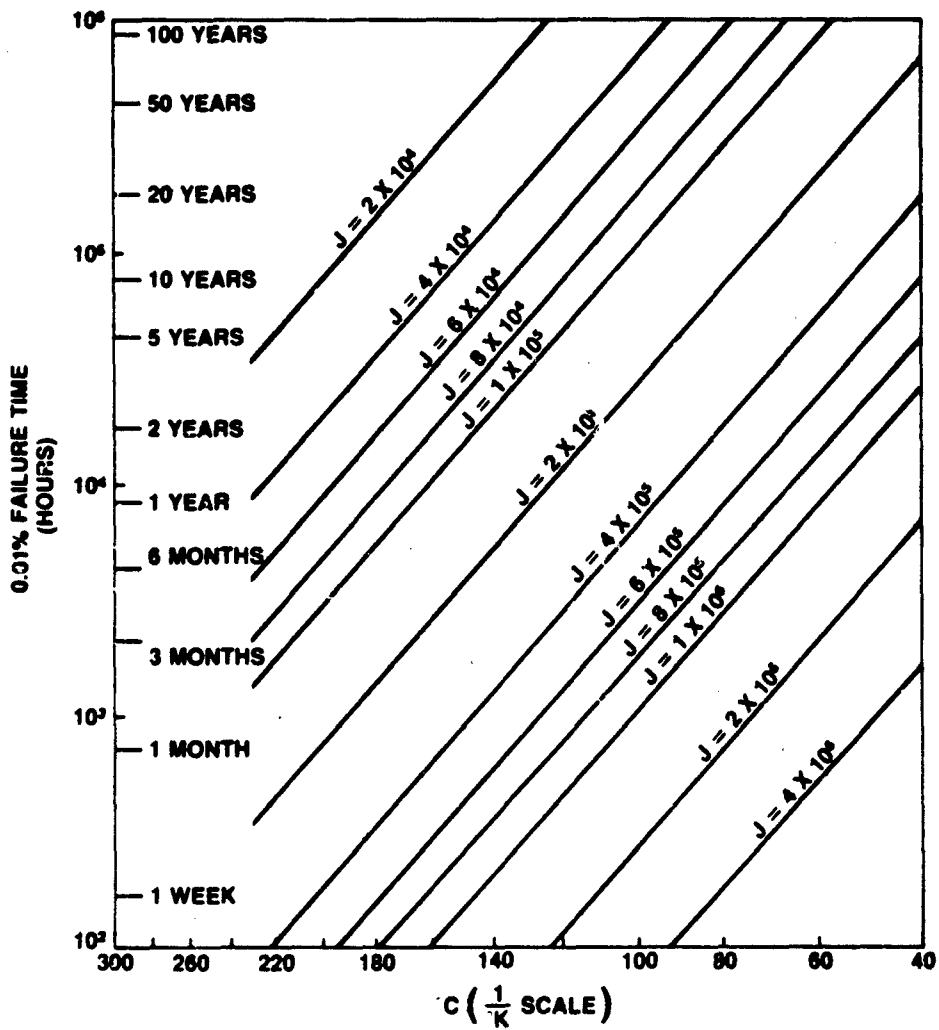
E3828

**FIGURE 30. 0.1% FAILURE TIME OF Al/Si ALLOY FILMS WITH
10⁻⁷ cm² CROSS-SECTIONAL AREA**



ES20

FIGURE 31. 0.01% FAILURE TIME OF Al/Si ALLOY FILMS WITH 10^{-7} cm² CROSS-SECTIONAL AREA



E3630

over pure aluminum. The failure mechanism for the alloy was a void which always formed at the negative end of the stripe indicating excessive stress causing gradients in temperature or current density at that region. The low activation energy was attributed to grain boundary and surface diffusion.

Learn's²⁰ results on non-glassed silicon alloys of aluminum were similar exhibiting longer lifetime at elevated temperatures than pure Al, but because of the lower activation energy the pure Al films provided greater lifetime below about 120°C.

The discrepancy between this present work and that of van Gorp and Learn may be attributed to the glass passivation. Besides causing the metal to compress during electromigration slowing the growth of hillocks and reducing the effects of electromigration, it may also reduce surface diffusion forcing the self diffusion of aluminum to take place through the grain boundaries with the generally accepted activation energy near 0.55 eV.

2.3.5 High Temperature Al/Si Alloy Electromigration

When silicon electromigrates at a rapid rate at elevated temperatures in Al/Si alloy films the definition of device failure must be redefined since the failure is not an open circuit. It could be defined as a shorted junction at a silicon-aluminum contact where electrons leave the silicon and enter the aluminum. Alternately it could be defined as a given rise in contact resistance at aluminum-silicon contacts where electrons leave the aluminum and enter the silicon. Both processes would be expected to accelerate as the contact areas decrease.

To study this high temperature mode of Al/Si alloy electromigration failure a test vehicle was designed and constructed where the contacts to the Al/Si alloy stripes were made to silicon at each end of the stripes. Figure 32 is a cross sectional diagram of the structure which consists of an n substrate with boron diffused contact regions 1.35 μm deep. The Al/Si alloy stripe contacts both boron doped regions at each end. Each boron doped region contains separate metallization regions which serve as wire bonding pads and make ohmic contact to the silicon.

Figure 33 shows micrographs of the test die and an enlarged view of one of the terminals showing the boron diffused region, the contact to the stripe and wire bonding pad. The test vehicle contained four stripes with a nominal width of 0.4 mils but differed in that the ohmic contact to the stripes varied in area. These ohmic contacts were 0.2 x 0.2 mils, 0.2 x 0.4 mils, 0.4 x 0.4 mils and 0.4 x 0.8 mils. For all of the work reported on here time was allowed to study only the 0.4 x 0.4 mil ohmic contacts. The parts were passivated in a manner identical to that in the previous experiment, pads opened by clearing the glass for wire bonding and the backs of the wafers were metallized with gold to provide a high temperature Au-Si eutectic die bond. The separated die were then bonded to TO-3 headers, wire bonded with 5 mil diameter aluminum wires using those stripes with the nominal 0.4 x 0.4 mil ohmic contacts. The parts were then sealed in a nitrogen ambient.

The silicon alloys used for the metal for this experiment were 0.35% Si, 1.4% Si, 2.5% Si and 3.6% Si. Half of the devices contained residual silicon

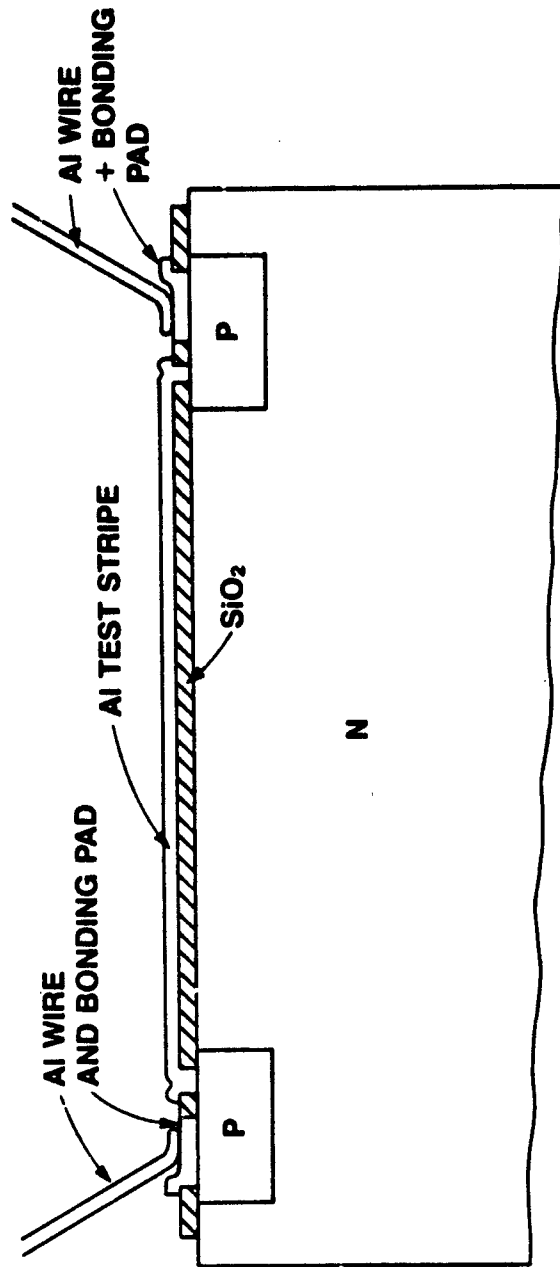
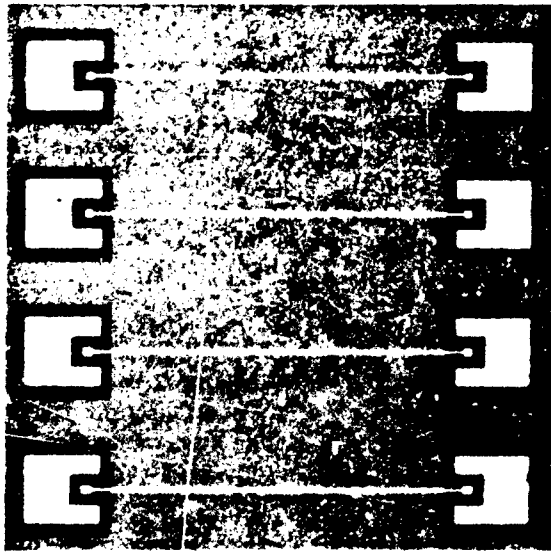
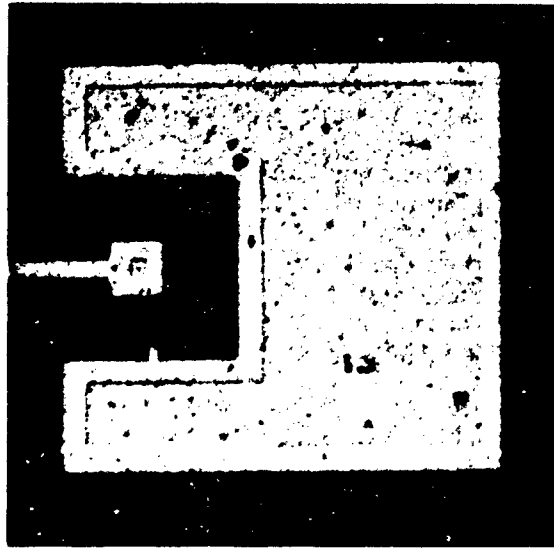


FIGURE 32. SCHEMATIC OF HIGH TEMPERATURE TEST STRUCTURE CROSS SECTION PRIOR TO PASSIVATION.

E3831



(a)



(b)

FIGURE 33. (a) 80 x 80 MIL HIGH TEMPERATURE TEST STRUCTURE (b) ENLARGED VIEW OF DIFFUSED REGION, OHMIC CONTACT AND WIRE BOND PAD.

in the areas cleared of aluminum during metal patterning while half of the devices had this residual silicon removed. Table VI presents the conductor dimensions of these alloy films and the measured dimensions of the stripe ohmic contacts.

Electrical resistance measurements were made of the parts and the very high and very low devices were culled from the lots. The devices were then placed under electromigration stress conditions at temperatures ranging between 240°C and 311°C with monitors for open circuits, resistance build up and negative terminal shorting. For this test device, it was not known at the start of the experiment which failure mode would predominate.

When the devices were placed under test the failures exhibited a bimodal distribution when plotted on log-normal probability paper. Figure 34 presents such a distribution. When this set of devices was inspected utilizing an optical microscope it was determined that six of the devices failed by the formation of voids randomly distributed along the stripes with one void per stripe eventually forming an open circuit. Five of the devices in this set failed due to etch pits which formed in the silicon at the negative terminals eventually shorting the junction. To study these failure modes each group within a set which failed either by the electromigration of aluminum in aluminum or by the electromigration of silicon in aluminum was treated as a separate set from which the median time to failure and the standard deviation were determined from log-normal plots. Unfortunately the sample sizes were not as great as desired introducing some scatter in the data.

Figure 35 presents SEM micrographs of the positive and negative terminals of a glass passivated stripe that had been stressed at 310°C at a current density of 4.95×10^5 A/cm². A pile up of Al and Si is observed at the (+) terminal cracking the glass passivation. Also a depression is observed at the (-) terminal where the Al and Si has been depleted also causing the passivation glass to crack. A hillock is also presented in Figure 35 which has cracked the glass and pushed up through it. Figure 36 shows the same features as does Figure 35, however the passivation glass has been etched away revealing the metal. Metal is observed to pile up at the (+) terminal while pitting of the Si substrate has occurred at the (-) terminal. The Al/Si alloy is also shown to have formed a void near the (-) terminal. The hillock appears flattened and distorted compared to the free growing structures found on non-glassed films.

Figure 37 shows the same terminals as were presented in Figures 35 and 36 however the aluminum metal has been selectively etched away. It is observed that the alloy build up at the positive terminal consisted of silicon being deposited at the silicon contact with aluminum on top of it. Coarsening of the silicon particles has occurred around the ohmic contact but appear depleted at the higher current density regions. The negative terminal exhibits severe vertical and lateral pitting with silicon build up near the contact where the current density drops due to radial spreading. Silicon build up is not observed where the alloy formed a void at the contact and therefore was not connected to the silicon source. In the stripe the silicon was observed to coarsen in an elongated fashion decorating aluminum grain boundaries.

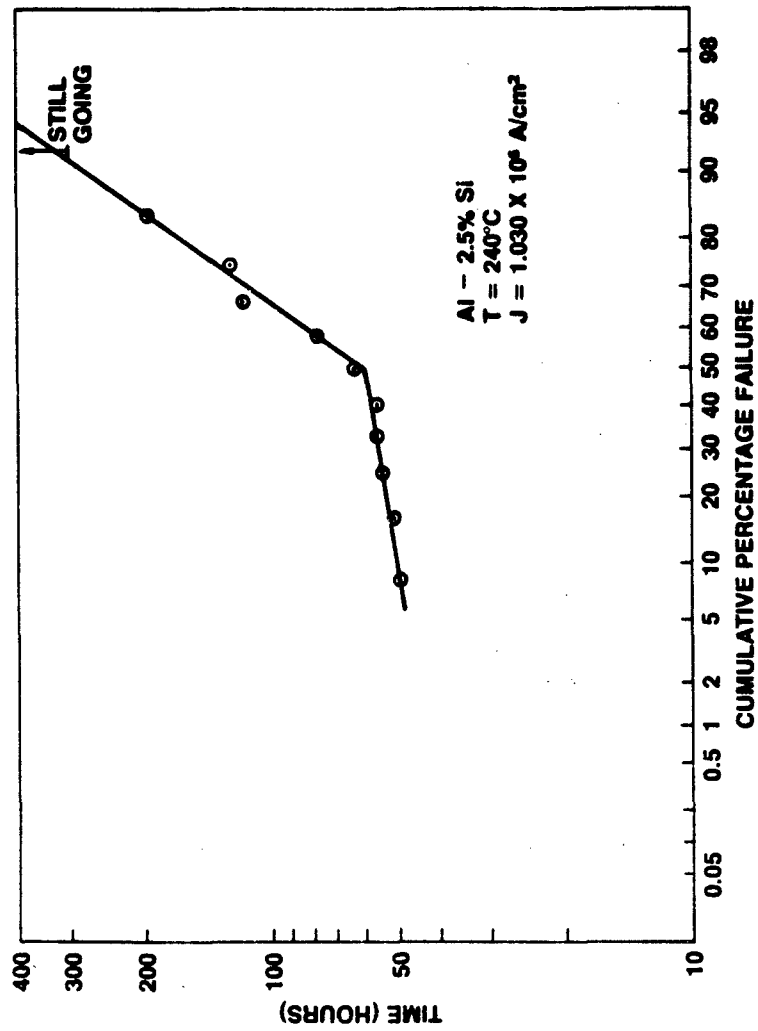
Figure 38 shows silicon build up at the positive terminal and etch pit

Table VI

High Temperature Test Device Dimensions

Alloy	Film Width (μm)	Film Thickness (μm)	Film Area (cm^2) $\times 10^8$	Contact Dimensions $\mu\text{m} \times \mu\text{m}$
0.35% Si	11.63	0.88	10.234	9.08 x 9.08
1.4% Si	10.32	0.84	8.669	9.30 x 9.30
2.5% Si	10.765	0.85	9.150	9.09 x 9.09
3.6% Si	10.568	0.83	8.771	9.09 x 9.09

FIGURE 34. BIMODAL FAILURE DISTRIBUTION



E300



+ TERMINAL

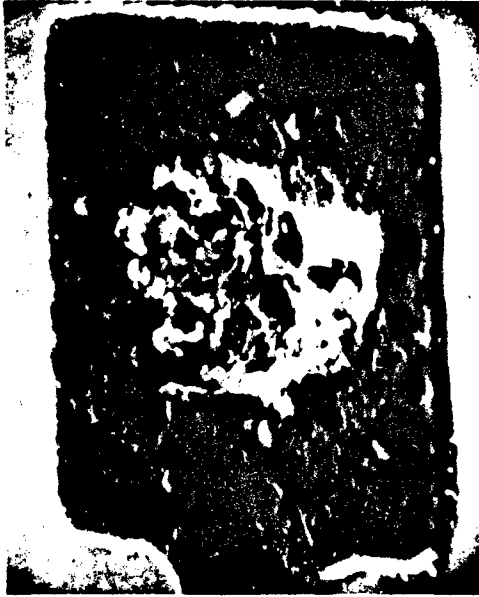


- TERMINAL



HILLOCK

FIGURE 35. DEVICE STRESSED AT 310°C AND $J = 4.95 \times 10^5$ A/cm² PRIOR TO PASSIVATION GLASS REMOVAL.



- TERMINAL



+ TERMINAL



HILLOCK

FIGURE 36. DEVICE SHOWN IN FIGURE 35 AFTER REMOVAL OF PASSIVATION GLASS. EX355



+ TERMINAL



- TERMINAL

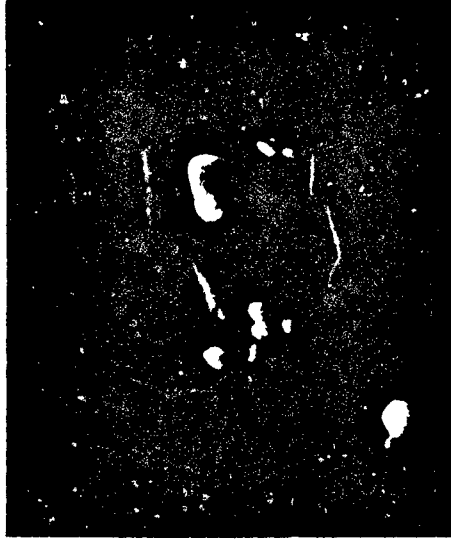


SI IN STRIPE

FIGURE 37. DEVICE SHOWN IN FIGURES 35 AND 36 AFTER ALUMINUM ETCH.



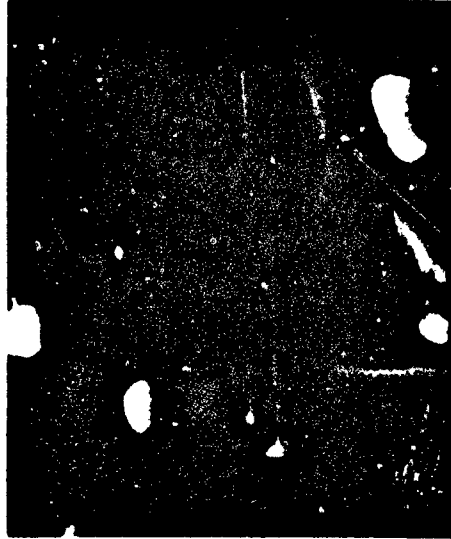
+ TERMINAL



- TERMINAL



+ TERMINAL WITH SEM LINES



- TERMINAL WITH SEM LINES

FIGURE 38. + AND - TERMINALS AFTER PASSIVATION GLASS, ALUMINUM AND THERMAL OXIDE ETCH. DEVICE FAILED BY VOID FORMATION. LOWER PICTURES SHOW SEM DEPOSITED LINES USED TO MEASURE DEPOSITED SI HEIGHT AND SI PIT DEPTH.

formation at the negative terminal of a stripe which failed due to the formation of a void along the stripe due to the electromigration of Al in Al. The top two views taken at 6081 X and an angle of 44° show the features of the contacts. The lower two views show how the SEM was used to accurately measure the height of the silicon build up and the depth of the silicon pits. At an angle of 0° the SEM electron beam was caused to scan a line across the features building up a fine line of polymerized vacuum pump oil. The samples were then tilted by an angle of 45°. The true height or depth can then be obtained by measuring the displacement of the line as it goes over the build up or down into the pit. The true depth or height then is equal to the apparent displacement divided by the sine of the angle of tilt. In the case shown in Figure 38 the silicon nodule height was determined to be 8,724 Å while the pit depth was 4,304 Å.

Figure 39 presents SEM micrographs of negative and positive terminals of a device tested at a temperature of 300°C and a current density of 4.98 x 10⁵ A/cm² before and after passivation glass removal. Vertical as well as lateral pit growth has occurred at the negative terminal and a void has grown over the contact and to one side of the contact forming the highest current through the bottom right of the alloy at the contact. Figure 40 shows these contacts after the aluminum has been etched away and indicates the build up of silicon near the negative terminal in the current carrying alloy and where the current spreads out reducing the current density. Silicon is also built up in the positive contact and considerable coarsening of silicon grains has occurred near that contact.

Typical void formation and hillock growth due to the electromigration of aluminum in aluminum are shown in Figure 41. The passivation glass has been etched off of three of the four stripes shown.

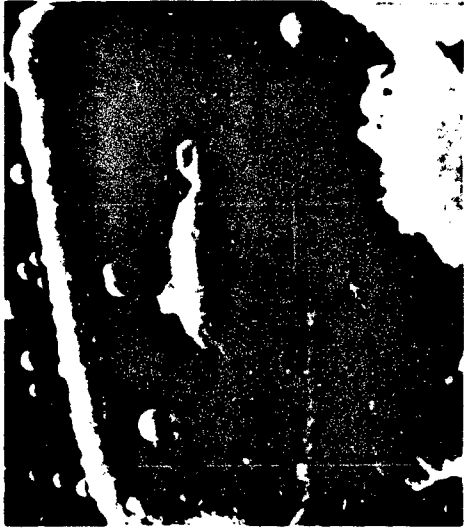
Table VII presents the high temperature test conditions and results obtained. Four alloys were used ranging from 0.35% Si to 3.6% Si. The temperature ranged from 240°C to 311°C and the current density varied from 4.565 x 10⁵ A/cm² to 1.038 x 10⁶ A/cm². The very high temperature oven could accept only one set of devices per run while two lower temperature ovens could accept three sets of devices per run. In general at the lower temperatures the predominant failure mode was due to the electromigration of Al in Al while at the higher temperatures the failure mode gradually switched predominantly to that due to the electromigration of Si in Al.

An Arrhenius plot of the data for failures due to the electromigration of Si in Al is presented in Figure 42. This relates the Al/Si alloy median time to failure due to this failure mode to the film geometry current density and temperature. The line drawn through the experimental points was constructed using the least squares technique can be expressed as:

$$\frac{wt.}{J^2 MTF} = 2.275 \times 10^{-13} \exp (-0.889/kT)$$

from which: $MTF = \frac{wt.}{J^2} 4.396 \times 10^{12} \exp (0.889/kT)$

The activation energy of 0.89 eV agrees well with the recent work of



+ TERMINAL



+ TERMINAL



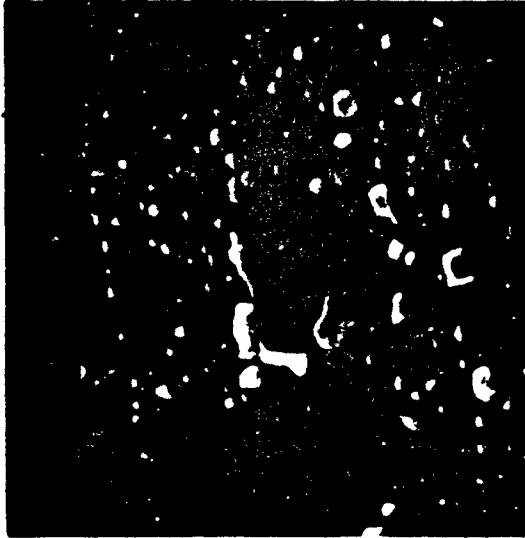
- TERMINAL



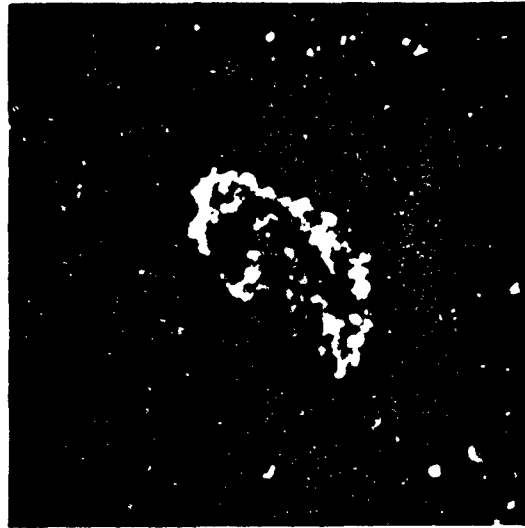
- TERMINAL

FIGURE 39. NEGATIVE AND POSITIVE TERMINALS BEFORE AND AFTER PASSIVATION GLASS REMOVAL. $T = 300^{\circ}\text{C}$, $J = 4.98 \times 10^5 \text{ A/cm}^2$. NOTE AI VOIDING AROUND (-) TERMINAL.

6200



+ TERMINAL



- TERMINAL

FIGURE 40. CONTACTS SHOWN IN FIGURE 39 AFTER AN ETCH. NOTE BUILD-UP OF Si AT HIGH CURRENT DENSITY REGION OF NEGATIVE CONTACT.

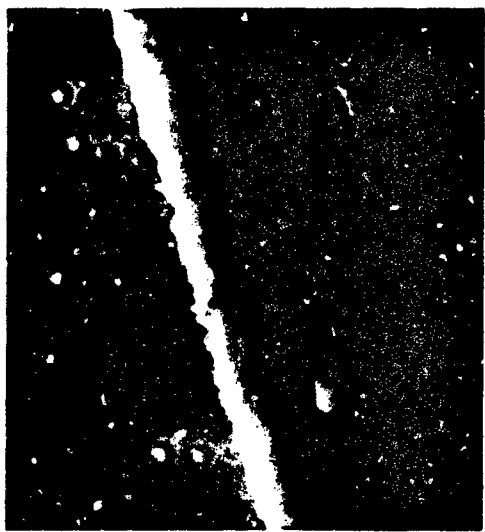


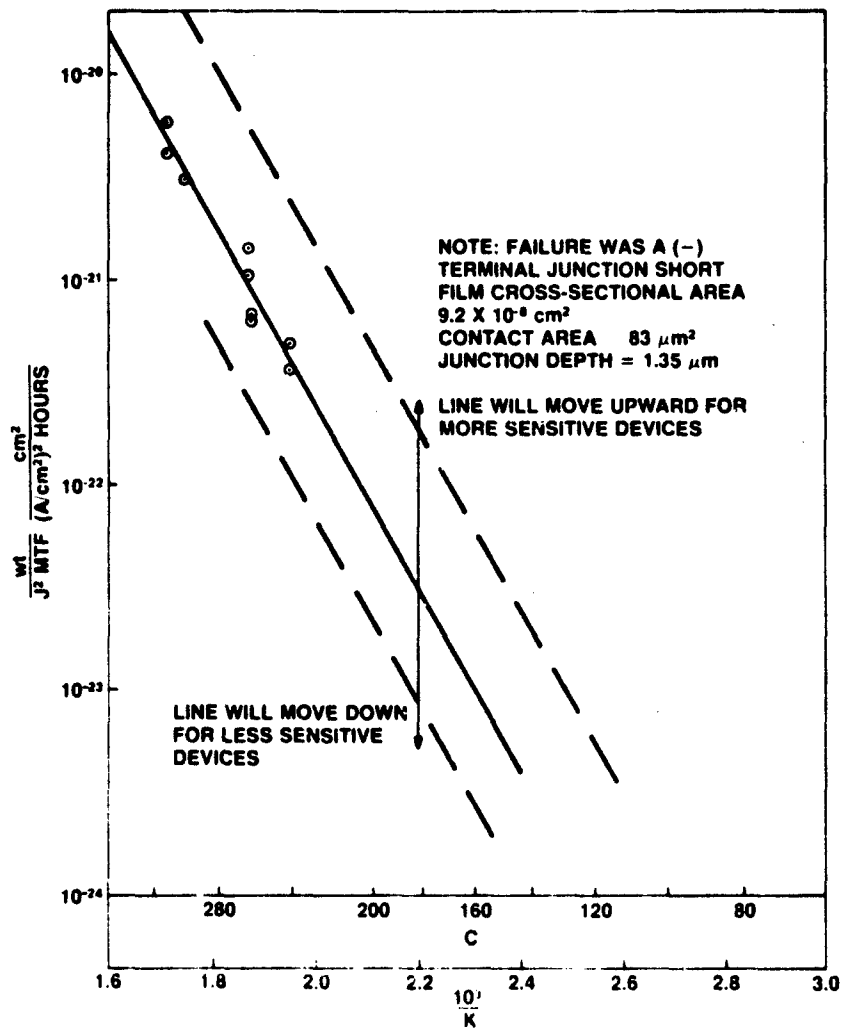
**FIGURE 41. TYPICAL VOIDS AND HILLOCKS OBSERVED IN HIGH TEMPERATURE
Al/Si FILMS DUE TO ALUMINUM ELECTROMIGRATION IN Al.**

00000

Table VII
High Temperature Al/Si Alloy Test Conditions and Results

Run #	Failure Mode	Alloy	Film Area x108 cm ²	Temperature °C	$\frac{10^3}{\sigma K}$	Current Density A/cm ² x10 ⁻⁶	MTF hours	Std. Dev. σ	wt $\frac{J^2 MTF}{x10^{22}}$
1	40% Si in Al	3.6% Si	8.771	260	1.876	1.0	61	.14	14.38
1	60% Al in Al	"	"	"	"	"	21	.48	41.77
2	62% Si in Al	3.6% Si	8.771	300	1.745	0.498	114	.11	30.96
2	38% Al in Al	"	"	"	"	"	65	.12	54.30
3	100% Si in Al	3.6% Si	8.771	310	1.715	0.495	85	.40	42.15
4	50% Si in Al	1.4% Si	8.669	260	1.876	0.8057	202	.36	6.574
4	50% Al in Al	"	"	"	"	"	92	.38	14.43
4	55% Si in Al	2.5% Si	9.150	260	1.876	0.8015	215	.36	6.624
4	45% Al in Al	"	"	"	"	"	60	.73	23.74
4	64% Si in Al	0.35% Si	10.234	260	1.876	0.7944	154	.49	10.53
4	36% Al in Al	"	"	"	"	"	56	.32	28.95
5	80% Si in Al	0.35% Si	10.234	311	1.712	0.4565	84	.26	58.49
5	20% Al in Al	"	"	"	"	"	60	.14	81.89
6	20% Si in Al	1.4% Si	8.669	240	1.949	1.038	245	-	3.543
6	80% Al in Al	"	"	"	"	"	93	.48	9.333
6	45% Si in Al	2.5% Si	9.150	240	1.949	1.030	174	.71	4.952
6	55% Al in Al	2.5% Si	"	"	"	"	75	.10	11.49
6	100% Al in Al	3.5% Si	8.771	240	1.949	1.037	49	.76	16.65

FIGURE 42. Al/Si ALLOY MEDIAN TIME TO FAILURE DUE TO THE ELECTROMIGRATION OF Si IN Al RELATED TO FILM GEOMETRY, CURRENT DENSITY AND TEMPERATURE



E3641

van Gorp¹⁹ who studied the precipitation of Si from a supersaturated Al-Si solid solution by resistance measurements and by microscopy. He found the activation energy for the diffusion of Si in Al for Al-1.8 at.% Si to be 0.9 ± 0.05 eV and is attributed to diffusion along dislocations. McCladin and Sankur⁴ found 0.8 eV for films with the Si content equal to the solubility limit.

It must be emphasized that the equations given above relate only to the specific test device used which failed by a shorted (-) contact junction whose contact area was about $83 \mu\text{m}^2$, the junction depth was $1.35 \mu\text{m}$ and the conductor cross sectional area was about $9.2 \times 10^{-8} \text{cm}^2$. Devices which are more sensitive to silicon electromigration (smaller contact areas, shallower junctions, larger conductor cross sectional areas to contact area ratios, more sensitive to increased resistance at the positive contacts) would be expected to operate along lines parallel to that of Figure 42 but moved upward. The pre-exponential constant for the first equation given would increase while that of the second equation would decrease.

In a like manner devices which are less sensitive to the effects of the electromigration of Si through Al would be expected to possess plots with slopes similar to that of Figure 42 but below that of Figure 42.

Figure 43 presents an Arrhenius plot of the data taken where the failure was an open circuit caused by the electromigration of Al in Al. Due to the generally small sample sizes available and the fact that some of the electrical opens appeared around the (-) terminal contact the data points were somewhat scattered. Using the least squares technique a line drawn through these points exhibited an activation energy of 0.7 eV. Rather than use that line the median time to failure line obtained at lower temperatures where failures were due to electrical opens caused by the electromigration of Al in Al (See Figure 27) was extrapolated to higher temperatures and is included in Figure 43. This indicates that at high temperatures the electromigration of Al through Al behaves similarly to that at low temperatures.

A composite Arrhenius plot of Al/Si small grain alloy median time to failure as a function of film geometry, current density and temperature where failures occur due to the electromigration of Al in Al or Si in Al for the test device used is presented in Figure 44. Except at the very high temperatures ($T > 210^\circ\text{C}$) devices constructed with Al/Si alloy metallization would be expected to fail by an open circuit due to the electromigration of Al in Al. Those devices which are very sensitive to the effects of electromigration of Si in Al may have to be limited to a lower maximum junction temperature (say 185°C).

2.4 Al/Si Alloy Film Corrosion

As part of this study on the reliability of Al/Si alloy films it was desirable to compare the corrosion rates of the alloys with that of pure Al films. The three alloy films characterized in Section 2.2 of this report were used for this study.

The Al/Si alloy films were deposited from a dual-source e-beam evaporator.

FIGURE 43. Al/Si ALLOY HIGH TEMPERATURE MEDIAN TIME TO FAILURE DUE TO VOID FORMATION RELATED TO FILM GEOMETRY, CURRENT DENSITY AND TEMPERATURE

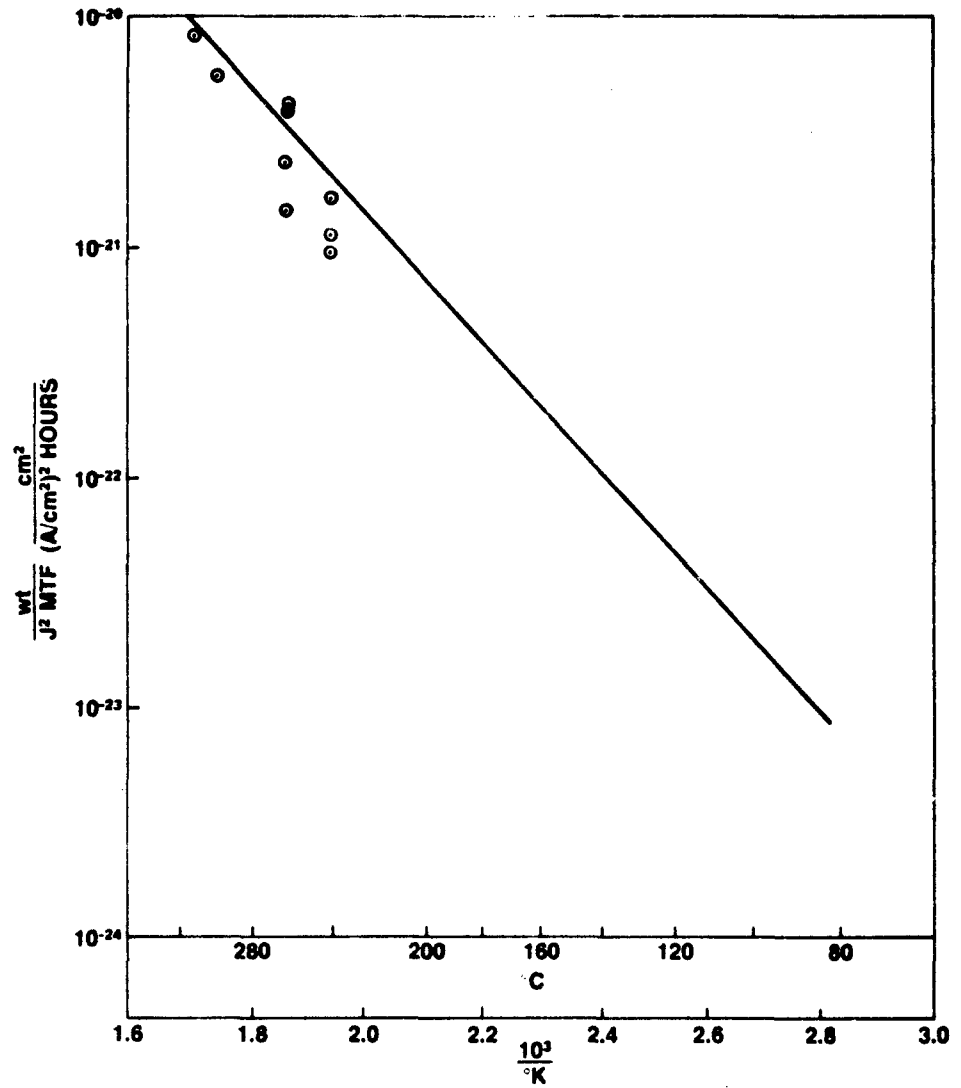
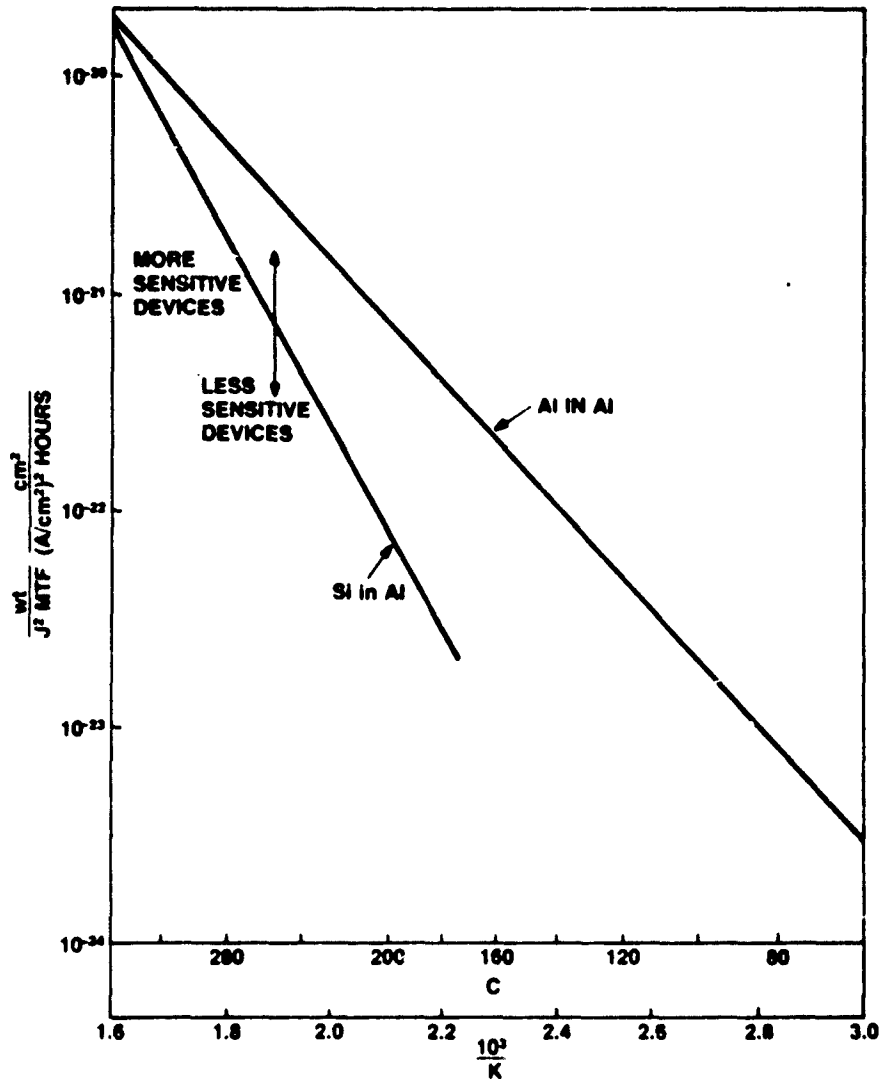


FIGURE 44. Al/Si ALLOY FAILURES DUE TO THE ELECTROMIGRATION OF Al IN Al AND Si IN Al



The substrates consisted of 10 $\text{K}\Omega$ of thermally oxidized Si wafers. The metallization was patterned (Figure 45) to form three pairs of 12.7 μm wide stripes with a separation of 12.7 μm . The test chips were eutectically bonded to T0-5 headers and contacts to the desired stripes were made using Al-1% Si wire. The samples were rinsed in 18 megohm water. Unencapsulated specimens were then exposed to the environmental stress of 85°C/85% R.H. with a 20 volt bias between adjacent metal stripes. The stripe resistance was periodically monitored to follow the corrosion process. An increase of 25% in the resistance was considered failure.

Three different alloy films were used; they contained 0.79% Si, 1.9% Si and 3.0% Si. A fourth set of specimens had 3.0% Si but were lightly etched (dilute $\text{HF}\cdot\text{HNO}_3$) to remove any Si between the metal stripes. The control group of specimens were pure Al with no alloy additions.

The corrosion results are shown in Figure 46 and Figure 47. Both the anode and cathode stripes were monitored. At the anode (Figure 46) all the Al/Si alloys corroded faster than the pure Al control specimens. Lines have been drawn to connect the data points for each alloy. At 180 hours there was no correlation between the corrosion rate and the silicon concentration. The 3% Si samples that were etched to remove the excess Si corroded slower than the unetched parts. The mean time to failure varied from 50 hours (0.79% Si) to 150 hours (1.9% Si) compared to a MTF greater than 250 hours for pure Al.

Different results were observed at the cathode. The samples with 0.79% Si corroded faster than the pure Al controls. However, the 1.9 and 3% Si alloys corroded at approximately the same rate. Also the etched samples (3% Si) failed at approximately the same rate as the pure Al samples. It should be noted that the anodic corrosion rate is much higher than the cathodic corrosion rate for the Al/Si alloys. For pure Al, however the failure rates are nearly identical for the cathode and anode.

Typical corroded samples are shown in Figures 48 and 49. Figure 48 shows the entire test pattern. The positive and negative stripes are indicated. The black spots are the corrosion products and can be seen mainly on the anode stripes. Figure 48b shows the center of the chip. The localized nature of the corrosion process can be seen. Similar local corrosion spots can be seen in the 0.79% Si samples (Figure 49). Again the spots are primarily on the anode (positive) stripes.

The corrosion characteristics are quite different for pure aluminum samples. The entire cathode stripe seems to corrode and turn dark as seen in Figure 50a. The cathode stripes appear dark in these pictures indicating a rough corrosion product on the surface. The failures at the anode stripes occur at very localized spots. Figure 50a shows a higher magnification of the Al anode and cathode stripe.

The addition of Si to the Al metallization results in Si precipitation after any heat treatments. These precipitates can occur at the top and bottom surface and in the grain boundaries. At the anode there are two competing reactions. First, anodic corrosion of the Al can occur according to:

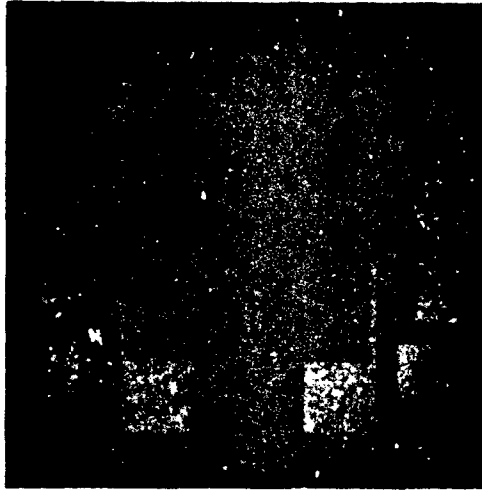


**FIGURE 45. THE CORROSION
TEST PATTERN
WITH 0.5 MIL LINE
WIDTHS AND 0.5 MIL
SPACINGS.**

E3844

FIGURE 46. THE ANODIC CORROSION FOR Al-Si ALLOY FILMS AND A PURE Al FILM

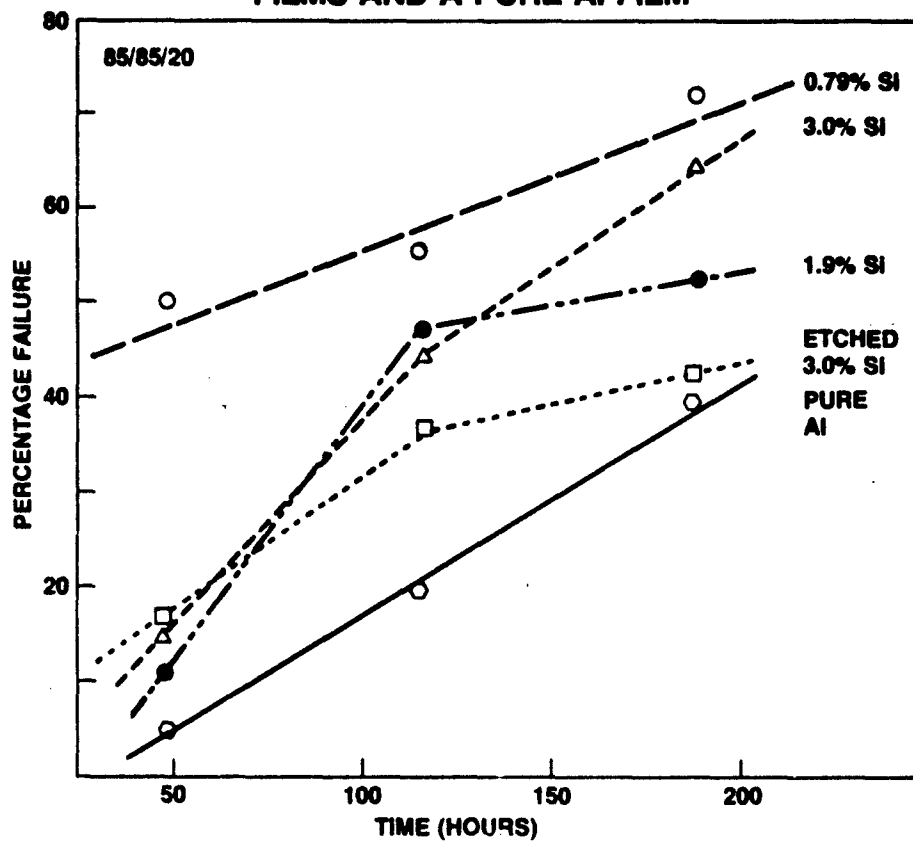
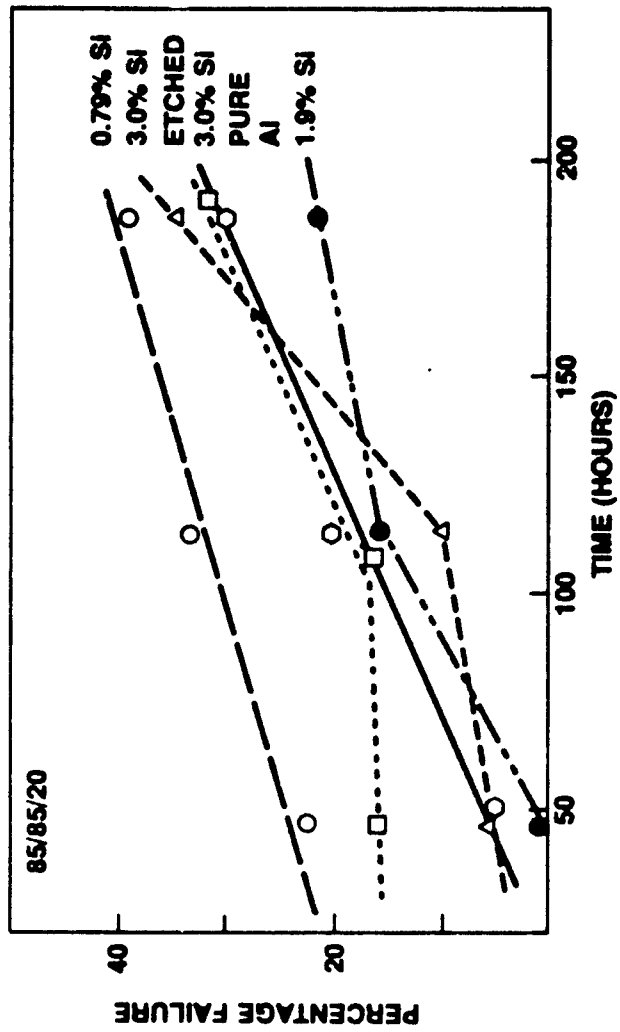


FIGURE 47. THE CATHODIC CORROSION FOR Al-SI ALLOY FILMS AND A PURE Al FILM



EX-49

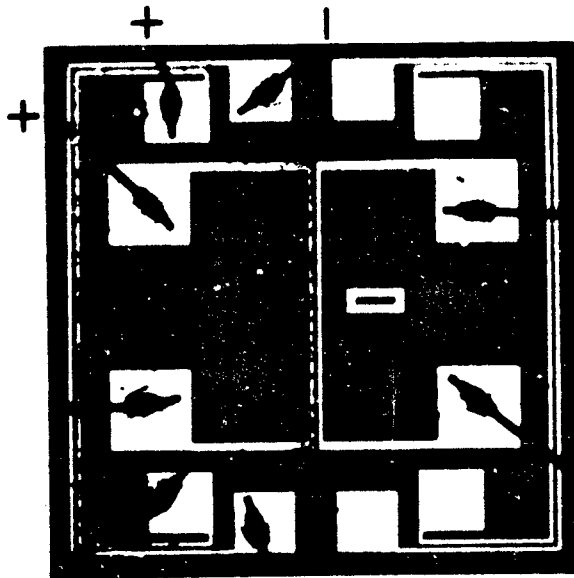
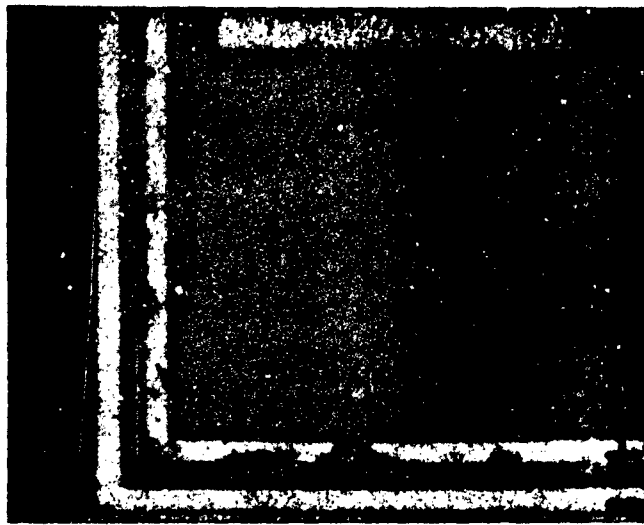


FIGURE 48A. A TYPICAL Al-3% Si SAMPLE SHOWING CHARACTERISTIC SPOTTY CORROSION AT THE ANODE STRIPES AFTER 180 HOURS AT 85/85/20.



FIGURE 48B. THE CENTER STRIPES AT HIGHER MAGNIFICATION SHOWING LOCAL CORROSION SPOTS.

ES847



**FIGURE 49. LOCAL CORROSION
SPOTS ON Al-0.79% Si
METALLIZATION AFTER
180 HOURS AT 85/85/20.**

E3048

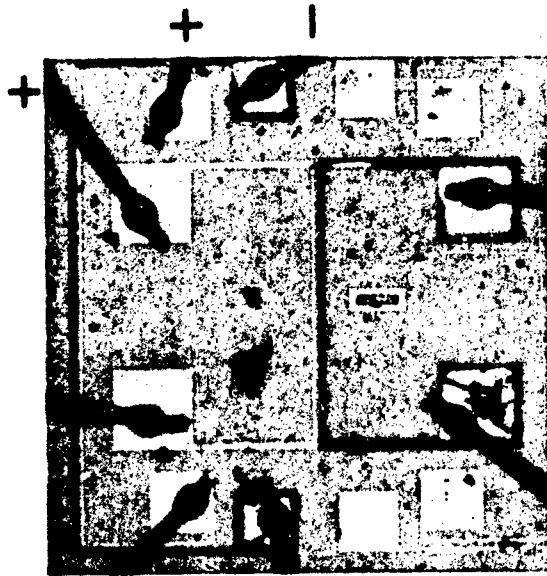


FIGURE 50A. A PURE Al TEST SAMPLE SHOWING THE CATHODIC CORROSION CHARACTERISTICS AFTER 180 HOURS AT 85/85/20.

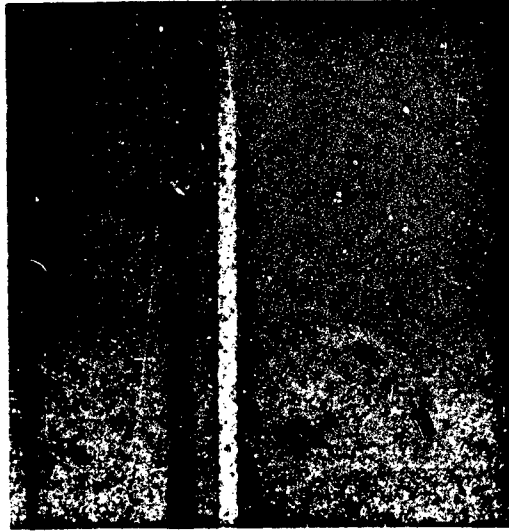


FIGURE 50B. A HIGH MAGNIFICATION VIEW OF THE TOP PART OF FIGURE 50A SHOWING CATHODIC CORROSION.

E3049



The anode will attract negatively charged ions such as Cl^{-} and OH^{-} which can accelerate the corrosion process. The second reaction is anodization by which the protective oxide film will grow thicker. The corrosion of Al is controlled by this surface oxide film. The presence of alloy additions of Si disrupts the surface oxide film. Also the presence of Si will affect the anodization rates. The Si causes discontinuities in the oxide film and allows the Al to corrode at areas adjacent to Si precipitates. This gives rise to the spotty corrosion characteristics seen in Figure 48 and 49. Since all the Al/Si alloys can result in Si precipitates at room temperature, similar corrosion rates are observed for all the alloys. The slower corrosion rate exhibited by the "etched" samples is attributed to the fact that any exposed silicon at the alloy surface was removed when the silicon was removed between the metal stripes. The "etched" alloy would then behave more nearly as pure aluminum.

The corrosion process is different at the cathode. Changes in pH cause the cathodic corrosion. Ions such as H^{+} , K^{+} and Na^{+} can migrate to the cathode and shift the pH. This results in Al corrosion. These pH changes cause more general corrosion so the corrosion rates are similar to the type and number of impurities and also the surface SiO_2 between the stripes. MTF's for pure Al has varied from 200 to 1000 hours. This is believed a result of local impurity variations.

In summary, Si alloy additions to Al accelerate the anodic corrosion rate and yield MTF's between 50 and 150 hours for samples exposed to 85/85/20 conditions. The cathodic corrosion rates are similar for Al and Al/Si alloys.

2.5 Al/Si Alloy Film Surface Reconstruction

Aluminum films deposited on oxidized silicon substrates undergo surface reconstruction when annealed at temperatures greater than about 150°C . It is often desirable to reduce the growth of hillocks or protrusions above the film surface since these may disrupt passivation layers or generate electrical shorts between layers of a multilayer metal device. It is therefore of interest to determine whether or not silicon additions to aluminum have an effect on hillock growth.

The underlying cause of surface reconstruction of aluminum thin films is the difference in thermal expansion coefficients of the aluminum thin film ($24 \text{ ppm}/^{\circ}\text{C}$) and the underlying silicon ($4 \text{ ppm}/^{\circ}\text{C}$) and SiO_2 ($0.5 \text{ ppm}/^{\circ}\text{C}$). A stress is generated in the film on any temperature excursion and the reconstruction is a result of the relief of the stress.

The specific mechanisms operating to cause surface reconstruction can be divided into two classes: those occurring at high temperatures--few cycles as would occur in device processing and those occurring at low temperature--many cycles as would occur in device operation. Looking first at the high temperature phenomenon, a number of investigators²⁶⁻²⁹ have reported surface reconstruction of aluminum films on silicon and SiO_2 after elevated temperature treatments. The form of the reconstruction has been found to vary as a

function of grain size, alloying elements, and annealing time and temperature. In small grained films the reconstruction is manifested in the form of many large hillocks and whiskers emanating from triple points and whole small grains. A model for the hillock and whisker growth has been proposed by Chaudhari³⁰ based on grain boundary sliding and diffusional creep playing a dominant role with the former controlling the incubation period and the latter controlling the kinetics of hillock growth. He shows qualitative agreement with observations made on lead films, but it is reasonable to expect that the model will hold up for observations on aluminum films.

As the grain size of aluminum increases, the number of hillocks and their size decreases and the form of reconstruction shifts to wrinkling within individual grains. A model for wrinkling has been proposed by Philofsky, et al²⁶ involving slip on planes where the maximum resolved shear stress is greater than the theoretical resolved shear stress. The effect of alloying additives to the aluminum such as Si, Cu, Sn, and Mn is to retard hillock growth^{26,27,31}. This is expected as grain boundary diffusion is substantially reduced by some of these alloying additions. Also, Si precipitates have been shown to form nucleating sites for hillock growth increasing the hillock density resulting in a larger number of smaller hillocks²⁶.

Surface reconstruction which occurs after many cycles at low temperature has been shown to be caused by an entirely different mechanism. Instead of diffusion controlled mass flow, the mechanism is plastic deformation induced by compressional fatigue. An engineering relationship was found to hold between the yield strength of the aluminum film, σ_y and the temperature required for the onset of this low temperature surface reconstruction as follows:

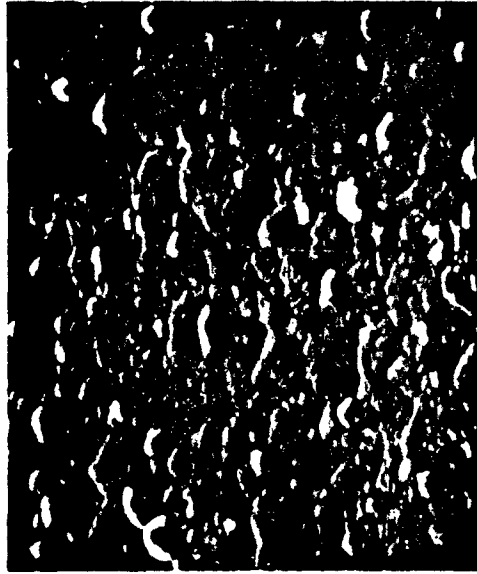
$$\sigma_y = 146 \Delta T$$

Since decreasing grain size and alloying additions both serve to increase yield strength, higher temperature cycles are required for the onset of this low temperature reconstruction which can lead to shorting between adjacent metal stripes.

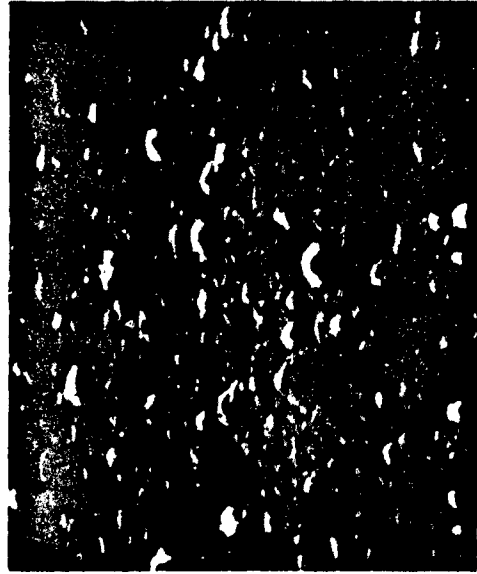
As briefly outlined above the effect of silicon alloy additions on surface reconstruction has been studied. A comparison between Figure 8 in Section 2.2 of this report and Figure 2 of reference 26 indicate that the introduction of Si tends to increase the density of hillocks and reduces their volume as was observed in reference 27.

Figure 51 presents SEM micrographs of three alloy films after ten temperature cycles from 25°C to 450°C with a ten minute dwell at each temperature. As previously discussed in Section 2.2 of this report the grains have grown rapidly promoted by the stress introduced by thermal cycling. The hillock density as shown in this figure ranges from 1.2×10^6 to 2.4×10^6 per cm^2 . It is obvious that the silicon does not prevent the growth of hillocks.

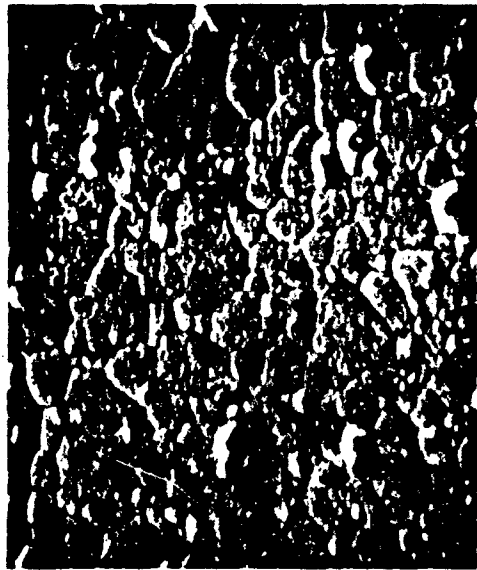
To study the effect of hillock growth and the stress introduced by the aluminum with its high thermal expansion coefficient on overlay glass films, alloys containing 1.5% Si, 2.5% Si and 3.5% Si about 7000 Å thick were patterned and coated with 3% phosphorous doped silica about 8000 Å thick. These were temperature cycled ten times from 25°C to 450°C being held at 10



1.9% Si



3% Si



0.79% Si

**FIGURE 51. Al/Si ALLOY FILMS
THERMALLY CYCLED 10
TIMES FROM 25°C TO 450°C
2000 X
 $\angle = 30^\circ$**

minutes at each temperature per cycle and examined using an SEM. Figure 52 shows glass cracking due to hillock growth as well as cracking which is attributed to the high rate of expansion of the aluminum as compared to that of the glass. SEM inspection of these samples prior to thermal cycling revealed no cracks in the passivation glass. It is believed that pure aluminum films thermally cycled in the same way would also cause cracks in the passivation glass.

2.6 Al/Si Alloy Wire Bondability

When one discusses wire bond strength to films and wire bondability one should first understand what gives metal its great strength. A single metal crystal can be considered to be an orderly array of an aggregate of metal ions which are sufficiently close to one another that they are able to share their valence electrons with the entire aggregate. The attraction of the positive metal ions to the common sea of electrons by-in-large is the "glue" which holds the structure together and provides the strength.

Most metal films and wires consist of a large number of crystals or "grains" which differ from one another in that their crystal lattices are oriented in different directions than their near neighbors. If one has two pieces of metal and wishes to join them or "weld" them together one must get the ions of the first metal sufficiently close to those of the second metal so they can share their valence electrons. This means that they must be brought within atomic spacings with one another. Since most metals contain layers of organic and inorganic films these must be disrupted by deforming the surfaces of both metals when pressed together to expose regions of clean metal to enable the weld to be completed.

Thermocompression welding essentially uses pressure and heat to deform both the wire and film to form the weld not unlike the technique of a blacksmith welding two pieces of wrought iron. Ultrasonic bonding relies on the dissipation of acoustic energy at the wire-film interface by friction to bring the two metals into intimate contact and to create the weld.

It is the purpose of this portion of the investigation of Al/Si alloy films to characterize the ultrasonic bondability of Al 1% Si 0.001" diameter wire to as deposited and heat treated Al/Si alloy films containing 0.79, 1.9 and 3% Si. This was done by obtaining "bond windows" of pull strengths as a function of ultrasonic power and time. At lower power settings (outside the window) the bonding wire does not adhere to the metallization. At higher power and/or time, the wires are necked down at the heel resulting in low pull strengths. These tests were made on a K and S 484 Hi Rel ultrasonic wire bonder with a UTI generator. All leads were 30 grams and the power setting was set on "low." The power setting was varied from 1.5 to 9 and the bond time ranged from 1.5 seconds to 9 seconds.

Figure 53 presents the bond windows for the as deposited alloy films and alloy films which have been aged in air at 210°C for 24 hours. Those settings within the windows exhibited less than 20% lifted bonds with a minimum of five bonds tested per setting. The numbers give the average destructive pull strength in grams. As indicated from this figure, the bond windows are

Handwritten notes and scribbles along the left margin of the page.

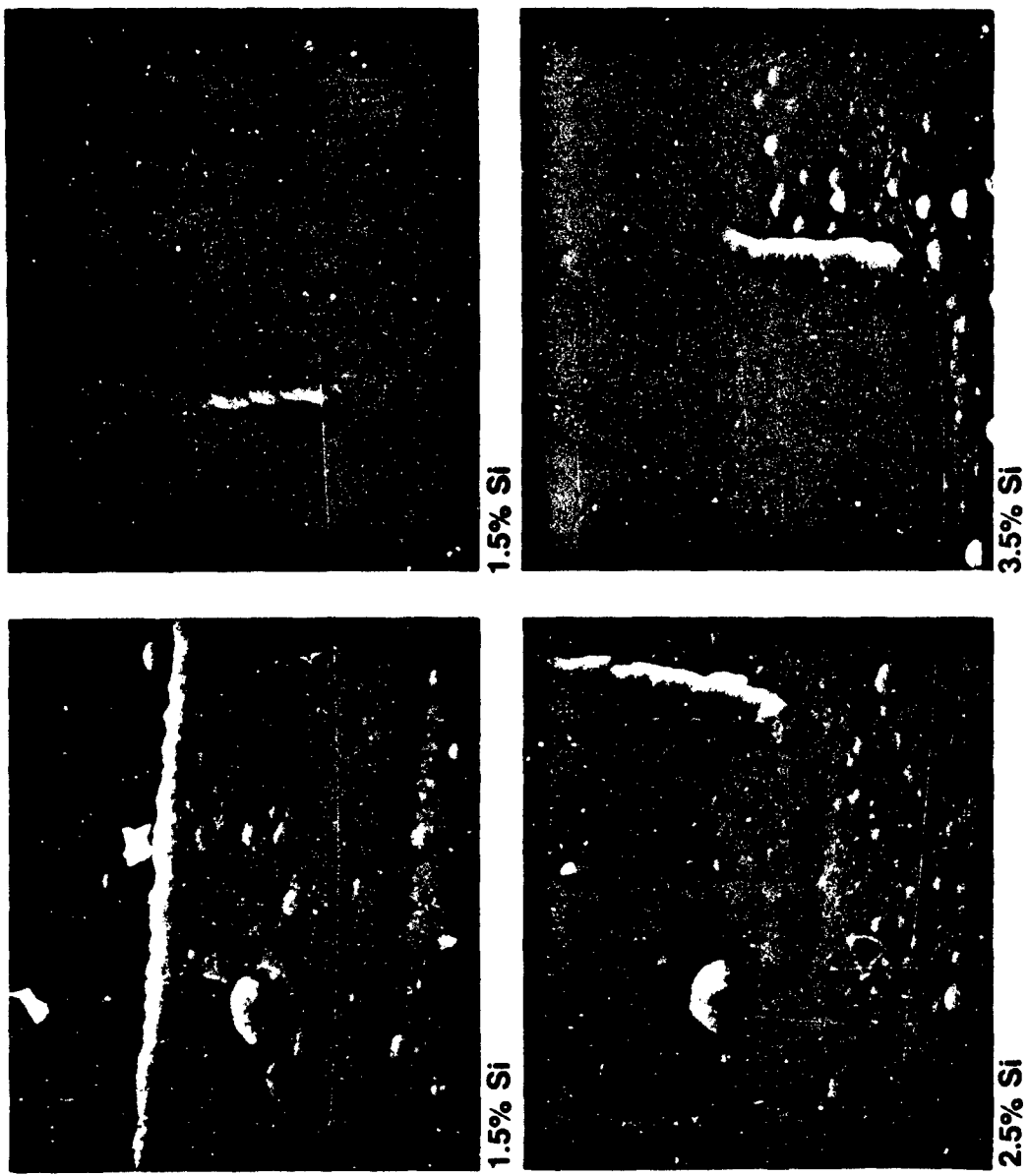
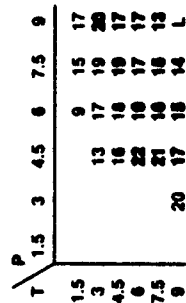
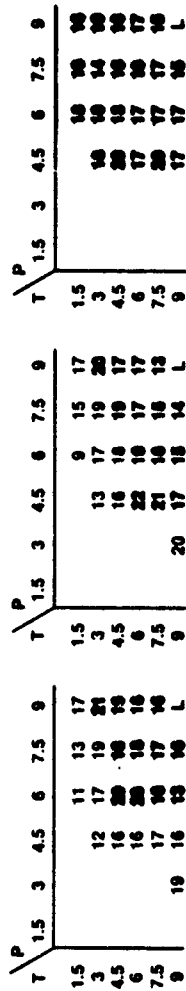


FIGURE 52. PASSIVATION GLASS CRACKS DUE TO THERMAL CYCLING

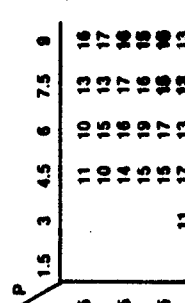
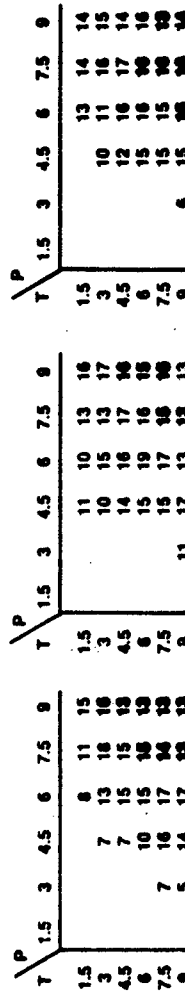
5271



3.0% Si

1.9% Si

As DEPOSITED
(g)



3.0% Si

1.9% Si

AFTER 24 HOURS AT 210°C IN AIR
(b)

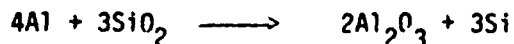
**FIGURE 53. POWER/TIME BONDING WINDOWS FOR Al/Si ALLOY FILMS TO 0.001''
Al 1% Si WIRE AT A LOAD OF 30 GRAMS. BOND WINDOWS HAVE 20%
OR LESS BOND LIFTS. NUMBERS GIVE AVERAGE DESTRUCTIVE
PULL STRENGTH IN GRAMS.**

quite large for the as deposited films and increase as the silicon content increases.

The bondability of the films aged in air at 210°C for 24 hours exhibited much smaller bonding windows than the as deposited films. It was originally postulated that the reason for the smaller bonding windows was due to a formation of a surface film of aluminum and silicon oxides, however, no difference could be detected between the baked and non-baked films when analyzed by the electron microprobe or the Auger electron spectrometer. The reason for the smaller bonding windows of the baked films is currently unknown. It is considered that this heat treatment prior to bonding was a severe test and no bonding problems are anticipated during normal manufacturing and wafer storage practices. It should be noted that the bonding windows on the as deposited films were made seven months after the films were deposited.

2.7 Adhesion of Al/Si Alloy Films to SiO₂

The solid state chemical reaction between aluminum films deposited on vitreous silicon dioxide is used by the semiconductor industry to provide excellent adherence of the aluminum to silicon dioxide. The free energy change in the reaction



is -150 kilocalories per mole at 500°C indicating that thermodynamically the reaction may proceed.

The fact that aluminum can successfully compete with silicon for the oxygen in silicon dioxide enables aluminum to form a strong adhesive bond to silica. When aluminum comes in intimate contact with silica it can break one of the two bonds oxygen has to silicon and chemically share the oxygen with silicon. This chemical bonding of aluminum to SiO₂ is called "chemisorbtion" and results in an extremely strong bond. Gold does not chemically react with SiO₂ and is poorly adherent to it. All metals that can reduce silicon dioxide and bond to it by chemisorbtion are utilized by the semiconductor industry for bonding metals to silicon dioxide. These are Mg, Al, Be and Ti. One other metal which is used extensively by the industry to bond to silicon dioxide is chromium and is an anomaly in the above discussion since it is incapable of reducing silica.

For chemisorbtion to take place the aluminum film must be in intimate contact with the silica. Any interfering film between aluminum and silica will generally result in poor bonding. Such films can be organic or inorganic. Organic films generally are removed by an HF etch prior to metal deposition or by heating the substrate under vacuum prior to metallization. One inorganic film that can form between the aluminum and silica is aluminum oxide by the reaction of aluminum with adsorbed layers of water. Such a film has been shown to interfere with the adhesion of aluminum to silica and can be prevented from forming by heating the silica in excess of 300°C under vacuum prior to metallization³².

An experiment designed to evaluate the adhesion of metal to SiO₂ was performed in an effort to compare the Al/Si alloys with pure aluminum. A special fixture was designed for use on an Instron tensile stress machine which enables vertical tensile stress to be applied to a 1/4 inch diameter rod epoxy bonded to the metal film. The results are given in Table VIII.

Although the test method was not capable of detecting differences of adhesion between the three Al/Si alloy films all three alloys exhibited extremely good adhesion to the silicon dioxide when deposited on a substrate held at elevated temperature.

2.8 Resistivity of Al/Si Alloys

The addition of Si to Al increases the resistivity of aluminum depending mainly upon how much silicon is in solid solution. The average increase in resistivity of aluminum per weight percent silicon is:

1.02 micro-ohm-cm in solution
0.088 micro-ohm-cm out of solution³³

Since the solubility of silicon is quite small (Figure 1) the change in resistivity, even when at its solubility limit, is small. The resistivity change when the silicon is out of solution is over a factor of eleven less than when solution. Thus when the silicon is randomly distributed it is difficult to measure any ΔR . Schnable et al³⁴ were unable to detect any ΔR in 2000 Å films of Al on silicon even when aged for 500 hours at 350°C.

Hall has observed that any change in resistivity in thin Al/Si alloy films could be brought about by the growth of large crystals of precipitated silicon extending an appreciable distance across the stripe². Such coarsening could be brought about by heat treatment or electromigration.

An experiment was performed during this present program to measure the resistivity of aluminum alloy films using the four point probe technique described by Lange³⁵. Here, the greatest error introduced would be in the measurement of the film thickness. The volume resistivity of three Al/Si alloy films over a temperature range 20°C to 160°C are plotted in Figure 54. The variation between films is believed to be within experimental error mainly due to thickness measurement error. Over this temperature range the alloys obey Matthiessen's law and the volume resistivity of the three alloys can be expressed as:

$$0.79\% \text{ Si} \quad \rho = 2.36 (1 + 0.0109 T) \mu\Omega \text{ cm}$$

$$1.9\% \text{ Si} \quad \rho = 2.39 (1 + 0.0107 T) \mu\Omega \text{ cm}$$

$$3.0\% \text{ Si} \quad \rho = 2.33 (1 + 0.0103 T) \mu\Omega \text{ cm}$$

For pure Al³³

$$\rho = 2.42 (1 + 0.0155 T) \mu\Omega \text{ cm}$$

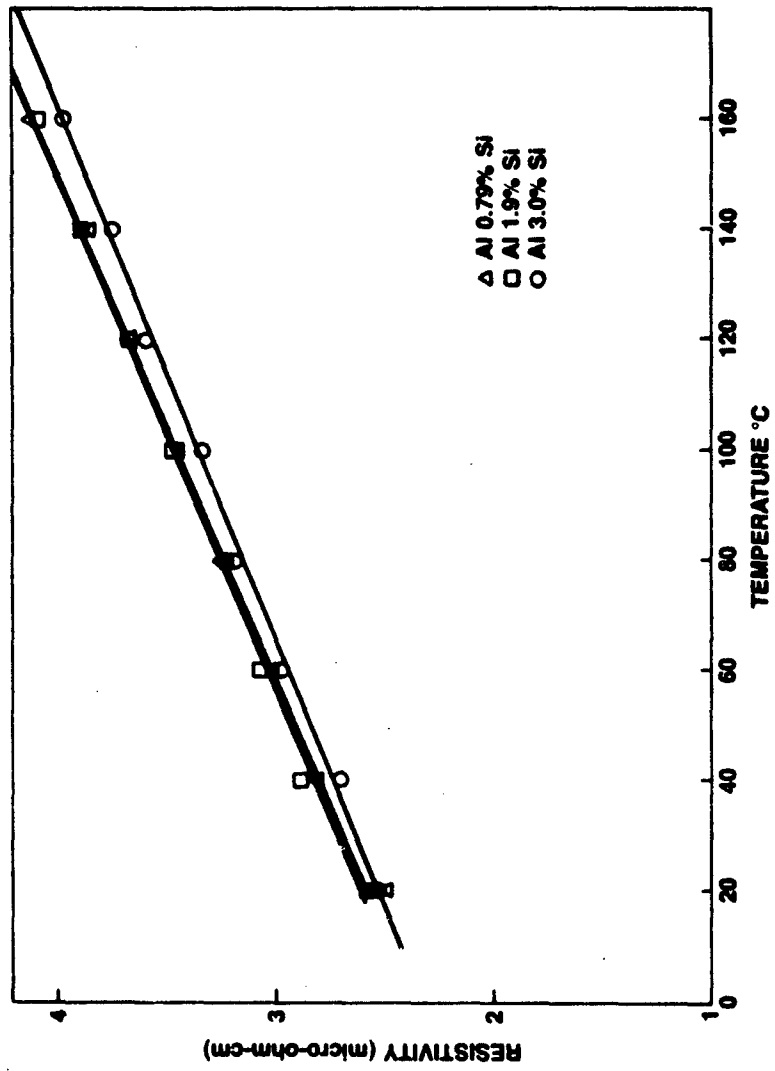
To evaluate the purity of the films resistivity ratios were measured between room temperature and liquid nitrogen temperature (-196°C). These are plotted in Figure 55 as a function of silicon content and indicates that

Table VIII

Metal - SiO₂ Adhesion Test Results

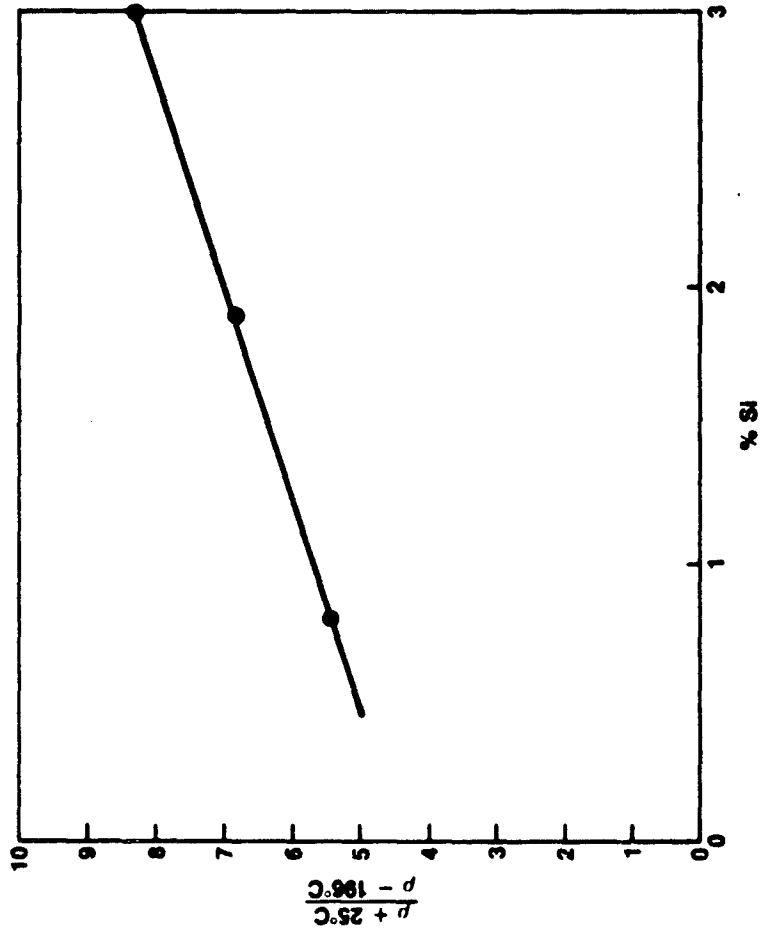
<u>Film</u>	<u>Rupture Force</u>	<u>Point of Rupture</u>
Pure Al deposited on a cold substrate	39 Killograms	Metal - SiO ₂ Interface
Pure Al deposited on a Hot Substrate >350°C	55 Killograms	In the Silicon
Al 0.79% Si deposited on a Hot Substrate >420°C	70 Killograms	In the epoxy
Al 1.9% Si deposited on a Hot Substrate at 420°C	73 Killograms	In the epoxy
Al 3% Si deposited on a Hot Substrate at 420°C	60 Killograms	In the epoxy and in the silicon

FIGURE 54. MEASURED RESISTIVITY OF THREE Al/Si ALLOY FILMS



6373

FIGURE 55. RESISTIVITY RATIO ROOM TEMPERATURE TO LIQUID NITROGEN TEMPERATURE AS A FUNCTION OF ALLOY SILICON CONTENT.



the resistivity ratio increases as the silicon content increases. This effect is believed due to the increased density of silicon nucleating sites as the silicon content is increased. Thus as the films are cooled the dissolved silicon has a greater opportunity to precipitate out of solution resulting in a purer aluminum lattice structure for the higher silicon content alloys. The purer aluminum lattice produces the higher resistivity ratios.

2.9 Sheet Resistivity at the Thermal Oxide-Passivation Glass Interface

One possible reliability problem area could arise due to leakage along the interface between the thermal oxide and the passivation glass. The concern here is that any residual silicon precipitated on the thermal oxide could lead to undesired electrical leakage paths.

To study this Al 3% Si alloy films were used which were deposited at the same time samples prepared for the low temperature electromigrations were made. Those films, however had the metal patterned identical to that shown in Figure 45 which was the metal pattern used in the corrosion experiments. One half of the samples were then treated to remove the residual silicon which remained on the substrate thermal oxide after the removal of the aluminum. The parts then received about 8000 Å of passivation glass with 3% phosphorus. Finally the samples were die bonded to 8 pin TO-5 headers and the outer long parallel stripes were wire bonded to the header leads. The outer stripes are separated by 0.5 mils and run parallel to each other for 105.5 mils distance making the space between the stripes equivalent to 1/211 of a square or 4.75×10^{-3} squares.

Ten volts were applied between the outside long parallel stripes on seven samples which had the residual silicon left at the thermal oxide-passivation glass interface and on seven samples which had the residual silicon removed. The leakage current between stripes was then measured using an electrometer. Table IX presents the data obtained.

The average current without the silicon was 4.2×10^{-11} A and with the silicon was 6.0×10^{-11} A. The respective resistance between the stripes was 2.381×10^{11} ohms and 1.667×10^{11} ohms. Since these resistances were measured across 1/211 of a square the sheet resistance for the case where the residual silicon was removed was 5.024×10^{13} ohms per square and 3.517×10^{13} ohms per square for the case where the residual silicon remained. It should be noted that the presence of the silicon at the interface between the thermally grown and passivation glass slightly reduces the sheet resistance, however these values with and without the silicon compare favorably to the surface resistivity of borosilicate electrical glass in a relative humidity greater than 50%³⁶.

It is concluded that if the spacing between metal stripes and other components is large compared to the silicon particulate size prior to the deposition of passivation glass, the residual silicon at the dielectric interface would not introduce functional problems. The silicon particulates do serve as centers for enhanced glass growth during passivation, forming a series of small lenses making it difficult to optically inspect underlying junctions for alignment, etc.

Table IX

Stripe Leakage Current at 10 Volts

<u>Without Residual Silicon</u>	<u>With Residual Silicon</u>
$2.0 \times 10^{-11} \text{ A}$	$4.1 \times 10^{-11} \text{ A}$
$1.7 \times 10^{-11} \text{ A}$	$3.5 \times 10^{-11} \text{ A}$
$2.0 \times 10^{-11} \text{ A}$	$7.4 \times 10^{-11} \text{ A}$
$5.5 \times 10^{-11} \text{ A}$	$8.5 \times 10^{-11} \text{ A}$
$6.3 \times 10^{-11} \text{ A}$	$4.1 \times 10^{-11} \text{ A}$
$5.3 \times 10^{-11} \text{ A}$	$8.4 \times 10^{-11} \text{ A}$
$6.5 \times 10^{-11} \text{ A}$	$6.3 \times 10^{-11} \text{ A}$

3.0 Further Observations of High Temperature Al/Si Alloy Electromigration

The Rome Air Development Center sponsored research program performed by Lewis, Bartels and Capobianco of the Raytheon Company²⁴ concluded that ECL Type 10,501 product manufactured by vendor A often failed at high temperatures due to an increase of the emitter resistance of an output transistor. The increase in emitter resistance was related to the build up of silicon in the emitter contact region by the electromigration of silicon in the Al/Si alloy metallization. The raw data for these experiments were presented by the authors. Although the number of devices placed on test at a given temperature and a given current density in the output transistor emitter stripe were usually five or less (and in one case only one) an attempt was made to determine the median time to failure. The purpose was to plot their data as $\log wt/J^2$ MTF vs. $1/^\circ K$ and to then compare this with the results obtained with the test device described in Section 2.3.5. Table X presents data extracted from the report for those parts that failed due to an increase in output emitter resistance.

An Arrhenius plot of this is presented in Figure 56 along with a line drawn using the least squares technique. Figure 56 also contains the data generated on this present program for high temperature Al/Si alloy data using the test device where the failure was due to etch pit formation shunting the negative contact junction. This line is parallel to the high temperature ECL data line indicating that they both have the same activation energy. The ECL data as shown by this figure is one order of magnitude more sensitive to failure than is the high temperature test device used on this present program. Failure for the ECL device was Si transport by electromigration to the emitter (+) contact while failure in the high temperature test device was silicon transport by electromigration away from the (-) contact generating etch pits.

The equation for the ECL data obtained from Figure 56 relating the median time to failure to emitter current lead geometry, the current density and time is:

$$\frac{wt}{J^2 \text{ MTF}} = 2.828 \times 10^{-12} \exp(-0.895/kT)$$

or

$$\text{MTF} = 3.536 \times 10^{11} \frac{wt}{J^2} \exp(0.895/kT)$$

The activation energy of 0.895 eV is surprisingly close to 0.889 eV obtained with the high temperature test device used in our present work.

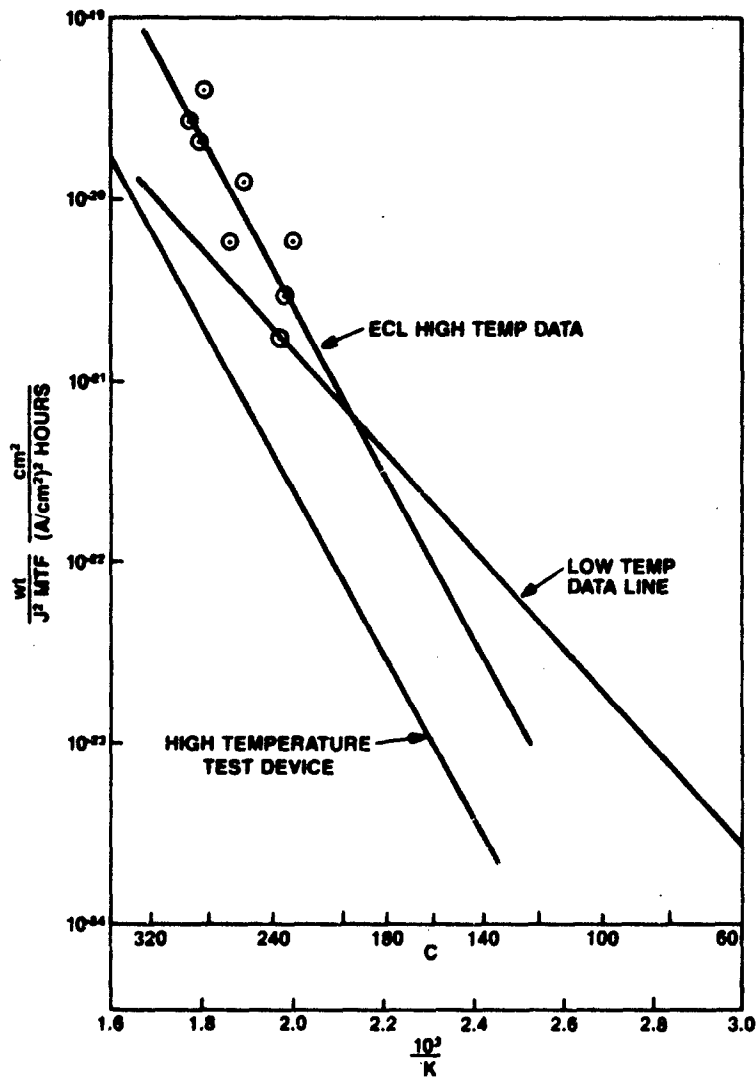
Figure 56 shows that the ECL devices which are more sensitive to the high temperature electromigration of Si through aluminum could be operated at junction temperatures near $180^\circ C$ and still fail mainly by open circuits due to the electromigration of Al in Al.

Table X

High Temperature ECL Test Data Obtained From Reference 24

Run #	Temperature °C	$\frac{10^3}{\sigma K}$	Current Density A/cm ² x 10 ⁻⁵	MTF (hours)	$\frac{wt}{J^2 MTF} \times 10^{21}$
1	226	2.00	1.05	3700	5.848
2	232	1.98	2.1	1850	2.917
3	235	1.97	2.94	1620	1.698
4	256	1.89	1.05	1500	14.42
5	265	1.86	2.1	930	5.803
6	282	1.80	1.05	540	40.07
7	286	1.79	2.1	260	20.67
8	292	1.77	2.94	100	27.51

FIGURE 56. ECL DATA COMPARED TO DATA GENERATED BY THE HIGH TEMPERATURE TEST DEVICE AND LOW TEMPERATURE DATA



E374

4.0 CONCLUSIONS AND RECOMMENDATIONS

From this study it is concluded that small grained and glassed Al/Si alloy metallization when used at normal device operating temperatures (below about 180-190°C) behaves much like pure small grained and glassed aluminum metallization. The glass overlay appears to increase its time to failure under electromigration conditions by a factor of two to three while the silicon addition appears to have very little influence on its electromigration rate. At the lower temperatures failure by electromigration is an electrical open circuit caused by void formation due to the electromigration of aluminum in aluminum. The activation energy for this was determined to be 0.54 eV, a value attributed to the electromigration of aluminum down grain boundaries.

At elevated temperatures (above about 180-230°C depending upon the device sensitivity) other electromigration modes of failure may predominate that due to the electromigration of silicon in aluminum. These are brought about by the electromigration of silicon in aluminum with the failure being either the shunting or shorting of junctions at ohmic contacts to the aluminum due to etch pit formation or the increase in resistance at ohmic contacts where electrons leave the aluminum and enter the silicon due to the build up of high resistive silicon at that contact. The etch pits generally are formed at the negative contacts to the metallization where electrons leave the silicon and enter the aluminum alloy. It is also possible for etch pits to form at positive ohmic contacts at regions where high current densities exist in the metal. As the overlying metal is depleted of silicon by electromigration the silicon substrate can serve as a silicon source to satisfy solid solubility in the aluminum, eventually forming an aluminum filled pit shorting an underlying junction. This mode of failure is often observed in r-f transistors³⁷ and I/C devices stressed at elevated temperatures²⁴. The activation energy for the electromigration of Si in Al for small grained and glassed films was found to be 0.89 eV being more sensitive to temperature than the small grain electromigration of Al in Al. This activation energy agrees well with that reported by van Grupp¹⁹ for the diffusion of Si in Al/Si thin films and is attributed by him to the diffusion of silicon along dislocations.

Caution should be taken by those stressing Al/Si alloy metallized devices at elevated temperatures to observe what the mode of failure is. If it is due to the electromigration of Si in Al for small grained and glassed films they should extrapolate to lower temperatures using an activation energy value of 0.89 eV until the temperature is reached when the failure mode becomes that due to the electromigration of Al in Al. For small grained alloy films extrapolation to lower temperatures from that point should follow an activation energy of 0.54 eV.

From this study it appears as though the MIL-M-38510C specification of a maximum current density of 5×10^5 A/cm² for glassed (99.99% pure or doped) aluminum is excessive for the glassed alloys studied. From Figures 28 through 31 the maximum temperatures allowable for the following percentage failures in the first year for a conductor continuously operating at 5×10^5 A/cm² and having a cross sectional area of 1×10^{-7} cm² are:

	T_j
50%	- 118°C
1%	- 98°C
0.1%	- 91°C
0.01%	- 85°C

If the current density for the above conductor was limited to 2×10^5 A/cm² the maximum allowable temperatures for the following percentage failure in the first year are:

	T_j
50%	- 171°C
1%	- 144°C
0.1%	- 135°C
0.01%	- 127°C

Motorola employs large grain (3-5 μ m) Al/Si alloy films on their MECL parts. The maximum current density design limit is 1.5×10^5 A/cm². Some of these have been in the field for a period approaching 10 years and have experienced as yet essentially no field failures due to electromigration. Also, temperature and current stress testing of these parts indicate a greater reliability for these larger grained Si alloy films than does this present work on small grain Si alloy films. It is believed that the improved performance of the large grain and glassed alloy films is based on the higher activation energy required for Al to electromigrate through Al of 1.2 eV. At about 180°C the lifetime of the large grained aluminum films shown in Figure 14 is an order of magnitude greater than the small grained glassed alloy films shown in Figure 27. At 100°C this improvement of the large grained glassed films over the small grained glassed films is about a factor of 300.

It is recommended, therefore, that a program be sponsored to study the electromigration failure of glassed large grain Al/Si alloy films.

The test devices used in the present study failed at elevated temperatures by shunting of an underlying junction by etch pit growth at the (-) terminal. In these tests the pit formed before a change in the (+) terminal contact resistance was noted. It would be useful to study test structures which are designed to fail by the increased resistance failure mode and which have various areas of ohmic contacts. It is desirable to know whether contact resistance increases can be detected at the upper device operating temperature ranges prior to failure due to an open circuit. Such a research program is recommended for large grained alloy films because of their extended lifetimes.

It has been shown that the alloy film structure and the distribution of Si throughout the film is a strong function of heat treatment above 300°C. Also at operating temperatures coarsening of the silicon particulates can occur promoted by electromigration of the Si in Al.

The corrosion rates of Al/Si alloys are similar to pure Al at the cathode. At the anode Si alloy additions to Al accelerate the anodic corrosion rate yielding MTF's between 50 and 150 hours at 85°C/85% R.H. with a 20 volt bias compared to about 250 hours for pure Al. Alloy films that were etched to remove the residual Si particles exhibited MTF's similar to pure aluminum.

* This could be critical when the devices are operated in a package ambient containing moisture, or in a non-hermetic package, and aggravated by ionic contamination, vis. solder flux, solvents, etc.

The addition of Si to Al tends to increase the density of hillocks during surface reconstruction reducing their size however the presence of Si does not prevent their formation. Passivated alloy films about 7000 Å thick have been shown to crack passivation glass when cycled 10 times from room temperature to 450°C.

The wire bondability of Al/Si alloy films has been shown to be good for ultrasonically bonding to Al 1% Si alloy wires. When the alloy films were heat treated at 210°C for 24 hours in air bondability was poor however the reason for this has not been identified. The wire bonds did not degrade during electromigration tests at temperatures below 210°C since the stripes failed due to an open circuit before any significant amount of silicon build-up could occur at the positive terminal bond.

The adhesion of Al/Si alloy films to thermally grown silicon dioxide has shown to be excellent when deposited on a hot substrate. In this case the substrate temperature exceeded 420°C, however it is believed that similar results can be obtained at temperatures as low as 300°C.

The electrical resistivity of pure Al is only slightly altered by the addition of small amount of Si. Only the silicon which remains in solid solution has much effect on the electrical resistivity and since this is greatly limited at operating temperatures the net effect is small.

The electrical sheet resistance at the interface between thermally grown silicon dioxide and chemically vapor deposited passivation glass was shown to be very high with or without the presence of residual silicon particulates at that interface. The particulates should not interfere with device operation if they are small compared to the separation between active elements and conductors. To assure small particulates the alloy film should be patterned prior to any heat treatments.

Finally, work done by others who observed the electromigration of Si through Al at elevated temperatures to cause device failure by resistance increase in the (+) ohmic contact was analyzed. It was found that their devices were more sensitive to the electromigration of Si in Al than was the device studied here. The degree of sensitivity depends upon the relative size of the ohmic contact to that of the conductor geometry, the depth of the underlying junction and the sensitivity of the device to contact resistance increase. Their work indicates that the activation energy for failure caused by the electromigration of Si through Al was identical to what was found in this present work.

APPENDIX I

References

1. J. R. Black, "Metallization Failures in Integrated Circuits," Tech. Report No. RADC-TR-68-243 Rome Air Development Center, Air Force Systems Command, Griffiss Air Force Base, New York, October 1968, AD# 844 307.
2. E. Hall, "Silicon RF Power Transistor Metallization," Final Report DAAB-7-C-0464 United States Army Electronics Command, Fort Monmouth, New Jersey, 1971.
3. H. Hansen, "Constitution of Binary Alloys," 2nd Edition, McGraw-Hill, New York, 1958.
4. J. O. McCaldin and H. Sankur, "Diffusivity and Solubility in the Al Metallization of Integrated Circuits," Appl. Phys. Lett. 19, (1971) 524.
5. G. J. van Gorp, "Diffusion-Limited Si Precipitation in Evaporated Al/Si Films," J. Appl. Physics, 44, No. 5 (1973).
6. M. Nanada, "Diffusion of Impurities in Thin Aluminum Films," Extended Abstracts Electrochemical Society Meeting, Atlantic City (1970) 478.
7. T. M. Reith and J. D. Schick, "The Electrical Effect on Schottky Barrier Diodes of Si Crystallization from Al-Si Metal Films," Appl. Phys. Lett. 25 (1974) 524.
8. J. Basterfield, J. M. Shannon and A. Gill, "The Nature of Barrier Height Variations in Alloyed Al-Si Barrier Diodes," Solid St. Electron. 18, (1974) 290.
9. F. M. d'Heurle and R. Rosenberg, "Electromigration in Thin Films," in Physics of Thin Films, Academic Press, Vol. 7 (1973) 257-310.
10. See for example, Th. Hehenkamp, "Study of Point Defects in Metals by Electro and Thermotransport," in Vacancies and Interstitials in Metals, ed., A. Seeger, D. Schumacher, W. Schilling and J. Diehel, Amsterdam North-Holland (1969) 91-122.
11. D. Shhabra, N. Ainslie, and D. Jepsen, "Theory of Failure in Thin Film Conductors, Abstr. Electrochem. Soc. Spring Meet. 1967.
12. J. R. Black "Electromigration- A Brief Survey and Some Recent Results," IEEE Trans. Electron Devices 16, (1969) 338.
13. F. M. d'Heurle, "The Effect of Copper Addition on Electromigration in Aluminum Thin Films," Met. Trans. 2, (1970) 681.

14. E. Hall, E. Philofsky and A. Gonzales, "A Scanning Electron Microscope Study of Electromigration in an Al-2% Cu Thin Film," *J. Electron Materials* 1, (1972) 333.
15. B. Agarwala, M. Attardo, A. Ingraham, "Dependence of Electromigration-Induced Failure Time on Length and Width of Aluminum Thin Film Conductors," *J. Appl. Phys.* 41, (1970) 3954.
16. N. G. Ainslie, F. M. d'Heurle, and O. C. Wells, "Coating, Mechanical Constraints and Pressure Effects on Electromigration," *Appl. Phys. Lett.* Vol 20, No. 4, Feb. 15, 1972.
17. T. Satake, K. Yokoyama, S. Shirakawa and K. Sawaguchi, "Electromigration in Aluminum Film Stripes Coated with Anodic Aluminum Oxide Films," *Jap. J. Appl. Physics*, Vol. 12, No. 4, April 1973.
18. I. A. Blech, "Electromigration in Thin Aluminum Films on Titanium Nitride," *J. Appl. Phys.* Vol. 47, No. 4, April 1976.
19. J. G. van Gorp, "Electromigration in Aluminum Films Containing Si," *Applied Physics Letters*, Vol. 19, No. 11 (1971) 476.
20. A. J. Learn, "Electromigration Effects in Aluminum Alloy Metallization," *J. Electronic Materials*, 3, No. 2 (1974) 531.
21. H. Buckle, *Z. Electrochem.* 49, (1943) 238.
22. R. F. Mehl, F. N. Rhines, K. A. von den Steiner, *Metals Alloys*, 13, (1941) 41.
23. C. J. Smithells, "Metals Reference Book," Vol. 2, 4th Ed., Plenum Press, New York, 662.
24. E. T. Lewis, D. Bartels, A. A. Capobianco, "Reliability Evaluation of ECL Microcircuits," RADC-TR-76-193, Rome Air Development Center, Air Force Systems Command, Griffiss Air Force Base, New York, 13441, June 1976. AD# A029 737.
25. D. S. Peck, "The Analysis of Data from Accelerated Stress Tests," 9th Annual Proceedings, Reliability Physics, IEEE Catalog No. 71-C-9-Phys., 1971, p. 69.
26. E. Philofsky and K. Ravi, E. Hall, and J. Black, "Surface Reconstruction of Aluminum Metallization--A New Potential Wearout Mechanism" *Rel. Phys. Symp.* Vol. 9, (1971) 120.
27. A. Paddock and J. Black, "Hillock Formation in Aluminum Thin Films," presented at the Electrochem. Soc. Meeting, Boston, May 5-9, 1968.
28. F. d'Huerle, L. Berenbaum, and R. Rosenberg, "On the Structure of Aluminum Films," *Trans. AIME* 242, (1968) 502.
29. J. Santoro, "Thermal Cycling and Surface Reconstruction in Aluminum Films," *J. Electrochem. Soc.* 116, (1969) 361.

30. P. Chaudhari, "Hillock Growth in Thin Films," J. Appl. Phys., 45, (1974) 4339.
31. K. Soto, T. Oi, H. Matsumaru, T. Okubo, T. Nishimara, "Hillock-Free Aluminum Thin Films for Electronic Devices," Metallurgical Transaction 2, (1971) 691.
32. J. R. Black, "The Reaction of Al with Vitreous Silica," 15th Annual Proceedings Reliability Physics, IEEE Catalog No. 77 CH-1195-7-Phy., 1977 p. 257.
33. K. van Horn, Ed., "Aluminum," Vol. 1, American Society for Metals, Metals Park, Ohio 1967.
34. G. Schnable, R. Keen, L. Lowenstein, "Study of Contact Failures in Integrated Circuits," Tech. Report No. RADC-TR-67-331, Rome Air Development Center, Air Force Systems Command, Griffiss Air Force Base, New York, Sept. 1967, AD# 820 554.
35. Julius Lange, "Method for Hall Mobility and Resistivity Measurements on Thin Layers," J. of Applied Physics, Vol. 35, No. 9, Sept. 1964, p. 2659.
36. "Properties of Selected Commercial Glasses," Corning Glass Works, No. B-83, Corning, New York 1949.
37. S. Gattesfeld, "A Life Test Study of Electromigration in Microwave Power Transistors," 12th Annual Proceedings Reliability Physics 1974, IEEE Cat. No. 74CH0839-1 Phy., 1974 p 94.

APPENDIX II

Acknowledgments

Several people at Motorola contributed to this work and deserve acknowledgment. Section 2.1 on the Solid State Dissolution of Si in Al was abstracted from work previously published by Dr. Edward Hall in reference 2. Sections 2.3, 2.3.1 and 2.3.2 were also originally prepared by Dr. Hall. Section 2.4 on Al/Si alloy corrosion presents the results of work done by Dr. Wayne Paulson. Dr. Edward Hall also contributed in part to Section 2.5 on Al/Si Alloy Film Surface Reconstruction. The experimental work presented in Section 2.6 on Al/Si Alloy Wire Bondability was performed by Ms. Kristie James. Mr. Curtis Mitchell designed the tensile fixture and performed the experimental work presented in Section 2.7 on the Adhesion of Al/Si Alloy Films to SiO₂. The Al/Si alloy resistivity measurements presented in Section 2.8 and the oxide interface sheet resistivity measurements of Section 2.9 were made by Dr. Michael Powell. Ms. Nancy Sutton prepared the experimental samples for the low temperature electromigration experiments while Mr. Robert Hovre made the high temperature test die.

The scanning electron microscope work was done by Ms. Lavoie Richardson, the electron microprobe analysis was performed by Ms. Donna Kirkman and the Auger electron spectrometer work by Mr. Anthony Gonzales. Ms. Marlene Robertson is recognized for her excellent work in preparing the manuscript.